Adhesion of cells on synthesized hydroxyapatite coatings with different morphologies

Mokabber, Taraneh; van Rijn, Patrick; Vakis, Antonis I.; Pei, Yutao T.

NBTE

Nederlandse vereniging voor
Biomaterialen en Tissue Engineering
Netherlands society for Biomaterials
and Tissue Engineering

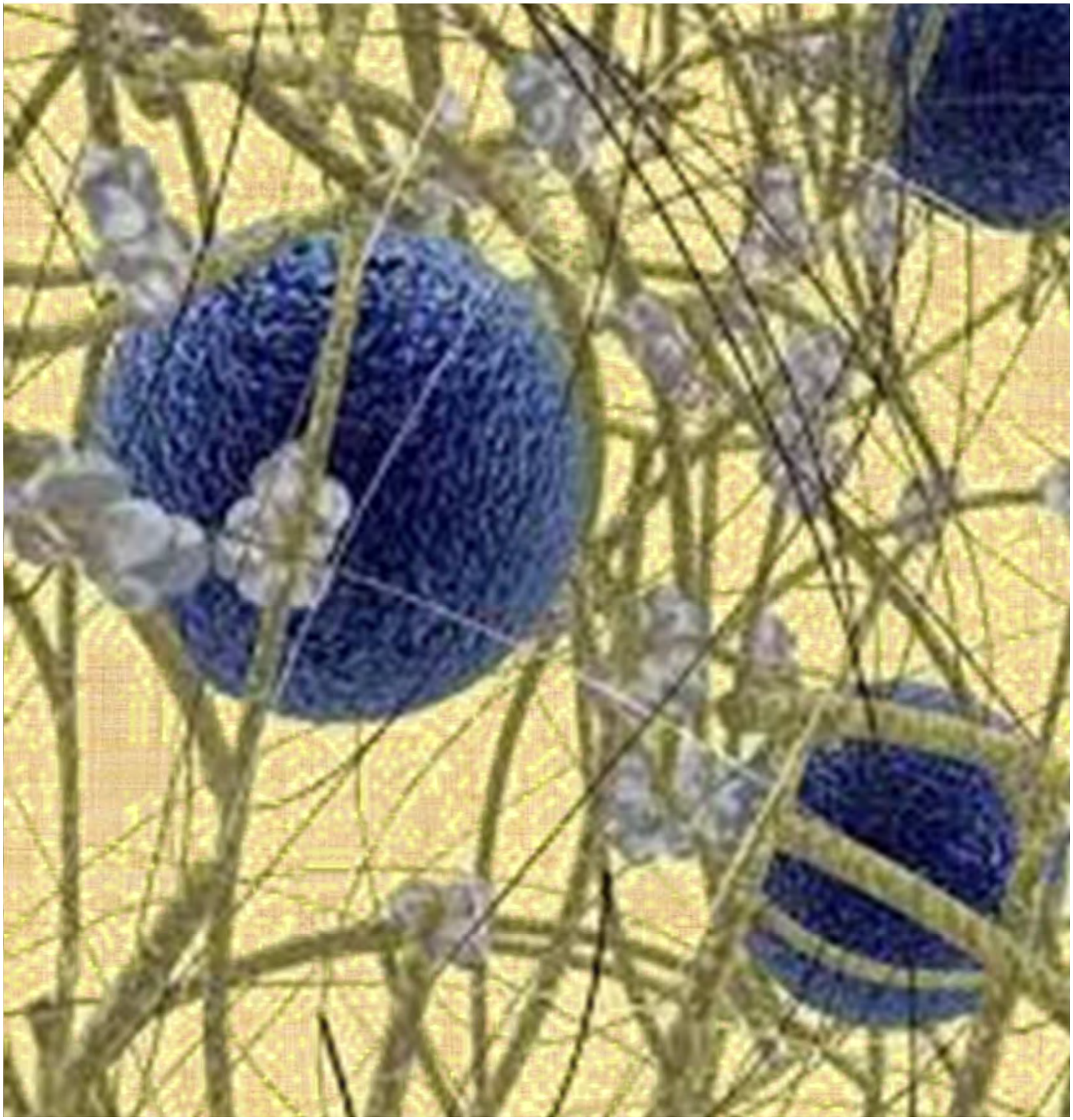

25th annual meeting

1-2 December 2016, Lunteren

NBTE
Netherlands society for
Biomaterials and Tissue Engineering

Program 25th Annual Meeting, 1 & 2 December 2016

at

"De Werelt congress center", Westhofflaan 2, 6741 KH Lunteren

Thursday, 1 December

09.15 – 09.45	***Registration and coffee***
09.45 – 10.00	***Welcome***

10.00 – 11.20 (8+2 min)	**Oral Presentations** **Chair: Mike Geven**
01	**Serdar Capar,** ErasmusMC-Orthopaedics, Rotterdam. *The inflammatory phenotype of infrapatellar fat pad can be modulated by triamcinolone acetonide, probably via the residing macrophages*
02	**Maurice van Dalen**, UTwente-Nanobiophysics & Developmental BioEngineering, Enschede. *Amyloid Micronetworks for Cartilage Tissue Engineering*
03	**Frances Bach**, UU-Veterinary Medicine, Utrecht. *The Regenerative Effects of Notochordal Cell Matrix (NCM) on Canine and Human Nucleus Pulposus Cells*
04	**Dafydd Visscher**, VUMC-Plastic, Reconstructive & Hand Surgery, Amsterdam. *3D-printed Injectable Poly- Ɛ-caprolactone Molds for Ear Cartilage Tissue Engineering*
05	**Anna Tellegen**, UU-Veterinary Medicine, Utrecht. *Controlled release of celecoxib from polyesteramide microparticles in a canine pre-clinical intervertebral disc degeneration model*
06	**Maurits Olthof**, UU-Veterinary Medicine, Utrecht. *Bone morphogenetic protein-2 release profile modulates bone formation in a novel phosphate modified oligo[(polyethylene glycol) fumarate] hydrogel*
07	**Ana Maria Almonacid**, UMCG-Pathology & Medical Biology, Groningen. *Nanostructured biomaterials for Skeletal Muscle Engineering*
08	**Maike Werner,** TU/e-Biomedical Engineering, Eindhoven. *Geometry-guided cell migration on competing length scales*

11.20 – 11.45	***Coffee break***

11.45 – 12.55 (8+2 min)	**Oral Presentations** **Chair: Marta Baroncelli**
09	**Ronald van Gaal,** TU/e-Biomedical Engineering, Eindhoven. *Supramolecular polymer based living membrane for kidney tissue mimics*
10	**Ilaria Geremia,** UTwente-Biomaterials Science and Technology, Enschede. *Development of New Strategies for the Removal of Urea from the Dialysate*
11	**Jeroen Buskermolen**, ACTA-Oral Cell Biology, Amsterdam. *Response of Gingiva Equivalents to Commensal and Pathogenic Oral Microbiomes*
12	**Bart Wullink**, UMCG-Ophthalmology, Groningen. *Type VII Collagen in the Human Accommodation System: Expression in Ciliary Body, Zonules and Lens Capsule*
13	**Jinlong Shao**, RadboudUMC-Biomaterials, Nijmegen. *Evaluation of Silver Nanoparticles incorporated Chitosan-based Membranes as Antibacterial Wound Dressing*
14	**Koen Dijkstra**, UMCU-Orthopedics, Utrecht. *BioAirbrush: Arthroscopic airbrush technology for cell-based treatment of knee cartilage defects – a pre-clinical in vitro study*
15	**Kavitha Sivasubramaniyan**, ErasmusMC-Orthopedics, Rotterdam. *A novel real-time migration assay identifies stem cell migration in 3D matrices*

12.55 – 13.55	***Lunch***

NVMB/NBTE Joint Symposium

13.55 – 15.10 (20+5 min)	**NVMB/NBTE Joint symposium: Part 1** **Chairs: Patricia Dankers, Reinout Stoop**
Symp 1	**Roeland Hanemaaijer**, TNO-Metabolic Health Research, Leiden *All you always wanted to know about ELISAs but were afraid to ask, and things you thought you know, but don't*
Symp 2	**Danny Duijsings**, Baseclear-Head R&D, Leiden. *Next generation sequencing*
Symp 3	**Andries van der Meer**, UTwente-Applied Stem Cell Technologies, Enschede. *Organs on Chips*

15.10 – 15.20	***Short Coffee Break***

15.20 – 16.35 (20+5 min)	**NVMB/NBTE Joint symposium: Part 2** **Chairs: Patricia Dankers, Reinout Stoop**
Symp 4	**Niels Geijsen**, Hubrecht Laboratories-Geijsen group, Utrecht. *Crispr/Cas9: tailoring the genome on demand*
Symp 5	**Beatriz Rocha**, Maastricht University-Multimodal Molecular Imaging Institute, Maastricht. *A better view with mass spec imaging*

Symp 6	**Patrick van Rijn**, UMCG-Biomedical Engineering, Groningen *Surface topologies determine cell behavior, not a superficial topic*
16.35 – 16.55	***Coffee Break***

16.55 – 18.00	***NBTE members Annual Meeting***

18.15 – 20.30	***Dinner***

20.30 – 21.30	**Invited lecture** ***Title: Biomaterials and cocultures for vascularized tissue engineering*** **James Kirkpatrick, MD, PhD, DSc** **Professor of Pathology, University Medical Center, Mainz, Germany,** **Fellow Royal College of Pathologists (FRCPath), London,** **Honorary, visiting professor in China, Singapore and Sweden.**

21.30 –	***Party time!***

Friday, 2 December

09.00 – 10.00 (8+2 min)	**Oral Presentations** **Chair: Vincenco Terlizzi**
16	**Renee Duijvelshoff**, TU/e-Biomedical engineering, Eindhoven. *In vivo performance of a bilayered supramolecular scaffold for in situ vascular tissue engineering*
17	**Aysun Guney,** UTwente-Biomaterials Science and Technology, Enschede. *Melt processable polymeric composites for additive manufacturing based on extrusion*
18	**Chella Hagmeijer**, UMCU-Orthopedics, Utrecht. *Development of a One-Stage Cell Therapy for Meniscus Regeneration Using a Combination of Meniscus Cells, Mesenchymal Stromal Cells and the Collagen Meniscus Implant*
19	**Tatiana Patricio***,* FUJIFILM Europe BV/ErasmusMC-Orthopedics, Rotterdam. *Bone-like magnetic microspheres obtained by bio-inspired synthesis, for controlled release of BMP-2 in bone tissue engineering*
20	**Nathan Kucko**, RadboudUMC-Biomaterials, Nijmegen *Towards load-bearing bioceramics: polymeric micro-fiber reinforcement of calcium phosphate bone cements*
21	**Philipp Kühn,** UMCG-Biomedical Engineering, Groningen. *Double Linear Gradient Biointerfaces for Determining Two-Parameter Dependent Stem Cell Behavior*

10.00 – 10.20	***Coffee break***

10.20 – 11.00	**Rapid fire Poster Presentations (1 min sharp, one slide)** **Chair: Angad Malhotra**
P1-P35	**Chris Arts,** MUMC-Orthopaedic Surgery, Maastricht. **David Barata**, MUMC/MERLN-Instructive Biomaterials Engineering, Maastricht. **Valentina Bonito**, TU/e-Biomedical engineering, Eindhoven. **Maaike Braham**, UMCU-Orthopedics, Utrecht. **Michiel Croes**, UMCU-Orthopedis, Utrecht. **Luuk van Dijk**, Xpand Biotechnology BV, Bilthoven. **Rongquan Duan**, UTwente-Biomaterials Science and Technology, Enschede. **Rachel Elzes**, UTwente-Biomaterials Science and Technology, Enschede. **Shorouk Fahmy-Garcia**, ErasmusMC-Orthopedics, Rotterdam. **Yao Fu**, UTwente-Developmental Bioengineering, Enschede. **João Pedro Garcia**, UMCU-Orthopedics, Utrecht. **Mike Geven**, UTwente-Biomaterials Science and Technology, Enschede. **Hatice Imran Güngördü,** RadboudUMC-Biomaterials, Nijmegen **Zhengchao Guo,** UTwente-Biomaterials Science and Technology, Enschede. **Dennie Hebels,** MERLN-Cell Biology-Inspired Tissue Engineering (cBITE), Maastricht.

	Jan Hendriks, UTwente-Developmental Bioengineering, Enschede. **Bastiaan Ippel**, TU/e-Biomedical Engineering, Eindhoven. **Lisanne Karbaat**, UTwente-Developmental Bioengineering, Enschede. **Caoimhe Kiernan**, ErasmusMC-Oral & Maxillofacial Surgery, Rotterdam. **Anne Leferink**, UTwente-BIOS Lab on a chip group, Enschede. **Kaizheng Liu**, RIMLS-Urology, Nijmegen. **Alessia Longoni**, UMCU-Oral and Maxillofacial Surgery and Special Dental Care, Utrecht. **Giulia Marchioli**, TU/e-Biomedical Engineering, Eindhoven. **Roel op 't Veld**, RadboudUMC-Biomaterials, Nijmegen. **Iris Pennings**, UMCU-Oral and Maxillofacial Surgery and Special Dental Care, Utrecht. **Daniela Petre**, RadboudUMC-Biomaterials, Nijmegen. **Stefan Remmers**, TU/e-Biomedical Engineering, Eindhoven. **Carl Schuurmans**, UU-Pharmaceutical Sciences, Utrecht. **Vincenzo Terlizzi**, UMCG-Pathology and Medical Biology, Groningen. **Patrycja Trepa**, UTwente-Biomaterials Science and Technology, Enschede. **Lizette Utomo**, ErasmusMC-Orthopedics, Rotterdam. **Steven Vermeulen**, MERLN-Cell Biology-Inspired Tissue Engineering, Maastricht. **Tamar Wissing**, TU/e-Biomedical Engineering, Eindhoven. **Dan Jing Wu**, TU/e-Biomedical Engineering, Eindhoven. **Yang Zhang**, RadboudUMC-Biomaterials, Utrecht.

11.00 – 12.30	***Poster presentations and drinks***

12.30 – 13.30	***Lunch Break***

13.30 – 14.30 (8+2 min)	**Oral Presentations Chair: Maike Braham**
22	**Gabriel Linguori**, UMCG-Medical Biology, Groningen. *Nano and Micro Directional Topographies Oppositely Influence Adipose Derived Stem Cells Differentiation to Smooth Muscle Cells*
23	**Taraneh Mokabber**, UMCG-Advanced Production engineering, Groningen. *Adhesion of cells on synthesized hydroxyapatite coatings with different morphologies*
24	**Yasaman Zamani**, ACTA-Oral Cell Biology, Amsterdam. *Surface Modification of 3D-Printed Polycaprolactone Scaffolds by Functional Carboxyl and Hydroxyl Groups Enhances MC3T3-E1 Pre-osteoblast Proliferation and Matrix Production*
25	**Matthijs Suijkerbuijk**, ErasmusMC-Orthopedics, Rotterdam. *Modulating JAK-STAT Signaling Pathways in Macrophages to Improve Tissue Regeneration*
26	**Sergio Spaans**, TU/e-Biomedical Engineering, Eindhoven. *Catechol-functionalized UPy-based biomaterials improve cardiomyocyte progenitor cell adhesion*
27	**Pia Kröger**, UTwente-Biomaterials Science and Technology, Enschede. *Single-chain nanoparticles: a new class of drug carriers*

14.30 – 14.50	***Coffee break***

14.50 – 16.00 (8+2 min)	**Oral Presentations Chair: Bastiaan Ippel**
28	**Eline van Haaften**, TU/e-Soft Tissue Biomechanics and Tissue Engineering, Eindhoven. *An in-vitro platform to culture vascular grafts under combined shear stress and circumferential stretch*
29	**Imke Jansen**, UMCU- Orthopedics, Utrecht. *Local Delivery of Triamcinolone Acetonide in an ACLT Model of Osteoarthritis Impairs Joint Regeneration, possibly by Inhibition of Wound Healing*
30	**Didem Mumcuoglu**, FUJIFILM Europe BV/ErasmusMC-Orthopedics, Rotterdam. *Development of Injectable BMP-2 Delivery Materials Using Collagen-I Based Recombinant Peptide*
31	**Thijs Pasman**, UTwente-Biomaterials Science and Technology, Enschede. *Fabrication of porous poly(trimethylene carbonate) membranes for lungs-on-chips using phase separation techniques*
32	**Qihui Zhou**, UMCG-Biomedical Engineering, Groningen. *High-throughput Screening of Cell Contact Guidance on Directional Micro/nanotopographical Gradients*
33	**Barbara Klotz**, UMCU-Oral and Maxillofacial Surgery & Special Dental Care, Utrecht. *Tailoring Gelatin-Transglutaminase Hydrogels for Pre-Vascularized Bone Analogs*

15.50	***Announcement of the chair, poster and presentation awards***

16.00	***Closure of the meeting***

Oral Abstracts

(Alphabetical order)

Nanostructured biomaterials for Skeletal Muscle Engineering

A.M. Almonacid Suarez, M.C. Harmsen, P.van Rijn
Department of Pathology and Medical Biology, University Medical Center Groningen, Hanzeplein 1 9713 GZ
Department of Biomedical Engineering, University of Groningen, University Medical Center Groningen, Antonius Deusinglaan 1, 9713 AV
Groningen, The Netherlands
Contact: a.m.almonacid.suarez@umcg.nl

Transplantation of autologous muscles is the current treatment for facial palsy, which requires long rehabilitation time.[1] Patients undergo a lot of physical and psychological trauma making a better treatment a necessity and the creation of adequate surrogate muscle tissue would provide a possible solution.[2]

Engineering of muscle tissue has had important developments in the last years with the creation of human muscle fibres able to contract.[3] However, it is still unknown how to engineered a muscle with proper vascularization and innervation.[4] In addition, much of the progress in muscle research has been with the use of the standard C2C12 cells of murine origin which is a disadvantage for engineering human muscle tissue.[5] Skeletal muscle has a highly aligned morphology and recreating this morphology is key in developing functional muscle. Aligned topographies have been shown to direct cellular orientation and understanding the cellular response to different topographies will aid in proper tissue scaffold engineering.[5]

Recently, gradient surfaces have improved the screening of cells in different topographies.[6] In our current research, previously generated knowledge from human satellite cells (hSCs) isolation and differentiation into muscle fibress[2] and developed gradient technology[7] were combined to assess hSCs response to topography. The gradient topography substrates were created by applying a unidirectional strain during shielded surface oxidation of polydimethylsiloxane (PDMS) with air plasma. As result wrinkles ranging from 1020 nm to 6930 nm in wavelength and 74 nm and 2843 nm in height were created within the same substrate. Human satellite cells (hSCs) were cultured on PDMS wrinkle gradients for 12 days. Cell alignment, area and elongation during proliferation after four days and differentiation after six and eight days were determined. Preliminary results showed that cells started to align after 16 hours of cell culturing in PM on the nanotopography gradients. Moreover, after 4 days in proliferation medium the preferred wrinkle size for cells were between 2200 nm and 3550 nm in wavelength and 319 nm and 793 nm in height. However, wavelengths between 4300 nm and 6930 nm and heights between 1142 nm and 2843 nm were optimal for alignment and differentiation after 12 days in culture. Additionally, it was observed that myofibre diameter changes across the gradient, larger diameters were obtained in larger wrinkle sizes. The minimum value found was in the smallest wrinkle sizes with a value of 16 um and the larger value found was in the largest wrinkle sizes with 125 um diameter. Additionally, cell area of differentiated myotubes varied significant across de gradient. After six days and eight days, the area of attached cells on the smallest wrinkles was significantly different from the rest of the gradient. Comparison tests suggested that the larger difference occurs from wrinkles features from 3550 nm wavelength and 793 nm height to the largest wrinkles, this results are consistent with cell density and diameter sizes across the gradient, suggesting that once cells start differentiating, they show a preferred migration and preference for greater wrinkle features.

In conclusion, satellite cell proliferation and differentiation into myotubes in PDMS wrinkled gradients was achieved. This preliminary study shows a cell behavior dependence on wrinkle size. However, further analysis is needed to determine exact correlation. Optimum feature dimensions will be translated to large area substrates to engineer muscle tissue sheets as a potential muscle surrogate to treat facial palsy.

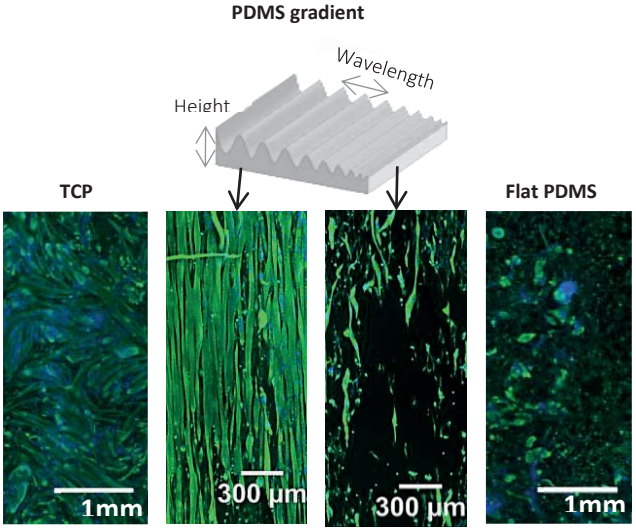

References

1. Chuang, D. C. *Facial Plast Surg* **24,** 194–203 (2008).
2. Koning, M. Tissue engineering of skeletal muscle for patients with facial paralysis. (University of Groningen, 2012).
3. Madden, L., Juhas, M., Kraus, W. E., Truskey, G. A. & Bursac, N. *Elife* **2015,** 1–14 (2015).
4. Juhas, M., Ye, J. & Bursac, N. *Methods* **99,** 81–90 (2016).
5. Qazi, T. H., Mooney, D. J., Pumberger, M., Geißler, S. & Duda, G. N. *Biomaterials* **53,** 502–521 (2015).
6. Kim, H. N. *et al. Adv. Drug Deliv. Rev.* **65,** 536–558 (2013).
7. Zhou, Q. *et al. Adv. Mater. Interfaces* (2016). doi:10.1002/admi.201600275

The Regenerative Effects of Notochordal Cell Matrix (NCM) on Canine and Human Nucleus Pulposus Cells

F.C. Bach[1], S.A.H. de Vries[2], L.B. Creemers[3], B.P. Meij[1], K. Ito[2,3], and M.A. Tryfonidou[1]

[1]Department of Clinical Sciences of Companion Animals, Faculty of Veterinary Medicine, Utrecht University, Yalelaan 104, 3584 CM, Utrecht, the Netherlands, [2]Orthopaedic Biomechanics, Department of Biomedical Engineering, Eindhoven University of Technology, De Rondom 70, 5612 AP Eindhoven, the Netherlands, [3]Department of Orthopaedics, University Medical Centre Utrecht, Heidelberglaan 100, 3584 CX Utrecht, the Netherlands

Introduction: Low back pain has been related to intervertebral disc (IVD) degeneration. Since dogs experience back pain and IVD degeneration with similar characteristics as humans, they are considered a suitable animal model for human IVD degeneration. Current treatments for IVD disease do not lead to repair, so there is urgent need for regenerative treatments resulting in functional IVD restoration. During IVD maturation, notochordal cells (NCs) are replaced by chondrocyte-like cells (CLCs) in the nucleus pulposus (NP). NCs produce soluble factors that induce cell proliferation and healthy extracellular matrix (ECM) production, but identification of these specific factor(s) has proven difficult. A novel approach would be to directly use the matrix of NP tissue rich in NCs, the so-called notochordal cell matrix (NCM), which has already been shown to exert anabolic effects on bovine CLCs. Therefore, as a first step towards translation, the regenerative effects of NCM on canine and human CLCs derived from degenerated IVDs were determined.

Material and Methods: NCM was produced from healthy porcine NC-rich NP tissue (n = 6, pooled) by lyophilization and resuspension in basal culture medium (10 mg/mL). The effect of NCM was determined on canine (n = 6) and human (n = 6) CLCs derived from degenerated IVDs (Thompson grade III) cultured in micro-aggregates (35,000 cells) for 28 days under hypoxic conditions. Main read out parameters (determined by RT-qPCR, histology, DMMB assay, and ELISA) were: ECM anabolism/catabolism, cell proliferation, morphology, apoptosis, inflammation, and Smad signaling (phosphorylated Smad1 & Smad2).

Results: Generally, the response of canine CLCs to NCM was more pronounced than the response of human CLCs to NCM. Although *ACAN* and *COL2A1* gene expression was not upregulated at day 7, NCM significantly increased the glycosaminoglycan content of human and canine CLC micro-aggregates compared with controls at day 28 (Figure). Furthermore, NCM induced mild collagen type I and abundant collagen type II deposition in human and canine CLC micro-aggregates (Figure). ECM catabolism and apoptosis marker gene expression was decreased by NCM treatment, whereas *CCND1* gene expression (marker for proliferation) was increased in human and canine CLCs. Collagen type X deposition and (anti-)inflammatory and notochordal/ nucleus pulposus marker gene expression were not affected by NCM treatment, but *VEGF* gene expression was increased in human and canine CLCs. Lastly, NCM significantly induced rapid Smad1 (BMP) and Smad2 (TGF-β) signaling in canine CLCs, whereas it decreased Smad1 and Smad2 signaling in human CLCs.

Discussion: NCM induced an anabolic, anti-catabolic, anti-apoptotic, and proliferative effect on human and canine CLCs derived from degenerated IVDs, indicating that it holds promise as regenerative treatment for IVD disease. Increased Smad signaling can explain the regenerative effects of NCM on canine CLCs, but future studies should focus on determining the mechanism(s) of NCM-mediated regeneration in human CLCs.

Conclusion: The current study shows that directly applying notochordal cell matrix of NP tissue could be a promising regenerative treatment for canine and human IVD disease, circumventing the (challenging) identification and application of bioactive NC-secreted substances.

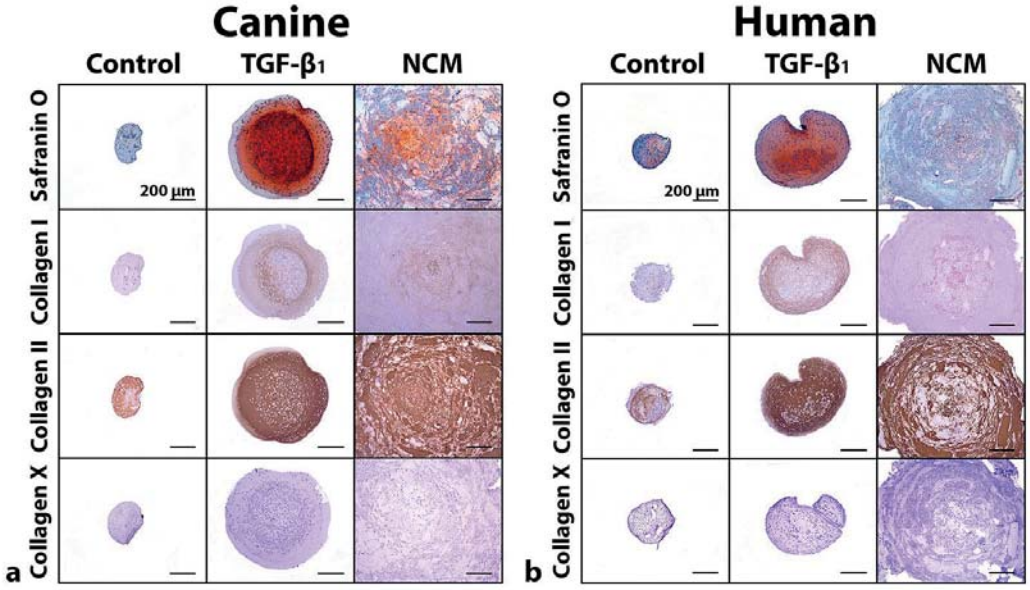

Fabrication of a bioprinted endosteal and perivascular bone marrow niche model for multiple myeloma

Maaike V.J. Braham [a], A. Rahul Akkineni [b], Tilman Ahlfeld [b], Monique C. Minnema [c], F. Cumhur Öner [a], Catherine Robin[d,e], Anja Lode [b], Michael Gelinsky [b] and Jacqueline Alblas [a]

[a] Department of Orthopaedics, University Medical Center Utrecht, Utrecht, The Netherlands
[b] Centre for Translational Bone, Joint and Soft Tissue Research, University Hospital Carl Gustav Carus and Faculty of Medicine, Technische Universität Dresden, Germany
[c] Department of Hematology, University Medical Center Utrecht Cancer Center, The Netherlands
[d] Hubrecht Institute-KNAW & University Medical Center Utrecht, Utrecht, The Netherlands
[e] Department of Cell Biology, University Medical Center, Utrecht, The Netherlands

Introduction: The bone marrow (BM) microenvironment is the preferred location of multiple myeloma (MM), supporting tumor growth and development. The BM microenvironment is composed of a collection of interacting subniches, the two most acknowledged are the endosteal niche and perivascular niche. Currently it is unknown whether preferred outgrowth of MM cells in either of these subniches exists, or if different subsets of MM cells are supported by these varying environments, as is seen for hematopoietic stem cells naturally residing in these subniches.
Aim: To fabricate a reliable culture model mimicking separate but interacting niches, in which primary MM cells can be cultured.
Methods: A 3D BM-MM model containing two subniches was created using three-dimensional (3D) bioprinting technology. A bioprintable pasty calcium phosphate cement (pCPC) scaffold was used to model the endosteal niche and Matrigel containing multiple cell types was used to mimic the perivascular niche. Optimal composition, function and interactions of the different subniches with primary MM cells was analyzed.
Results: A BM model with separate but interacting subniches was successfully created. The perivascular model showed a sustained viability of the cultured primary CD138+ MM cells. The endosteal model was not capable of sustaining the cultured CD138+ MM cells. When adding both niches within one model, a significant increase in the proliferation of CD138+ MM cells was observed, when compared to the perivascular model alone.
Conclusions: The developed model is the first to incorporate both the perivascular and the endosteal niche within one model, showing an added value by increasing the survival of primary MM cells *in vitro*. This bioprinted model can be used as a relevant tool to study the outgrowth of MM cells in either of these subniches, and MM interactions with these varying sub microenvironments.

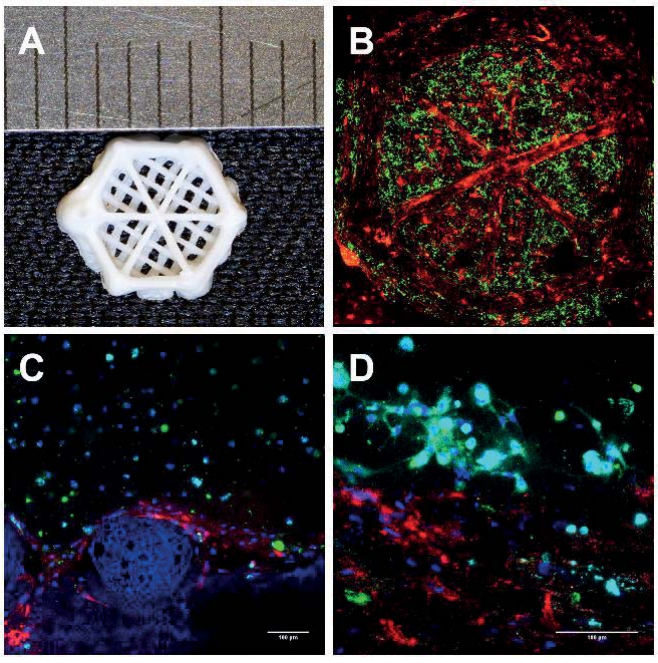

Figure 1: Fabrication of a bioprinted endosteal and perivascular bone marrow niche model
(A) Bioprinted p-CPC scaffolds, (B) with an added Matrigel coculture. The p-CPC scaffolds were functionalized with O-MSCs (DiI, red) before adding the soft BM-coculture containing both MSCs and EPCs (DiO, green). (C) At both day 2 and (D) day 10 migration of MSCs (DiO, green) and EPCs (DiD, cyan) could be observed from the Matrigel towards the endosteal compartment, indication interactions between both compartments. At day 10 of culture, networks of MSCs and EPCs have formed, in close proximity of the endosteal compartment. Hoechst, blue.

Response of Gingiva Equivalents to Commensal and Pathogenic Oral Microbiomes

J.K. Buskermolen[1], M.M. Janus[2], B.P Krom[2], S. Gibbs[1,3]
j.k.buskermolen@acta.nl

Department of 1) Oral Cell Biology and 2) Preventive Dentistry, Academic Centre for Dentistry Amsterdam, University of Amsterdam, and VU University Amsterdam, MOVE Research Institute Amsterdam, The Netherlands. 3) Department of Dermatology, VU University medical center, Amsterdam

Introduction

Host-microbiome interactions play an important part in regulating human health. Microbiomes consist of up to 200 different species of bacteria. Whereas commensal oral microbiomes do not damage the host tissue, pathogenic oral microbiomes cause diseases such as gingivitis or caries. The aim of this study was to determine the host response to commensal and pathogenic oral microbiomes with the aid of 3D tissue engineered gingiva equivalents (GE).

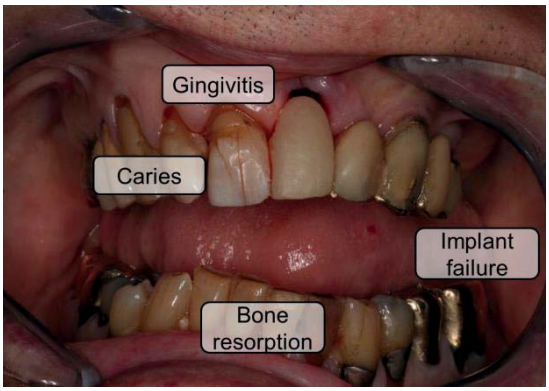

Figure 1: *In vivo* pathology caused by different oral microbiomes.

Materials and Methods

The GE consisted of a fully differentiated epithelium on a fibroblast populated collagen hydrogel. Three distinct oral microbiomes were grown, resembling a commensal, gingivitis and cariogenic phenotype. GE were exposed to the microbiomes for 24 hours. GE response to the different microbiomes was analyzed by histology and inflammatory mediator release (ELISA).

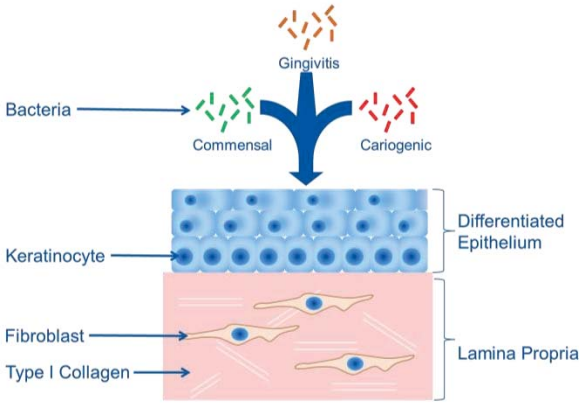

Figure 1: *In vitro* 3D model to study the effects of different oral microbiomes on oral mucosa.

Results

A dense layer of commensal, gingivitis or cariogenic bacteria were observed on GE tissue sections. Commensal and cariogenic bacteria had no detrimental effects on GE histology. However gingivitis bacteria caused a disruption in tissue integrity in the upper epithelial layers. Notable differences were observed in the secretion of inflammatory cytokines. IL-6, CXCL8 and CCL20 secretion was higher when the GE were exposed to commensal microbiomes than to pathogenic microbiomes. In contrast, CCL5 upregulation was similar for all three microbiomes.

Conclusions

Commensal microbiomes and pathogenic microbiomes induce a different inflammatory cytokine response in gingiva tissue. Notably, GE secreted higher amounts of pro-inflammatory cytokines in response to the commensal microbiome than in response to the pathogenic microbiome. Our results indicate that the pathogenic microbiome might actively evade the immune response.

The inflammatory phenotype of infrapatellar fat pad can be modulated by triamcinolone acetonide, probably via the residing macrophages.

S. Çapar[1], W. Wei[1], J.A.N. Verhaar[1], S. Clockaerts[2], G.J.V.M. van Osch[1], Y.M. Bastiaansen-Jenniskens[1]
[1]Erasmus MC, University Medical Center, Rotterdam, the Netherlands
[2] Department of Orthopaedic Surgery and Traumatology, AZ Groeninge Kortrijk, Belgium.

Introduction – Joint injuries are common and often result in cartilage defects and inflammation of the joint. Joint inflammation however may prevent successful cartilage defect repair. The inflamed infrapatellar fat pad (IPFP) in the knee joint secretes factors that inhibit successful cartilage repair by inhibiting chondrogenic differentiation and stimulating degradation. Pro-inflammatory macrophages residing in the IPFP are suspected to contribute to this effect (1). To improve cartilage repair, restoration of the joint homeostasis is necessary. Therefore, we aim to reduce inflammation in the IPFP focusing on macrophages residing in the tissue to create an environment that allows cartilage repair.

Materials and methods – IPFP tissue was obtained as leftover material from patients with OA who underwent a total knee arthroplasty. The IPFP was cut into small pieces and cultured in Dulbecco's Modified Eagle Medium with Glutamax (DMEM-HG) supplemented with 1% insulin-transferrin-selenium (ITS+) and Triamcinolone acetonide (0.1µM-100µM TAA; #T6501), celecoxib (#PZ0008), pravastatin (#P4498) or fenofibrate (#F6020). After 24 hours of culture, IPFP explants were snap frozen in liquid nitrogen for gene analysis of Tumor Necrosis Factor alpha (*TNFA*), Interleukin beta (*IL1B*), *IL6*, *IL10*, Cluster of differentiation 206 (*CD206*), and *CD163*, or immediately processed for flow cytometric analysis using conjugated antibodies against CD14-APC-H7, CD80-PECy7, CD86-PE, CD163-PerCP-Cy5.5, and CD206-FITC.

Results – Only TAA significantly reduced the gene expression of pro-inflammatory cytokines *TNFA*, *IL1B,* and *IL6* in IPFP explants and increased the expression *IL10*, *CD206* and *CD163* as markers for anti-inflammatory processes (Figure 1). We therefore continued with TAA to examine whether TAA indeed modulates the phenotype of the macrophages residing in the IPFP. Only the low dose of TAA decreased the percentage of CD80+/CD14+ and CD86+/CD14+ cells (regarded as pro-inflammatory macrophages, figure 2 upper panel). TAA in both concentrations increased the percentages of CD163+/CD14+ cells. Only with the high concentration of TAA, the percentage of CD206+/CD14+ within the IPFP increased (regarded as anti-inflammatory macrophages, figure 2 lower panel).

Discussion and Conclusion - IPFP can become inflamed and secrete factors that influence the joint environment. Based on gene expression, TAA seems to decrease general IPFP inflammation, whereas celecoxib, pravastatin and fenofibrate had a less clear anti-inflammatory effect on IPFP. In conclusion, our data indicate that TAA can be used to specifically reduce IPFP inflammation through modulation of the pro-inflammatory macrophages residing in IPFP to an anti-inflammatory state. This might eventually improve the joint environment for better cartilage repair.

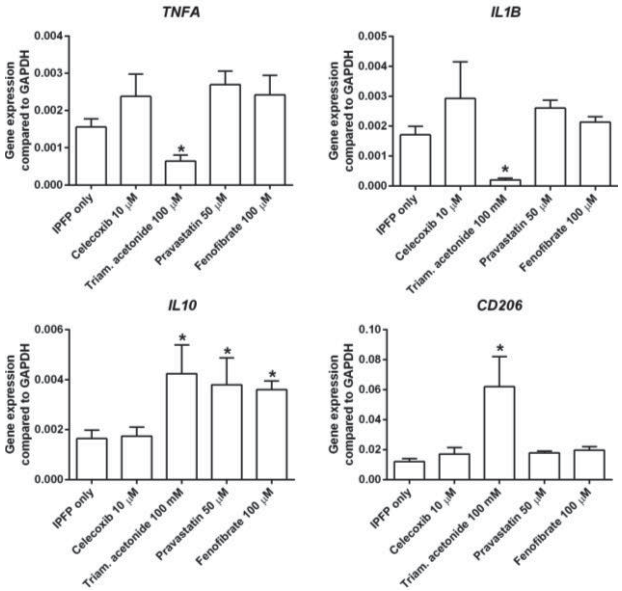

*Figure 1: Relative gene expression of from 3 donors with 2 samples per donor (n=6). Values are mean ± SD. *P<0.05 versus non treated IPFP only condition.*

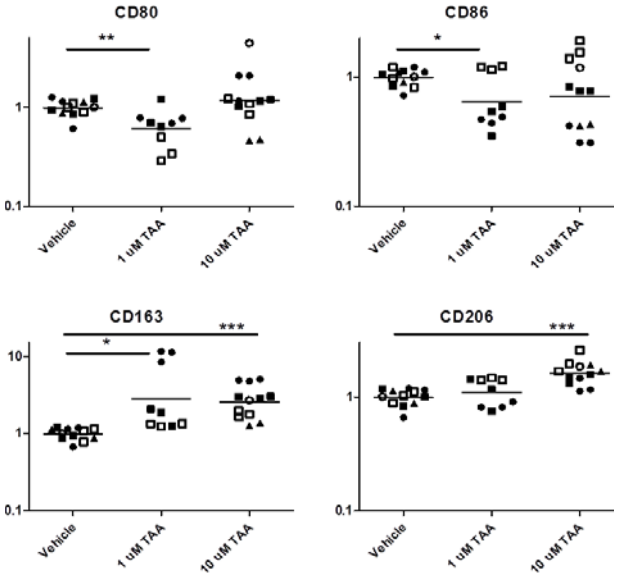

*Figure 2: . Effect of TAA treatment on presence of pro-inflammatory (upper panels) and anti-inflammatory (lower panels) surface markers among CD14+ macrophages. Percentages of cells that are positive for marker are normalized to their respective control samples . P < 0.001; *** P < 0.05; ** = P < 0.01; **

Reference -

1. Wei W. et al. 2015

Amyloid Micronetworks for Cartilage Tissue Engineering

M.C.E. van Dalen[1,2], M. Karperien[2], J.N. Post[2], M.M.A.E. Claessens[1]
1. MESA+, PO Box 217, 7500 AE, Enschede, the Netherlands
2. MIRA, PO Box 217, 7500 AE, Enschede, the Netherlands

Introduction

Most people obtain some degree of articular cartilage damage. As a result of the low self-repair capacity of cartilage, more than 1 out of 4 people suffer from osteoarthritis. Current clinical tissue engineering-based treatments results in tissue that is often the wrong type of cartilage, does not fully fill the defect, and that poorly integrates with native tissue. By using a scaffold that mimics the extracellular matrix (ECM) of articular cartilage, cells experience a more relevant local environment leading to healthy cartilage formation.

Cartilage tissue consists of collagen bundles providing tensile strength and proteoglycans that form a hydrogel-like structure resisting compression. A scaffold for cartilage tissue engineering should mimic the properties of these components to provide native cues to the cells.

In this work we propose the use of amyloid micronetworks (AMN) as a cartilage ECM mimicking scaffold. Amyloid fibrils are polypeptide based and self-assembled structures with a high occurrence in nature. The fibrils consist of proteins coupled by inter-protein β-sheets and have diameters up to 15 nanometres and lengths of a few micrometres. Amyloid fibrils have a Young's modulus comparable to collagen and can self-assemble into AMN that resemble hydrogels. Therefore, we hypothesized that AMN are a scaffold material for cartilage tissue engineering.

Amyloid micronetwork self-assembly

Briefly, self-assembly of the similarly sized but differently charged proteins α-synuclein (αS, -), β-lactoglobulin (βLG, -) and lysozyme (LZ, +) was induced by incubation at defined pH, temperature and salt concentration. The self-assembly into AMN was confirmed by the amyloid binding fluorescent dye Thioflavin T, atomic force microscopy, CD-spectroscopy, and electron microscopy, all confirming successful self-assembly of the proteins into AMN.

Amyloid micronetworks alter chondrocyte response

Maintaining chondrocyte viability is key to ensure ECM formation over time. Bovine chondrocytes were cultured in a monolayer with proliferation medium containing the different AMN. After 3 days, Calcein AM staining was used in combination with flow-cytometry to show that AMN did not alter the fraction of cells with intact membranes. However, the bulk metabolic activity of the cells, determined by the MTT assay, was lowered to 60% in the presence of αS and βLG AMN, and to 25% with LZ AMN present.

Chondrocytes are metabolic inactive cells and therefore the chondrocyte phenotype might be better persevered in the presence of LZ AMN. This was confirmed by studying changes in cartilage marker gene expression levels by qPCR. Cartilage ECM related genes ACAN (proteoglycan) and COL2A1 (collagen) were significantly upregulated in the presence of LZ AMN, while MMP1 and MMP3 (collagenases) were upregulated in presence of αS or βLG AMN.

Lysozyme micronetworks increase matrix formation

To investigate the long-term effects of AMN on chondrocytes and cartilage ECM formation, chondrocytes were mixed with different AMN and cultured in proliferation medium for 5 weeks in 3D. Afterwards, nuclei and sulphated glycosaminoglycans (part of proteoglycan) were stained. Intact nuclei were observed in all samples, suggesting that chondrocytes remained viable after prolonged exposure to AMN. αS and βLG AMN decreased the overall glycosaminoglycan content, while LZ AMN increased this content as compared to the agarose control.

Collagen production was visualized with electron microscopy. LZ AMN allowed the formation of collagen bundles with characteristic D-banding (Figure 1). However, αS and βLG AMN, and to some extent agarose samples, showed twisted bundles without D-banding. Apparently, collagen bundle formation is hampered in presence of the AMN. qPCR analyses support the histological findings: ECM formation related genes are significantly upregulated in the presence of LZ AMN while overall collagenase expression was not significantly altered after 5 weeks.

Conclusion

We show that AMN can be used as scaffold material for cartilage tissue engineering. Interestingly, despite the similar secondary structure of the proteins in the fibrils and comparable morphology of the AMN, the differences are determined by the protein used to form the AMN. In addition, we provide evidence that LZ AMN might be chondroinductive. Possibly, the net charge of the proteins influences this observation, since only LZ has a positive net charge. Therefore, by choosing or designing the self-assembling polypeptide, increased tissue formation could be induced for cartilage tissue engineering with AMN.

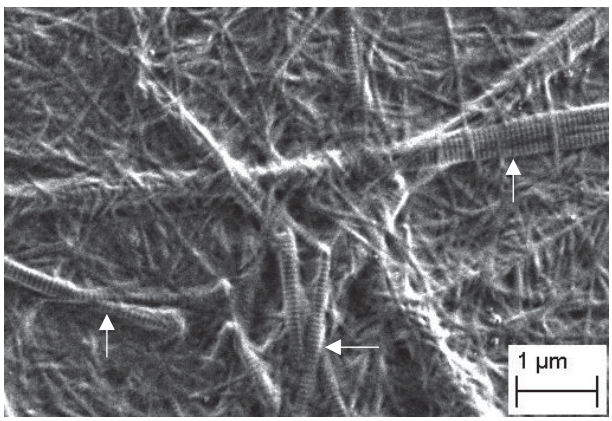

Figure 1: Electron microscopy image of collagen bundles (arrows) between LZ amyloid fibrils after 5 weeks of culture.

BioAirbrush: Arthroscopic airbrush technology for cell-based treatment of knee cartilage defects – a pre-clinical *in vitro* study

K Dijkstra, D.B.F. Saris, L.A. Vonk
UMC Utrecht, dept. of Orthopedics, PO Box 85500, 3508 GA, Utrecht, The Netherlands
k.dijkstra-4@umcutrecht.nl

Introduction

Recent research has shown the feasibility of arthroscopic airbrush assisted filling of cartilage defects using fibrin glue [1]. However, currently available fibrin spray device-nozzles need to be optimized for arthroscopic use. Current changes include internal to external mixing to prevent fibrin clogging and developing a 45-degree tip for increased arthroscopic maneuverability. Our work aims at (I) optimizing current technology with the design of custom-made spray nozzles and (II) at investigating cell viability after spraying at varying pressures and nozzle-substrate distances.

Materials & Methods

Custom-made spray nozzles were designed with 3D CAD software and produced by high-resolution 3D printing (fig 1). Two commercially available fibrin spray devices using an internal mixing nozzle (Baxter® DuploSpray, for endoscopic use), and external mixing nozzle (Baxter® EasySpray, for topical use only) were used as a comparison. To study the influence of the spraying pressure on cell viability, human chondrocytes, human MSCs, and immortalized MSCs were sprayed *in vitro* in culture medium under increasing pressure ranging from 0 to 1.5 bar, from a distance of 1.5 cm. This distance was varied to study the influence of nozzle-substrate distance. Cell viability was determined after 24 hrs (AlamarBlue) and normalized to the DNA content (PicoGreen). To evaluate the homogeneity of the mixing of the fibrin glue components with the BioAirbrush nozzle, blue and yellow microparticles were added to the fibrinogen and the thrombin component, respectively. A 250µl fibrin gel was sprayed onto a glass slide and visualized under microsopy to evaluate mixing.

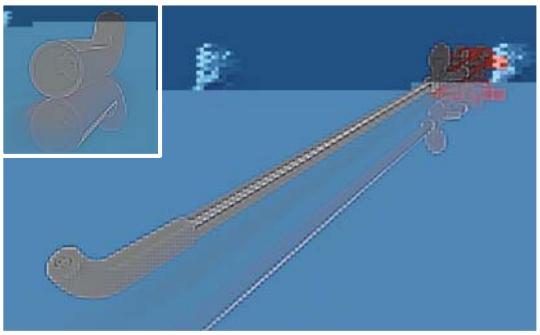

Figure 1: Design of the custom-made BioAirbrush nozzle

Results & Discussion

Spraying under increasing air pressure (0-1.5 bar) with an internal mixing nozzle (DuploSpray) had a highly destructive effect on cell viability (<20% viability at 1.0 bar) (fig.2A), while an external mixing nozzle (EasySpray) had a limited effect on cell viability (>90% viability at 1.0 bar) (fig.2B). Using custom-made external mixing nozzles for the endoscopic DuploSpray system, the destructive effect of increasing air pressure on cell viability of hMSCs, iMSCs and chondrocytes was not statistically significant for pressures up to 1.0 bar (>90% viability) (fig.3). The nozzle-substrate distance was shown to have only a minor effect at a short distance of 5 mm. Additionally, it was shown that homogenous mixing of the fibrin glue components was achieved using the newly developed system.

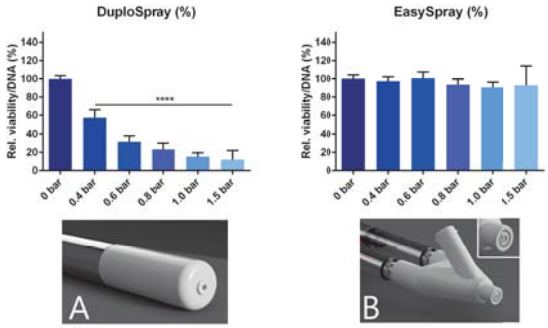

Figure 2: Relative viability 24h after spraying, normalized to DNA content

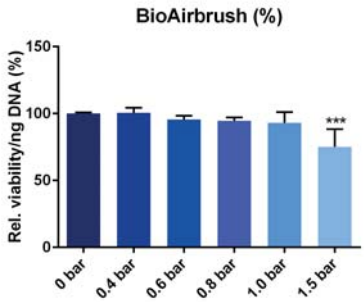

Figure 3: Relative viability 24h after spraying, normalized to DNA content. Custom-made BioAirbrush nozzle

Conclusion

The current commercially available spray nozzles are not applicable for arthroscopic cell spraying due to their design or influence on cell viability. However, modification of this technology with 3D-printed custom-made nozzles enabled cell spraying at a short distance without significantly affecting cell viability. This provides an easy-to-use technology for arthroscopic application of (cell-laden) hydrogels as well as a useful tool that can potentially be used in tissue engineering.

References

[1] T. S. de Windt et al, "Arthroscopic airbrush assisted cell implantation for cartilage repair in the knee: a controlled laboratory and human cadaveric study.," *Osteoarthritis Cartilage*, vol. 23, no. 1, pp. 143–50, Jan. 2015

In vivo performance of a bilayered supramolecular scaffold for in situ vascular tissue engineering

R. Duijvelshoff[1,2], A. di Luca[1], S. Dekker[1], S.H.M. Söntjens[3], H.M. Janssen[3], P.Y.W. Dankers[1,2], C.V.C. Bouten[1,2]

1. Eindhoven University of Technology, Department of Biomedical Engineering, PO Box 513, 5600 MB Eindhoven, The Netherlands
2. Institute for Complex Molecular Systems (ICMS), PO Box 513, 5600 MB Eindhoven, The Netherlands
3. SyMO-Chem BV, Eindhoven, The Netherlands

Introduction

In situ vascular tissue engineering (TE) holds great potential as an alternative for current small-diameter vascular replacement therapies, which often fail as a consequence of thrombosis and stenosis. This in situ TE approach aims to induce endogenous regeneration directly at the site of implantation using biodegradable synthetic scaffolds [1,2]. Here, we present a small-diameter, biodegradable, bilayered tubular scaffold based on a supramolecular elastomer. Scaffolds consisted of a porous inner layer to allow cellular infiltration from the bloodstream, and a dense outer layer to restrict transmural ingrowth from the adjacent tissues. Scaffolds were evaluated in vivo for arterial remodeling during 5 months in a rat model.

Materials and Methods

Tubular bilayered scaffolds (inner diameter 1.5 mm) were obtained by electrospinning of the supramolecular elastomer. Scaffold morphology and mechanical properties were characterized in vitro by scanning electron microscopy (SEM) and equibiaxial tensile tests. The scaffolds were then implanted in 20 healthy male Lewis rats as an interposition graft into the abdominal aorta. Grafts were explanted after 1 month (n=6), 3 months (n=7), and 5 months (n=7) for histological assessments and SEM.

Preliminary results

Electrospinning resulted in tubular bilayered scaffolds, with a porous inner layer (wall thickness 270 ± 17 µm) and a dense outer layer (wall thickness 85 ± 26µm) (Fig. 1). Equibiaxial tensile tests were performed to obtain the elastic modulus. This resulted in an elastic modulus of 2.63 ± 0.43 MPa in the longitudinal direction, and an elastic modulus of 1.96 ± 0.27 MPa in the circumferential direction (Fig. 2).

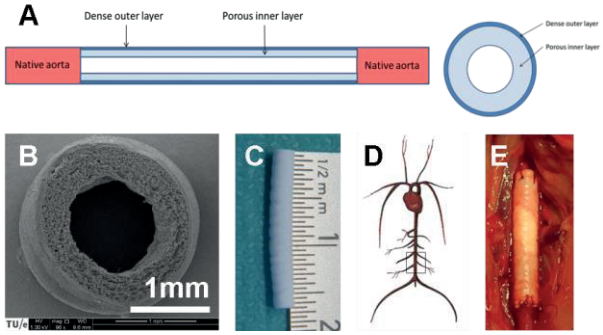

Fig. 1: Bilayered scaffold composition and study design
(A) Schematic overview of the bilayered tubular scaffold, (B) SEM image of a cross-section of the scaffold, (C) Scaffold prior to implantation, (D) Schematic representation of the implantation site (infrarenal abdominal aorta of male Lewis rats), (E) Scaffold in situ.

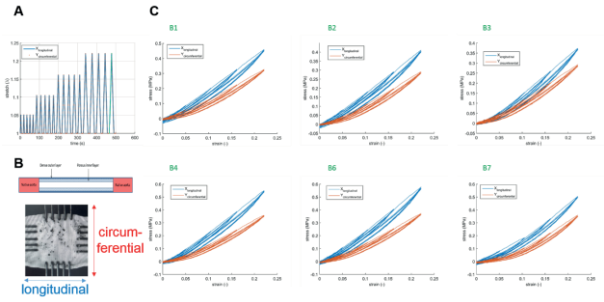

Fig. 2: Equibiaxial tensile tests of bilayered scaffolds (n=6)
(A) Displacement controlled testing protocol, (B) Schematic representation of the scaffold and image of a scaffold during the equibiaxial tensile test, (C) Engineering stress-strain curves of the individual scaffolds (n=6).

Grafts were explanted after 1, 3, and 5 months. All grafts remained patent with no signs of occlusion. However, most grafts demonstrated aneurysmal changes, ranging from saccular to fusiform. Histological analyses further revealed the local presence of calcium (Fig. 3). Histologically and by SEM, only in 1-month explants scaffold could be observed.

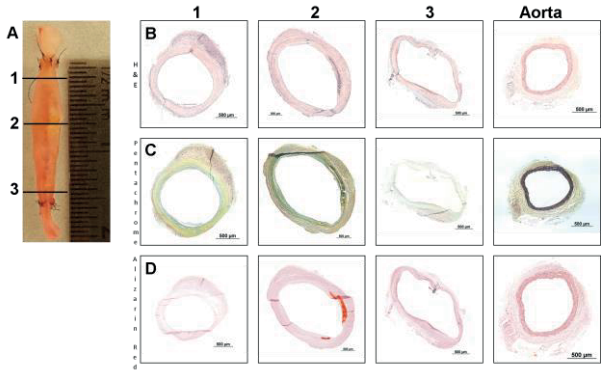

Fig. 3: Gross morphology of a 5-month explant
(A) Macroscopic view of a 5-month explant and schematic overview of the proximal (1), center (2), and distal (3) transection of the explant, (B) Weigert's Hematoxylin and Eosin staining, (C) Pentachrome staining, and (D) Alizarin red staining of cross-sections of the explant (position 1, 2, 3) and native aorta. Scale bars: 500 µm.

Conclusion

In this in vivo study, we have evaluated the remodeling of a bilayered supramolecular scaffold. The results of the study reveal major aneurysmal changes with a large interindividual variation, possibly related to fast scaffold degradation. Further analyses of the explants are currently performed to identify possible causes of the aneurysm formation in order to optimize scaffold designs for next generation scaffolds for in situ vascular TE.

The authors would like to acknowledge EE van Haaften for her assistance with the equibiaxial tensile tests

References

1. Bouten CVC *et al.* Adv Drug Del Rev. 2011; 63: 221-241.
2. Rocco KA *et al.* Tissue Eng Part B Rev. 2014; 20: 628-640.

Supramolecular polymer based living membrane for kidney tissue mimics

R.C. van Gaal[1,2], M. Fedecostante[4], R. Masereeuw[4] P.Y.W. Dankers[1,2,3]

1 Laboratory for Cell and Tissue Engineering, Department of Biomedical Engineering, Eindhoven University of Technology, PO Box 513, 5600 MB Eindhoven, The Netherlands
2 Institute for Complex Molecular Systems, Eindhoven University of Technology, PO Box 513, 5600 MB Eindhoven, The Netherlands
3 Laboratory of Chemical Biology, Department of Biomedical Engineering, Eindhoven University of Technology, PO Box 513, 5600 MB Eindhoven, The Netherlands
4 Division of Pharmacology, Utrecht Institute for Pharmaceutical Sciences, Universiteitsweg 99, 3584 CG Utrecht, The Netherlands.

Introduction

Currently, there is a strong need for systems that mimic kidney tissue for disease modelling, nephrotoxicity assessment of drugs, and renal replacement therapies. To mimic kidney function renal proximal tubule epithelial cells (RPTEC) are essential, as they are responsible for fine tuning the urine through active handling of nutrients, drugs, and toxins. Important is that the employed culture substrate has the capacity to induce long-term functional tight monolayer formation of RPTEC. This is currently achieved by coating polyethersulfone (PES) membranes with L-3,4-dihydroxyphenylalanine (L-DOPA) and collagen type IV.[1,2] PES membranes lack easy adaptability of mechanical properties and convenient bio-functionalization. Therefore, we propose to use supramolecular polymers and bioactive groups based on ureido-pyrimidinone (UPy) moieties. These moieties self-assemble via hydrogen bond arrays and allow for the creation of a large modular toolbox for material design.[3,4] Here, we propose a membrane based on UPy-functionalized polycaprolactone (PCLdiUPy) and UPy-modified DOPA (UPyDOPA) to substitute L-DOPA coating and to induce a long-term functional monolayer of RPTECs.

Materials and Methods

Membranes were electrospun composed of either PCLdiUPy, or a blend of PCLdiUPy + 10 mol% UPyDOPA. Membranes were subjected to hydrophobicity measurements, scanning electron microscopy and qualitative analysis for DOPA moieties. Conditionally immortalized proximal tubule epithelial cells (ciPTEC) were cultured on membranes with several coating strategies (pristine, Col IV or L-DOPA/Col IV) for 7days. Cells were stained with relevant markers to assess monolayer formation. Monolayer tightness was investigated through the potential of the cell layer to block diffusion of inulin-FITC.

Results and Discussion

Membranes were successfully spun with a fiber diameter of around 1 µm to prevent cellular infiltration (PCLdiUPy 0.9±0.3µm and PCLdiUPy + UPyDOPA 0.8±0.2µm). Incorporation of UPyDOPA drastically reduced the hydrophobicity of the membranes, and resulted in a strong positive signal in a qualitative assay for DOPA moieties. Taken together these results indicated that DOPA moieties are presented at the surface of the fibers. L-DOPA was insufficiently substituted by UPyDOPA to aid in the formation of a long-term ciPTEC monolayer. However, cell morphology hints to a synergistic effect of UPyDOPA and L-DOPA/Col IV coating on monolayer induction. Diffusion was severely impeded by the membranes alone. It is likely that the cellular contribution in diffusion blockage is undetectable.

Conclusions

Here, we present a membrane based on PCLdiUPy and UPyDOPA that shows potential in monolayer induction of RPTECs, an essential step forward to the creation of kidney tissue mimics. Future work will focus on monolayer functionality, new membrane fabrication techniques, and applying the membranes to natural flow conditions for further tissue mimicry.

References

1 Oo Z.Y. *et al.* Biomaterials 2011
2 Jansen J. *et al.* Scientific Reports 2015
3 Mollet B.B. *et al.* Journal of Materials Chemistry B 2014
4 Dankers P.Y.W. *et al.* Nat Mater *2005*

Development of New Strategies for the Removal of Urea from the Dialysate

I. Geremia, D. Stamatialis
i.geremia@utwente.nl

Department of Biomaterials Science and Technology, MIRA Institute, Faculty of Science and Technology, University of Twente, Enschede, The Netherlands

Introduction. Hemodialysis is a life-saving therapy, which however has quite high environmental impact. More than one hundred liters of ultra-pure water are used per session per patient and every session has to be performed usually three times per week. The environmental reasons, as well as the advantages of having continuous patient treatment, stimulated research towards development of portable or wearable artificial kidney systems with the regeneration of the dialysate. In this work we focus on two strategies for the removal of urea from the dialysate (Fig.1): urea adsorption using mixed matrix membranes (MMMs) where sorbent particles are incorporated into membrane matrix and rejection of ammonium ions obtained by the enzymatic degradation of urea using nanofiltration membranes.

Methods. Flat sheet MMMs were prepared via phase inversion by casting polyethylene vinyl alcohol polymer solution containing functionalized chitosan beads. Membrane morphology was characterized via scanning electron microscopy and adsorption of urea to the beads was investigated via the detection of ammonium ions obtained by the hydrolysis of urea using urease.

Polyetherimide nanofiltration hollow fibers (HFs) were produced via wet-dry spinning and positive charges were introduced by crosslinking the membrane forming polymer with polyethylenimine simultaneously to the HFs production. The morphology of the positively-charged HFs was characterized via scanning electron microscopy, FTIR and zeta potential measurement. Their performance was studied via ammonium ions retentions and water permeability experiments.

Results and discussion. The beads are very well distributed in the MMMs (Fig.2). Their embedding to the membrane prevents their aggregation and decreases the pressure drop which is a typical problem of columns with beads. Comparison of urea adsorption isotherms for beads alone and for the MMMs indicates that the accessibility of the beads in the MMMs is very good. Moreover, new studies of urea adsorption on mesoporous silica show promising results which open room for a new class of MMMs forming materials.

The positively-charged nanofiltration HFs here produced via "chemistry in the spinneret" method (Fig. 3) show a well-defined finger-like macrovoids structure with a dense inner layer obtained by the crosslinking of the two components (Fig. 3). The HFs so obtained have a water permeability in the nanofiltration range and are able to reject more than 50% of ammonium ions in solution.

Conclusions. New MMMs for urea sorption for dialysate regeneration were developed. In the future, efforts will focus on the optimization of the membrane transport properties, increase of the sorption capacity and possible upscaling. Mesoporous silica particles will be embedded in MMMs and their urea adsorption capacity will be tested. Positively charged nanofiltration HFs have shown promising ammonium ions retention results and future works will be dedicated to their optimization.

Acknowledgment. This work is financially supported by EU Marie Curie ITN-TheLink (grant agreement no. 642890).

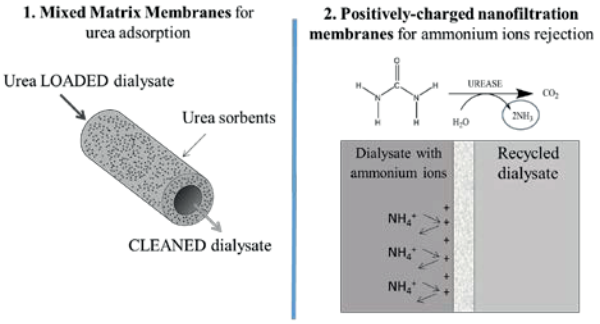

Figure 1. Scheme of the two strategies for urea removal from spent dialysate studied in this work.

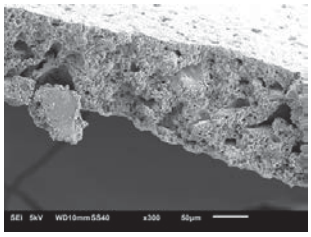

Figure 2. SEM image of MMM's cross section.

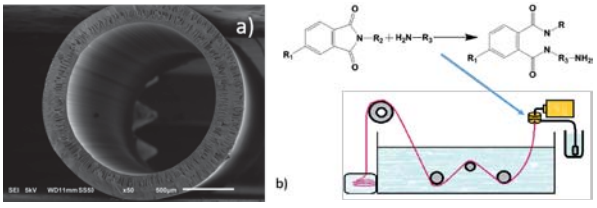

Figure 3. a) SEM image of nanofiltration HF's cross section; b) Scheme of "chemistry in the spinneret" for the crosslinking of polyetherimide with polyethylenimine.

MELT PROCESSABLE POLYMERIC COMPOSITES FOR ADDITIVE MANUFACTURING BASED ON EXTRUSION

A. Guney1, J. Malda2,3, W.J.A. Dhert2,3 and D.W. Grijpma1,4
1Dept. of Biomaterials Science and Technology, University of Twente, 7522 LG Enschede, The Netherlands,
2Dept. of Orthopaedics, University Medical Center Utrecht, 3584 CX Utrecht, The Netherlands
3Faculty of Veterinary Sciences, University of Utrecht, 3584 CM Utrecht, The Netherlands,
4Dept. of Biomedical Engineering, University Medical Center Groningen, 7600 AD Groningen, The Netherlands,
a.guney@utwente.nl, j.malda@uu.nl, w.dhert@uu.nl, d.w.grijpma@utwente.nl

Introduction.

3D biomaterial printing has great potential in biomedical applications [1]. Additive manufacturing based on extrusion processing of a thermoplastic polymer is of great interest in preparing designed scaffolds for tissue engineering applications [2]. However, the number of thermoplastic materials available for extrusion is very limited [3]. This research is focused on the development of new polymeric materials and their composites for additive manufacturing based on extrusion processing.

Methods.

Synthesis of PCL-b-PTMC-b-PCL

Biodegradable thermoplastic elastomers were synthesized from trimethylene carbonate (TMC) and ε-caprolactone (CL) using 2,2-dimethyl 1,3-propanediol as initiator and diphenyl phosphate as catalyst. A dihydroxy group-terminated PTMC oligomer was first prepared by ring opening polymerization under argon atmosphere for 72 h at 70°C. Subsequently, this PTMC oligomer was used to initiate the ROP of ε-CL. This reaction was let to proceed for another 24 h under the same conditions, leading to the formation of a PCL-*b*-PTMC-*b*-PCL triblock copolymer. Here we prepared high molecular weight PCL_{26}-*b*-$PTMC_{50}$-*b*-PCL_{26} (P), which corresponds to a molecular weight of around 102 kg/mol. Also, the solution of the copolymer and two different weight to weight ratios of nano-hydroxyapatite (n-HA) (app. 300x35 nm^2) were used to prepare non-porous composite films by casting on glass plates. P to HA ratio were 100:20, 80:20 and 60:20. The thermal properties of the composite materials were evaluated using differential scanning calorimetry. The tensile properties of films with varying HA contents was assessed.

3D printing of PCL-b-PTMC-b-PCL triblock copolymers

The mixture of PCL-*b*-PTMC-*b*-PCL and nano-hydroxyapatite *(40 wt.%)* were prepared. By dissolving polymers in ethylene carbonate at elevated temperatures and subsequently cooling down to (-20°C) to below its melting temperature, porous polymeric structures can be obtained after extraction with water. The solution was printed using a BioBots (USA) apparatus at 60°C and 145kPa on glass.

Results.

Reinforcement of the polymer matrix with HA resulted in decreased melting temperatures. Moreover, increased HA contents in the films lead to increased tensile modulus and toughness, and decreased elongations at break. Following the investigation of the thermal and mechanical properties, we prepared polymeric composites for extrusion.

Table 1: Thermal properties of P0, P20 and P40 dissolved in EC

P/HA (w/w)	Tg_1 (°C)	Tg_2 (°C)	T_c (°C)	T_m (°C)	Td_1 (°C)	Td_2 (°C)
100/0	-57.8	-19.4	-9	42	350	433
80/20	-60.1	-19.2	-10	34	325	412
60/40	-58.3	-20.3	-20	32	323	410

Table 2. Tensile properties of P0, P20 and P40 (of non-porous films)

P/HA (w/w)	E (MPa)	σ_{yield} (MPa)	ε_{yield} (%)	ε_{break} (%)	Toughness (N/mm^2)
100/0	142±19	6±1	4±1	826±34	476±95
80/20	179±16	6±1	3±1	510±27	585±157
60/40	243±10	7±1	3±1	445±12	589±133

Porous scaffolds were obtained by printing successive layers of polymeric (composite) strands.

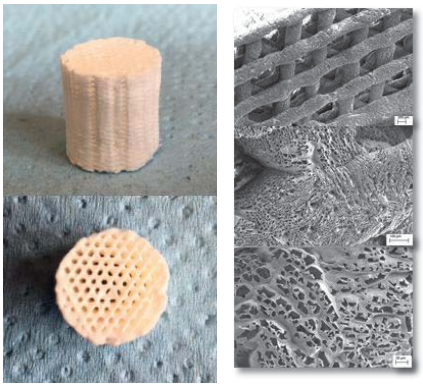

Figure 1. PCL_{26}-*b*-$PTMC_{50}$-*b*-PCL_{26} with nano-hydroxyapatite (40 wt.%)

Conclusions.

Using low melting ethylene carbonate as a crystallizable solvent, tissue engineering scaffolds with a macro- and microporous porosity could readily be prepared by 3D printing. These triblock copolymers and composites may find wide in tissue engineering.

Acknowledgements.

Foryou Medical Devices provided TMC, XPand Biotechnology provide

An in-vitro platform to culture vascular grafts under combined shear stress and circumferential stretch

E.E. van Haaften[a], M.C.M. Rutten[b], J.A. Bulsink[b], A.I.P.M. Smits[a], N.A. Kurniawan[a], C.V.C. Bouten[a]

Eindhoven University of Technology, [a]Soft Tissue Biomechanics and Tissue Engineering, [b]Cardiovascular Biomechanics, Eindhoven, The Netherlands

Introduction: The leading cause of vascular access dysfunction in hemodialysis patients is the occlusion of the graft due to thrombosis. *In-situ* tissue-engineered vascular access grafts are envisioned to improve primary maturation rates and long-term functionality. Bio-functionalization, structural organization, and degradation rate are thought to be important parameters in the design of instructive scaffolds for *in-situ* vascular tissue engineering. The relevance of these design parameters is ideally tested *in-vitro* under hemodynamic conditions to make a better translation to the *in-vivo* situation. This study presents the design and validation of a mesofluidics-based *in-vitro* platform that allows for independent control of circumferential stretch and fluid shear stress in a 3D tubular scaffold. This platform enables systematic assessment of the impact of hemodynamic conditions on cell-produced matrix and mechanical properties of developing vascular constructs.

Materials and Methods: The test platform consists of a custom-made tubular 3D scaffold culture chamber (Figure 1). The scaffolds, centered in a glass tube, are pressurized from the inside, generating circumferential stretch, and perfused through the annular gap between the scaffold and glass wall, generating wall shear stress (WSS). Using this approach, circumferential stretch (0-10%, 1Hz) and WSS (0-5Pa) can be controlled independently. The system has been validated numerically and experimentally. As a proof-of-concept, tubular polycarbonate bisurea (PC-BU) scaffolds (ø3mm) will be seeded with human vena saphena cells (HVSCs) and exposed to four types of mechanical loading during 7 days: (1) static culture, (2) circumferential stretching only, (3) perfusion at predefined WSS only, and (4) circumferential stretching and perfusion combined. Collagen architecture and cellular infiltration will be assessed using confocal laser scanning microscopy.

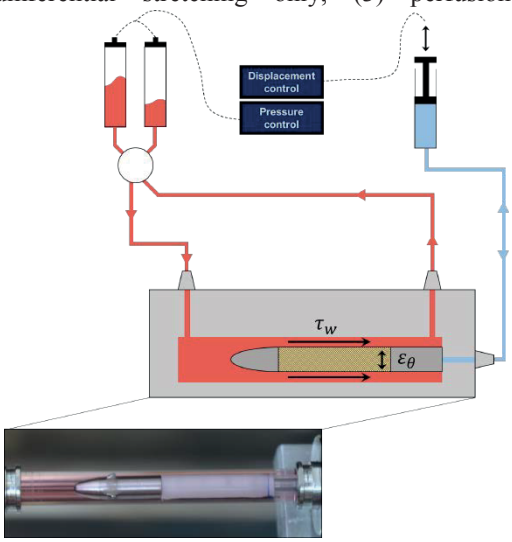

Fig. 1: Schematic of the main components of the bioreactor system. Flow rate is controlled by a pressure pump generating shear stress (τ_w) at the outer surface of the scaffold. Circumferential stretch (ε_θ) is controlled by volume displacements using a linear motor.

Results and Discussion: To minimize flow disturbance due to changing channel dimensions as a result of stretch, the length of the graft and the slit height between the scaffold and glass wall were optimized (Figure 2).

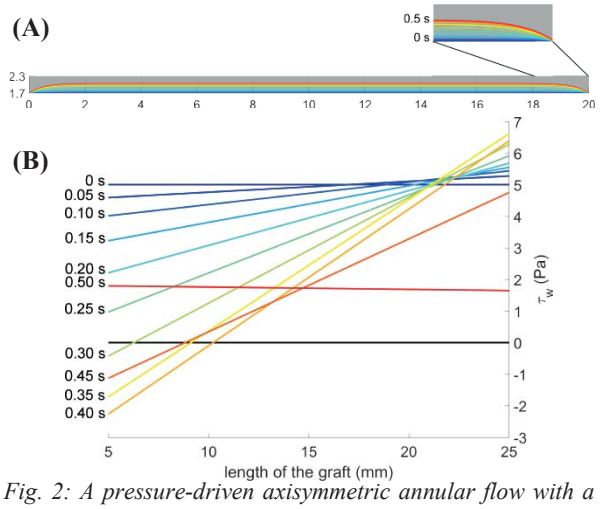

*Fig. 2: A pressure-driven axisymmetric annular flow with a 1Hz sinusoidal moving membrane (20% stretch) **(A)** shows temporally and spatially inhomogeneous WSS **(B)**. The simulation results were used to tune the graft length and slit height towards more homogenized loads.*

With the optimized channel dimensions, the flow could be successfully controlled during a 7-day culture experiment (WSS 1.6Pa, 80mmHg). Preliminary experiments showed that perfusion alone resulted in a preferential direction of collagen matrix deposition in the flow direction (Figure 3, indicated with arrow).

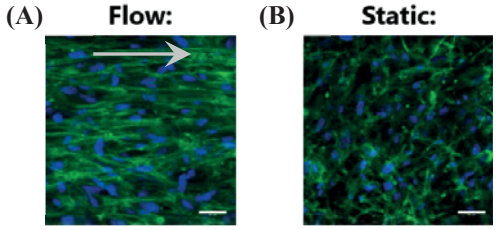

*Fig. 3: Collagen (green) and nuclei (blue) in an isotropic scaffold after 7 days of perfusion **(A)** and static culture **(B)**. Arrow indicates flow direction, bar = 50µm.*

Current work is directed to incorporating the straining device in the bioreactor system to evaluate the effect of mechanical stretch on tissue maturation.

Conclusion: A mesofluidics-based platform was developed to study cell–scaffold interactions under hemodynamic conditions. This platform will be used for culturing and testing vascular (access) graft.

Development of a One-Stage Cell Therapy for Meniscus Regeneration Using a Combination of Meniscus Cells, Mesenchymal Stromal Cells and the Collagen Meniscus Implant®

M.H. Hagmeijer[1], D.F.B. Saris[1,2], L.A. Vonk[1]
[1]University Medical Center Utrecht, [2]MIRA institute, University of Twente, Enschede, The Netherlands

INTRODUCTION: Damage to the meniscus is a very common intra-articular knee injury in young active patients. Since meniscus tissue has a very limited healing capacity, surgical treatment is often directed towards removal of the damaged tissue (partial or subtotal meniscectomy), frequently causing early osteoarthritis. To overcome this, the Collagen Meniscus Implant (CMI®) is already used in clinics, providing an environment for ingrowth of cells and tissue formation while the biomaterial is slowly degraded. However, this is a slow process and could be accelerated using a cell-based treatment. Therefore, the aim of this study was to investigate the feasibility of a one-stage cell-based treatment for meniscus regeneration by augmenting the CMI with a combination of meniscus cells and mesenchymal stromal cells (MSCs). A cell combination of autologous recycled cartilage cells and allogeneic MSCs has been shown safe and feasible for one-step cartilage repair.

METHODS: Human meniscus cells isolated from meniscus tissue of patients receiving a total knee replacement and bone marrow derived MSCs were cultured in different ratios in cell pellets and type I collagen hydrogels (n=6 donors). The same cell types (n= 3 donors) were seeded in a 10:90 ratio (based on previous results of chondrocytes and MSCs) with 500.000 cells per 150mm^3 of CMI in fibrin glue. To mimic clinical circumstances of *ex vivo* pre-seeding and *in vivo* seeding during arthroscopy, dry CMIs and CMIs immersed in culture medium were used and seeded either statically or by injection. All cultures were harvested after 28 days and analyzed for glycosaminoglycan (GAG, by DMMB), DNA and total collagen (by HYP) content, histology (H&E and Safranin-O) and immunohistochemistry for type I and II collagen.

RESULTS: No significant differences were observed in GAG, DNA and collagen content between various ratios of meniscus cells to MSCs, but there was a trend that the contents of 20 : 80 ratio were more similar to cultures of meniscus cells alone in both pellets and collagen hydrogels (Fig. 1). Although no differences were found in GAG and DNA content between wet and dry seeded CMI's (Fig. 2), more homogenous cell distribution was found in dry seeded CMI's and the tissue that was produced consisted mainly of type I collagen with minimal deposition of type II collagen and proteoglycans (Fig. 3).

DISCUSSION: Seeding a CMI with a combination of meniscus cells and mesenchymal stromal cells leads to fibrocartilage-like tissue formation. Static seeding of a dry CMI appears to be the best method, resulting in a homogenous distribution of cells and neotissue. Ratios of 10 : 90 and 20 : 80 meniscus cells : MSCs are clinically feasible for one-stage procedures and perform as well as only meniscus cells. This translates to the clinic as seeding the CMI before arthroscopic implantation with cells (10-20% meniscus cells and 90-80% MSCs) in fibrin glue to retain the cells in the scaffold during implantation.

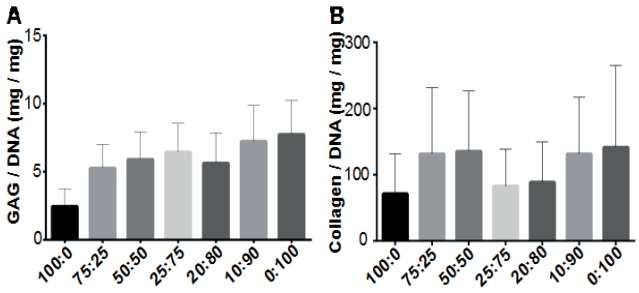

Figure 1: glycosaminoglycan (GAG, A) and collagen (B) content, both normalized for DNA content, of pellets containing various ratios of meniscus : mesenchymal stromal cells cultured for 28 days.

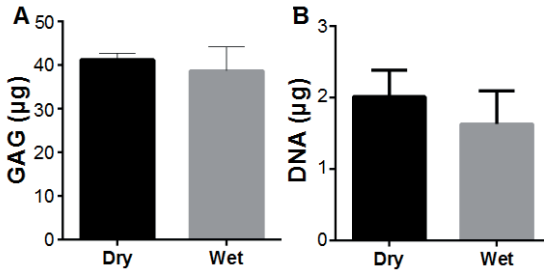

Figure 2: glycosaminoglycan (GAG, A) and DNA (B) content of dry and wet seeded Collagen Meniscus Implants with a combination of human meniscus and mesenchymal stromal cells (10 : 90) cultured for 28 days.

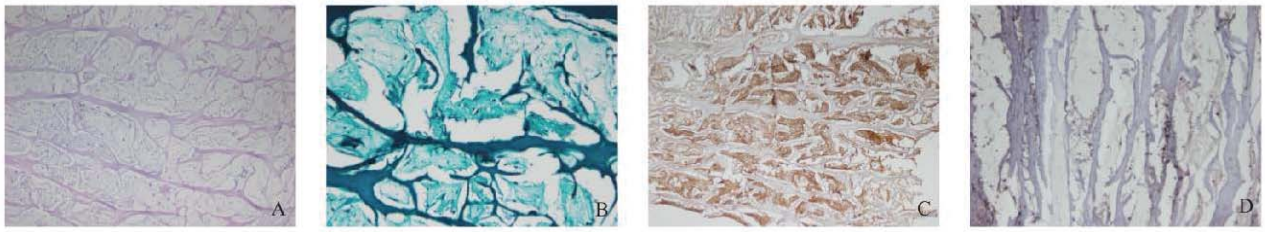

Figure 3: histological stainings (A: H&E magnification 40X, B: Safranin-O/Fast green, 100X) and immunohistochemistry for type I (C, 40X) and type II collagen (D, 100X) of dry seeded Collagen Meniscus Implants with a combination of human meniscus and mesenchymal stromal cells (10 : 90) cultured for 28 days.

Local Delivery of Triamcinolone Acetonide in an ACLT Model of Osteoarthritis Impairs Joint Regeneration, possibly by Inhibition of Wound Healing

Imke (I). Jansen[1], Anna Tellegen[2], Saskia Plomp[2], Julien Berard[4], Pieter Emans[5], Erin de Gendt[1], Rachel Thomas[3], Huub de Visser[1], Marja Kik[3], Guy Grinwis[3], George Mihov[4], Jens Thies[4], Nina Woike[4], Ken Messier[4], Björn Meij[2], Marianna Tryfonidou[2] and Laura Creemers[1]

[1]Department of Orthopedics, University Medical Center Utrecht, the Netherlands [2]Department of Clinical Sciences of Companion Animals and [3]Department of Pathobiology, Faculty of Veterinary Medicine, Utrecht University, The Netherlands [4]DSM Biomedical, Geleen, The Netherlands [5]Department of Orthopedics, Maastricht University Medical Center Utrecht, the Netherlands.

INTRODUCTION: Corticosteroids such as triamcinolone acetonide (TAA) are used to alleviate pain symptoms of osteoarthritic patients. Although usually pain relief is achieved, the effect wears off with time. The use of biomaterial-based local delivery systems would overcome this problem. However, little is known on the appropriate dosing of corticosteroids in the joint. In a previous study on collagenase-induced mild OA in the rat, a limited effect on cartilage degeneration was found of TAA, either as bolus or in a polyesteramide microsphere (PEAMs) controlled release platform system. In the current study, safety, effectivity and possible side effects of TAA locally delivered by the microsphere platform at different dosages was studied in an anterior cruciate ligament transection (ACLT) and partial meniscectomy (DMM) model of rat OA, which is a more severe OA model. As damage of ligamentous structures leading to instability is a contraindication for corticosteroid therapy, despite lack of clear evidence with this respect, this was further examined.

METHODS: The Utrecht University Ethical Committee for Animal Care and Use approved the study protocol (# 2014.III.10.086). OA was induced by transection of the anterior cruciate ligament and partial meniscectomy in 24 rats. Four weeks after surgery, the experimental joint was injected intra-articularly with PEAMs loaded with 0.70 mg, 1.0 mg or 1.6 mg TAA. Empty PEAMs were included as control, in addition to the contralateral healthy and untreated joints. PEAMs were administered by two injections on two consecutive days. Serum TAA levels were determined the first two weeks post-injection using HPLC analysis. Weekly pressure plate measurements were performed to monitor static weight bearing and thereby indirectly pain during a 16 week follow up. Post-mortem, histology (Mankin score) and microCT scans of all knee joints showed disease progression and possible effects on bone tissue. From healthy animals, patella, collateral and cruciate ligament explants were cultured in expansion medium consisting of DMEM (high glucose, GlutaMAX(TM), pyruvate) supplemented with 10% fetal bovine serum, 1% ascorbic acid 2-phosphate and 1% penicillin/streptomycin for 10 days with or without TAA (100 μM) added to the medium. After culture, the presence of fibroblasts migrating out of the tissue and adhering to the bottom of the culture dish was assessed. Differences in calcium deposition by microCT were evaluated by one-way analysis of variance (ANOVA). *In vitro* data on ligament cell outgrowth was categorized into ‘’migration/adherence’’ and ‘’no migration/adherence’’ and a Fisher’s Exact test was performed to evaluate significant differences in the migration/adherence of ligament fibroblasts in the presence or absence of TAA. $P<0.05$ was taken to indicate statistical significance.

RESULTS: Load bearing did not differ between the OA hind limb compared to the untreated limb in any of the treatments (n=6 per group), although degeneration was moderate (Mankin score 6). In the PEAM+TAA treated rats, serum TAA was undetectable 8 days after injection. MicroCT analysis revealed extensive dystrophic calcification in all TAA-treated knee joints (figure 1 and 2). Histopathological analysis of knee joints treated with TAA showed a significant increase in cartilage degeneration, reflected in a loss of tidemark, cartilage structure degeneration, and chondrocyte cell damage, with basal degeneration. No effects were found of empty microspheres. Cell outgrowth from ligaments was almost completely inhibited by TAA, independent of the ligament type studied (table 1).

DISCUSSION: Although moderate degeneration was induced, pain could not be detected in the ALCT OA model. Empty microspheres were found to be safe, but dystrophic calcification and destruction of the knee joint was observed with the TAA-loaded microspheres, independent of the dose. Ligament fibroblasts did not migrate out of cultured explants and adhere to the culture dish in the presence of TAA, indicating that TAA might impair wound healing processes in damaged joints thereby extending the instability of the joint. Controversy remains on the treatment of OA with corticosteroids, since both beneficial and adverse effects have been reported: dystrophic calcifications have also been reported in human patients. We hypothesize that in the present OA model, where joint instability is induced by transection of the cruciate ligaments and partial meniscectomy, the continuous presence of TAA impairs joint stabilization and tissue healing, thereby providing support for the notion that damage-induced instability of a joint is a contra-indication for corticosteroid treatment. Calcification may suggest inhibition of clearance of cell debris by immune cells, although corticosteroids have been suggested to directly induce calcification without alterations in osteogenic markers in MSCs (de Mos *et al.,* 2007). Future studies may show the effect of slow release of TAA at lower dosages and/or in different joint disease models. Effects on joint pain of local TAA delivery may be more appropriately studied by using models such as the peptidoglycan polysaccharide-induced pain model.

Tailoring Gelatin-Transglutaminase Hydrogels for Pre-Vascularized Bone Analogs

B.J. Klotz[1], M. Wright Clark[1], K.S. Lim[2], I. Pennings[1], T.B.F. Woodfield[2], J. Malda[3,4], A.J.W.P. Rosenberg[1], D. Gawlitta[1].

[1] Department of Oral and Maxillofacial Surgery & Special Dental Care, Regenerative Medicine Center Utrecht, Uppsalalaan 8, 3584CT, Utrecht, The Netherlands
[2] Department of Orthopaedic Surgery and Musculoskeletal Medicine, Christchurch Regenerative Medicine and Tissue Engineering (CReaTE) Group, University of Otago Christchurch, Christchurch 8011, New Zealand
[3] Department of Orthopaedics, Regenerative Medicine Center Utrecht, Uppsalalaan 8, 3584 CT, Utrecht, The Netherlands
[4] Department of Equine Sciences, Faculty of Veterinary Sciences, Utrecht University, Yalelaan 112, 3584 CM, Utrecht, The Netherlands

Introduction: In maxillofacial surgery, large bone defects are currently treated with autologous vascularized bone flaps. This strategy is associated with drawbacks, such as an additional operation procedure and limitations in quantity as well as quality of the harvested bone graft. Tissue engineering aims to fabricate bone analogs by designing hydrogels that mimic and support growth of bone tissue. During this process, nutrient and oxygen supply of the developing bone tissue needs to be ensured. Therefore, the engineering of bone tissue needs to be accompanied by vascularization strategies throughout the construct.
A challenge in engineering bone and capillaries in one construct is presented by the differences in matrix stiffness that are required. In the present approach a soft hydrogel, based on gelatin-transglutaminase (TG) is investigated to support capillary-like network formation. The aim of this study is to tailor gelatin-TG hydrogels for engineering prevascularized bone constructs. The strategy of this approach will be to guide osteogenic differentiation of mesenchymal stromal cells (MSCs) in a soft hydrogel by means of a co-culture with endothelial colony forming cells (ECFCs).

Materials and Methods: Gelatin hydrogels crosslinked by transglutaminase (TG) were characterized physico-mechanically. The gelatin concentration was varied from 3-6% (w/v) and the TG concentration from 0.75- 1.5% (w/v). Dynamic mechanical analysis (DMA) and rheology measurements were conducted to investigate the effect of gelatin concentration on hydrogel characteristics (E-modulus, point of gelation).
Biological compatibility of the crosslinking process was tested by live-dead staining one day after MSC encapsulation.
This study was based on a previously established co-culture model of MSCs and ECFCs (1). MSCs were derived from the iliac crest and ECFCs from human umbilical cord blood samples upon donor informed consent. MSCs and ECFCs were combined in a 4:1 ratio at a total of $6.25*10^6$ cells/ml in gelatin-TG hydrogels and cultured for 10 days under osteogenic culture conditions. In whole mount constructs, capillary-like structures were identified by CD31 immunohistochemical staining, network stabilizing cells by α-smooth muscle actin and as an early osteogenic marker expression of alkaline phosphatase (ALP) was assessed.

Results and Discussion: In this study, a gelatin-TG hydrogel system was characterized for engineering pre-vascularized bone tissue analogs. The cells' intrinsic abilities were used to assemble pre-vascular structures in an osteogenically differentiated construct.
Physico-chemical characterization showed that gelatin-TG hydrogel stiffness could be tuned from 2.93 ± 0.87 kPa to 31.28 ± 9.11 kPa when applying gelatin concentrations from 3 to 6% (n=2). The sol gel transition for 3.5% (w/v) gelatin occured after 13 minutes, whereas 5% (w/v) gelatin took 7 minutes, both with 1.25% TG (n=1).
To evaluate the suitability of this hydrogel system for cell culture, MSCs were encapsulated in 5% (w/v) gelatin hydrogels with TG concentrations of 1, 1.25 and 1.5% (w/v). Approximately 90% of the cells were viable one day post encapsulation (n=3). Consequently, MSC viability was high and independent of the TG concentration.
Three different gelatin concentrations were chosen to further select the most appropriate composition for pre-vascular network formation and cell distribution within the gel. To do so, 3.5% gelatin (4.2kPa), 4.5% (10.8kPa), and 5% (20.5kPa) were selected for MSC-ECFC co-culture. Results showed positive ALP expression and pre-vascular network formation (Figure 1) in all three hydrogel concentrations. However, pre-vascular networks were only able to assemble in 3D throughout the 3.5% gelatin-TG hydrogels. For this reason, 3.5% gelatin-TG hydrogels were chosen as the optimal hydrogel composition for further experiments.

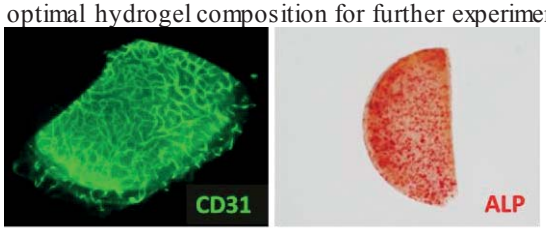

Figure 1. Pre-vascular network formation (CD31) and early osteogenesis (ALP) in gelatin-TG hydrogels (here 3.5%).

Conclusions: In the present study, gelatin-TG hydrogels were identified as a suitable matrix for engineering of pre-vascularized bone constructs. Low gelatin concentrations of 3.5% proved to be most promising in terms of cell distribution throughout the gel and vascular network formation. Future work will investigate additional stimulation of osteogenesis in these soft hydrogels to improve bone formation.

(1) Gawlitta D, Fledderus JO, van Rijen MHP, et al. Hypoxia Impedes Vasculogenesis of In Vitro Engineered Bone. Tissue Engineering Part A. 2012;18(1-2):208-218.

SINGLE-CHAIN NANOPARTICLES: A NEW CLASS OF DRUG CARRIERS

A.P.P. Kröger[a], R.J.E.A. Boonen[a] and J.M.J. Paulusse[a,b]
[a]Department of Biomaterials Science and Technology, MIRA Institute for Biomedical Technology and Technical Medicine, University of Twente, Enschede, the Netherlands; [b]Department of Nuclear Medicine and Molecular Imaging, University Medical Center Groningen, Groningen, the Netherlands
E-mail: piakroger@utwente.nl

Introduction

Due to their chemical diversity, polymeric nanoparticles have gained popularity in a multitude of medical applications, and importantly in drug delivery. Whereas large nanoparticles up to 200 nm display prolonged blood circulation times, small particles below 5 nm avoid accumulation in the body through renal excretion, thus circumventing the need for biodegradability.[1,2] Furthermore, smaller particles have shown enhanced penetration through dense tissues such as solid tumors.[3] The blood-brain barrier (BBB) is the tightest endothelium of the body, and drug carrier systems able to cross this barrier are essential for effective drug delivery, to treat diseases such as Alzheimer's disease. In particular, gold nanoparticles display a clear size dependence for BBB passing of nanoparticles. [4,5] Whereas the smallest gold nanoparticles of 10 nm have demonstrated the highest brain uptake, size investigations of polymeric nanoparticles are still pending.

Currently employed polymeric nanoparticles are typically in the size range of 20-100 nm.[6] In order to widen the range of existing polymeric drug carrier systems to the sub-20 nm size regime, *single-chain polymer nanoparticles* (SCNPs) are investigated here. SCNPs are prepared through intramolecular crosslinking of individual polymer chains into individual nanoparticles and thus offer tremendous control over size and dispersity. Through exclusively intramolecular crosslinks, SCNPs are a magnitude smaller than conventional polymer nanoparticles, without the requirement of complex synthetic strategies.

Results and Discussion

In this work, SCNPs were prepared via intramolecular crosslinking of vinyl polymers with bifunctional crosslinkers. To gain monodisperse and size-controlled precursors, the polymers were polymerized using RAFT, whereby two kinds of monomers were implemented. The first monomer forms the backbone of the polymer and therefore, determines general physicochemical properties, such as solubility and hydrophobicity/hydrophilicity. The second monomer, which was incorporated between 10-20 mol%, provides the crosslinkable units. Polymers were added dropwise into a dilute solution of crosslinker to form SCNPs. Before isolation of the particles, remaining crosslinkable units were removed through endcapping.

Methyl and benzyl methacrylate were used as backbone monomers for standard systems in organic solvents. Size exclusion chromatography showed a size reduction of up to 90%, indicating formation of SCNPs. Moreover, a clear dependence of the particle sizes on the precursor chain length was demonstrated. AFM and STEM images illustrate the flat shape of the particles and confirm the sub-10 nm diameters, which were observed by DLS (Figure 1).

Through employing solketal methacrylate as backbone monomer, polymers were achieved that can be rendered water-soluble by hydrolysis at low pH. The resulting diglycol copolymer was successfully crosslinked with a PEG-based crosslinker, both in water as well as in DMSO. The resulting nanoparticles were imaged via AFM and a diameter of 12 nm was confirmed by DLS.

After incubation of COS-7 kidney cells with these nanoparticles, no significant toxicity was observed, even at particle concentrations of up to 100 µg/mL, making these nanomaterials highly promising for biomedical applications. Furthermore, labeling the glycol moieties with *N*-methylisatoic anhydride resulted in blue-fluorescent nanoparticles with an excitation/emission maximum of ~360/436 nm. These particles represent a preliminary model for evaluation in a BBB *in vitro* model.

Conclusion

Owing to the ease of preparation, the majority of currently developed SCNPs are soluble only in organic media, impeding their biomedical application. By means of hydrolyzed solketal moieties, water-soluble and fluorescent SCNPs were developed. These particles are currently under investigation for BBB crossing in *in vitro* models.

References

(1) Li, S.-D.; Huang, L. *Mol. Pharm.* **2008**, *5*, 496.
(2) Kukowska-Latallo, J. F.; Candido, K. A.; Cao, Z.; Nigavekar, S. S.; Majoros, I. J.; Thomas, T. P.; Balogh, L. P.; Khan, M. K.; Baker, J. R. *Cancer Res.* **2005**, *65*, 5317.
(3) Kawai, M.; Higuchi, H.; Takeda, M.; Kobayashi, Y.; Ohuchi, N. *Breast Cancer Res.* **2009**, *11*, R43.
(4) De Jong, W. H.; Hagens, W. I.; Krystek, P.; Burger, M. C.; Sips, A. J. A. M.; Geertsma, R. E. *Biomaterials* **2008**, *29*, 1912.
(5) Sonavane, G.; Tomoda, K.; Makino, K. *Colloids Surf. B. Biointerfaces* **2008**, *66*, 274.
(6) Kumari, A.; Yadav, S. K.; Yadav, S. C. *Colloids Surf. B. Biointerfaces* **2010**, *75*, 1.

Towards load-bearing bioceramics: polymeric micro-fiber reinforcement of calcium phosphate bone cements

N. W. Kucko[1,2], D. G. Petre[1], R. P Herber[2], S. C. G. Leeuwenburgh[1]

[1]*Department of Biomaterials, Radboudumc, Transistorweg 5, 6534 AT, Nijmegen, The Netherlands*

[2]*Cam Bioceramics BV, Zernikedreef 6, 2333 CL, Leiden, The Netherlands*

INTRODUCTION: Calcium phosphate cements (CPCs) are self-setting, injectable cements considered to be a favourable bone substitute material primarily due to their excellent biocompatibility, osteoconductivity, and injectability [1]. However, in most cases their clinical applications are restricted to non-load bearing sites due to their inherent brittleness and poor mechanical integrity [2]. The main aim of this study was to investigate how the incorporation micro-fibers, specifically PLLA or PVA, along with fiber length, concentration and dispersion would influence the mechanical properties of CPCs. Further, modification of the fibers with bisphosphonate (BP) groups to tailor the fiber-cement matrix interface affinity was also investigated.

METHODS: Fiber-reinforced CPC specimens were prepared by mixing a solid phase (α-tricalcium phosphate with PLLA or PVA fibers) with a liquid phase (4 wt% aqueous solution of $NaH_2PO_4 \cdot 2H_20$) in compositions listed in Table 1. The CPC paste was cast in a silicon mold to create bars (4 x 4 x 25 mm) to perform three-point bending tests. The resulting stress versus strain curves were used to calculate the flexural strength, flexural modulus, and toughness (expressed herein as work-of-fracture (WOF)) of the CPC bars.

For the BP modification of PLLA fibers, the fibers were first subjected to a chemical process known as aminolysis in order to add amine functional groups to the surface of the fibers. Next, the functionalized fibers were soaked in a glutaraldehyde/alendronic acid solution for 12 hours to bind BP groups to the functionalized fibers before being incorporated into the CPC to run mechanical tests as stated previously.

Table 1. Fiber-reinforced CPC compositions.

Fiber Type	Length (mm)	Diameter (µm)	Concentration (wt%)
PLLA	1.5, 3 and 6	11	1.25, 2.5, and 5
BP-PLLA	1.2 and 1.7	11	2.5 and 5
PVA	3 and 6	26	1.25, 2.5, and 5

RESULTS: The stress vs. strain curves (Fig. 1) demonstrate how fiber-free CPCs can only withstand a stress of ≤ 7 MPa before complete failure under minimal strain whereas fiber-reinforced CPCs can withstand stresses as high as 25 MPa before succumbing to a slow, gradual reduction in stress over an extended strain. This phenomenon is typical for tougher, more ductile materials. For PLLA fibers, the WOF increased from 15 J/m^2 (fiber-free control) to 1.4 kJ/m^2 for CPC compositions containing 5wt% 1.5mm fiber lengths, confirming that an increase in fiber content results in a dramatic increase in WOF values (Fig. 2A). The same trend was observed for CPCs reinforced with PVA fibers where WOF values as high as 10 kJ/m^2 were observed (Fig. 2C). When compared to the literature, the values for PVA-reinforced CPCs rank among the best-performers [3].

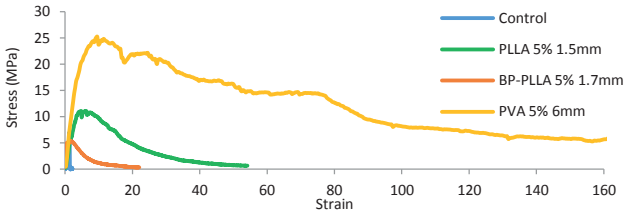

Fig. 1: Stress vs. strain curves for fiber-reinforced CPCs.

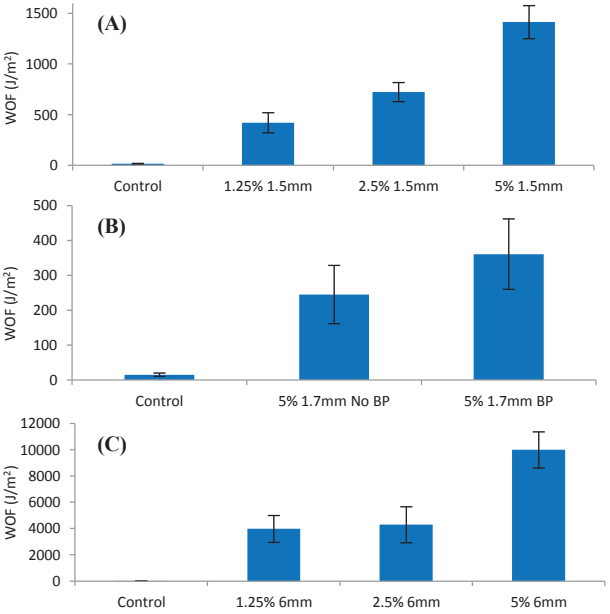

Fig. 2: Work-of-fracture values for CPCs reinforced with (A) PLLA , (B) BP-Modified PLLA and (C) PVA fibers.

DISCUSSION & CONCLUSIONS: Incorporation of different fiber types, lengths, and concentrations all significantly influenced the mechanical properties of CPCs. The dramatic increase in the WOF was indicative of the CPC becoming a tougher and more ductile material, making it less prone to catastrophic fracturing. Scanning electron microscopy revealed that incorporated fibers hindered crack propagation and bridged cracks together, thereby redistributing the applied loads throughout the entire sample and increasing their load-bearing capacity. Finally, it was determined that although aminolysis was a successful strategy for binding BP groups to the fibers, this chemical process inhibited the mechanical integrity of the fiber structure and thus the overall mechanical properties of the CPCs were hindered.

REFERENCES: [1] W. Liu, J. Zhang, G. Rethore et al (2014*) Acta Biomaterialia* **10**:3335-45. [2] Z. Yi, F. Yang, F. Wolke et al (2010) *Acta Biomaterialia* **6**:1238-47. [3] R. Kruger and J. Groll (2012) *Biomaterials* **33**:5887-900.

ACKNOWLEDGEMENTS: This study was funded through a VIDI grant (#13455) from the Dutch Technology Foundation (STW).

Double Linear Gradient Biointerfaces for Determining Two-Parameter Dependent Stem Cell Behavior

Philipp T. Kühn, Qihui Zhou, Torben A. B. van der Boon, Aneta M. Schaap-Oziemlak, Theo G. van Kooten and Patrick van Rijn
Department of Biomedical Engineering, W.J. Kolff Institute, University Medical Center Groningen and University of Groningen, PO Box 196, 9700 AD Groningen, The Netherlands. E-mail: p.t.kuhn@umcg.nl

Introduction: In the fields of regenerative medicine and tissue engineering it is pivotal to have full control over cellular behavior such as adhesion, spreading, migration, proliferation and differentiation. It is well-known that cells respond to their micro-environment. Most frequently targeted parameters on biomaterial surfaces are wettability, stiffness and topology, which have been shown to influence cell behavior in various ways. To obtain a high degree of control over cellular behavior, the influence of these parameters needs to be well-understood. General approaches for determining cell behavior often use one particular parameter, such as wettability, stiffness or topology. To elucidate the influence of surface properties on cells, gradients of these properties are time/cost efficient tools, because they can replace multiple separate experiments. A problem with altering the surface of a biomaterial is that often several parameters are altered at the same time and that specific combinations of these parameters may affect cellular behavior more than the individual parameters would do themselves. Here we developed a double linear gradient based on PDMS, using a single step shielded air plasma treatment which generates upon oxidation a more hydrophilic and stiffer material. By using a wettability gradient and the coupled gradient in wettability and stiffness, the combinatorial effect of both parameters towards human bone marrow mesenchymal stem cells (hBM-MSCs) can be tested.

Methods: The double gradients are generated on polydimethylsiloxane (PDMS, silicon rubber) which is cheap, non-toxic, transparent, flexible, biocompatible, and does not swell in aqueous media. Air plasma changes the surface properties of PDMS resulting in a stiffer and more hydrophilic surface. The amount of surface modification and the depth of penetration depends on the exposure time and intensity. By selectively masking the surface, a double gradient in wettability and stiffness is created. In addition, hydrophobized glass is treated the same way in order to obtain a single gradient in wettability, which can be used to uncouple the two parameters. hBM-MSCs adhesion behavior was tested in terms of cell density, spreading and focal adhesion area using florescence microscopy.

Results: The generated double gradients showed gradual changes in wettability and stiffness orthogonal to each other. Static water contact angle (WCA) measurements displayed a wettability gradient from 30° to 90° while atomic force microscope (AFM) indicated a surface stiffness gradient from 4MPa up to 80MPa. The wettability gradient on glass showed a WCA ranging from 20° to 140°. Macroscopic cell adhesion as well as cell spreading and focal adhesion area per cell measurements of the stem cells show that the hBM-MSCs on the single gradient follow a different trend than on the double gradient.

Conclusion: The obtained results showed clearly, that the introduced method is capable of generating double gradients on PDMS surfaces using a one-step modification. The results of the hBM-hMSC experiments show, that double gradients are a very officiant way of testing cellular response to different surface parameters. Also the results proof, that the investigation of combination of these parameters is in need in order to get control over cell behavior.

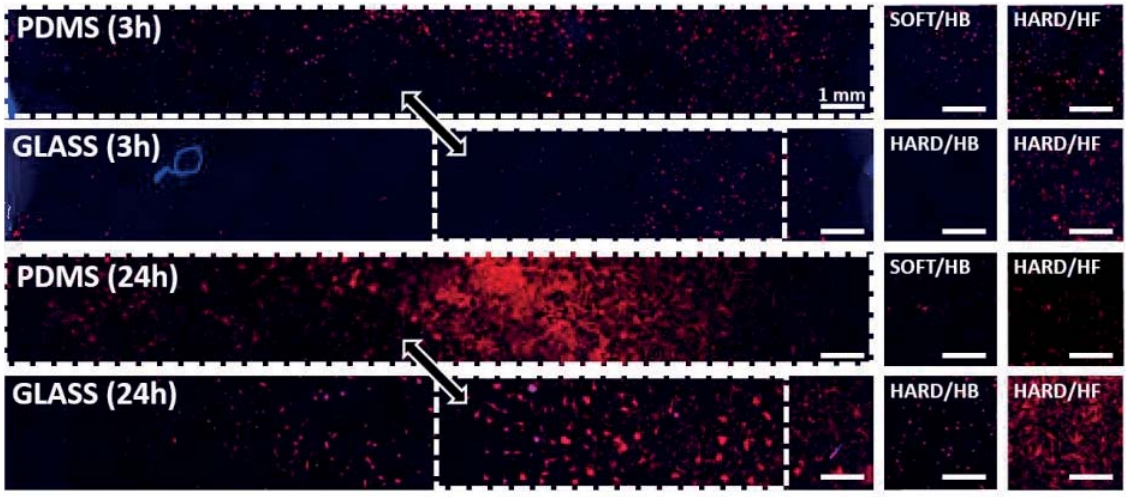

Figure 1: Combined fluorescence microscopy pictures of hBM-MSCs on the different gradients are shown. As comparison representative parts of the controls are sown as well. Here, the red marker is for TRITC-phalloidin and the blue is for DAPI. The areas surrounded by the white dashed lines and connected with the arrow, represent the same regions of wettability on the samples and are added for better comparison.

Nano and Micro Directional Topographies Oppositely Influence Adipose Derived Stem Cells Differentiation to Smooth Muscle Cells.

G.R. Liguori[1,3], Q. Zhou[2], G.G. Barros[1,3], P.T. Kühn[2], L.F.P. Moreira[3], P. van Rijn[2], M.C. Harmsen[1]

1. Cardiovascular Regenerative Medicine Research Group (CAVAREM), Department of Pathology and Medical Biology, University Medical Center Groningen
2. Biomedical Engineering Department-FB40, University of Groningen, University Medical Center Groningen
3. Laboratory of Cardiovascular Surgery and Circulation Pathophysiology (LIM-11), Heart Institute (InCor), Hospital das Clínicas da Faculdade de Medicina da Universidade de São Paulo

INTRODUCTION: Directional topographies in biomaterials such as 'wrinkles' influence adhesion, alignment and differentiation of (stem) cells. However, to date, little is known how linear topographies could be exploited to direct cell behavior to optimize biomaterials to generate Tissue- Engineered Biological Vessels (TEBV). Thus, we investigated the biological response of adipose tissue-derived stromal cells (ASCs) to gradient wrinkle sizes, varying unidirectionally the wavelength and amplitude from nanometer to micrometer scale.

METHODS: Polydimethylsiloxane (PDMS) samples with nanometer and micrometer topography linearly directional gradients (wavelength (w) range: 361nm to 10μm; amplitude (a) range: 16nm to 2μm) were fabricated. ASCs were cultured on the PDMS patterned samples, as well as in PDMS and plastic controls, and stimulated with 0ng/mL and 1ng/mL TGF-β1 to induce SMC differentiation. After 7 days, differentiation was assessed using SM22-α immunofluorescence microscopy.

RESULTS: Adhesion, proliferation and alignment of ASC preferentially occurred in the micrometer-sized wrinkles (w:1808nm/a:517nm or above). Although, nanometer-sized wrinkles allowed adhesion, these inhibited TGF-β1-induced differentiation of ASC. In the group stimulated with TGF-β1, at size range w:361nm/a:16nm to w:2823nm/a:847nm, SMC differentiation was lower compared to the wrinkle-free controls (One-way ANOVA, $p<0.001$).

CONCLUSIONS: ASCs' differentiation to SMCs was inhibited in nanotopography directional patterns while adhesion, proliferation and alignment were preferably found in microtopography directional patterns. These findings could indicate ways to both avoid or induce ASCs differentiation into SMCs, respectively by using nano and microtopography directional patterns, as well as the best topography setups to achieve aligned cell layers to generate TEBV.

Adhesion of cells on synthesized hydroxyapatite coatings with different morphologies

T. Mokabber[1], P. van Rijn[2], A.I. Vakis[1], Y.T. Pei[1]

[1]Department of Advanced Production Engineering, Engineering and Technology Institute Groningen (ENTEG), Faculty of Mathematics and Natural Sciences, University of Groningen (RuG), Groningen, The Netherlands;
[2]Department of Biomedical Engineering, Faculty of Medical Science, University of Groningen, University Medical Center Groningen (UMCG), Groningen, The Netherlands

t.mokabber@rug.nl

Introduction: Hydroxyapatite coated on titanium is extensively used in orthopedic implants. This is attributed to the advantages of titanium offering desirable mechanical properties and to the biocompatibility of hydroxyapatite. Synthetic hydroxyapatite has great structural and compositional similarity to natural bone and exhibits a surface chemistry that accelerates the growth of bone. Electrochemical deposition (ECD) is the most frequently used technique to produce hydroxyapatite coatings. The parameters of electrochemical deposition significantly affect the crystallinity, stoichiometry and morphology of the deposited coating [1-3]. The morphology of the deposited coatings is a critical issue since it strongly influences the interaction with tissue cells. Here we present methods for controlling the morphology of the coatings in order to enhance the biocompatibility and bioactivity. Morphology control is obtained by varying the deposition time under specific conditions. The morphologies will affect the mechanical and physical properties of the coating which will, in turn, affect clinical usability. Tissue compatibility is investigated by assessing the interactions of bone-like cells with the HA surface coatings.

Materials and Methods: The electrochemical deposition was performed in a conventional electrochemical cell with two electrodes in which platinum and pure titanium plates were used as anode and cathode, respectively. An electrolyte solution of 0.042 M $Ca(NO_3)_2.4H_2O$, 0.025 M $NH_4H_2PO_4$, and 1.5 vol.% H_2O_2 was used. The deposition time was varied in order to investigate its influence (1, 3, and 30 min) on the coating morphology. All other deposition parameters were kept unchanged. SaOs cells with cell density of 4×10^4 were seeded and cultured on the various coatings with distinct morphology. Finally, the cells' behaviour was observed via SEM and fluorescence microscopy using immunostaining after 2 days and 7 days culture.

Results and discussion: a 1 min deposition time resulted in a flat and smooth coating with minimum roughness. By increasing the deposition time to 3 min, HA nanoplates start to grow on coating surface which increases the surface roughness. Coating deposited at 30 min had the highest roughness due to the elongated sharp ribbons formed on the surface. Different morphologies with different roughness significantly affected the cellular behavior. In the case of the 1 min coating deposition, SaOs cells can grow and adhere to the coating very well, displaying high spreading area. On the coating deposited in 3 min with plate-like morphology cells appeared less viable and many rounded cells were observed. Finally, on the coating with a ribbon-like morphology and highest surface roughness cells appeared non-viable, and it was found that the sharp ribbons of the coating were able to completely penetrate the cells.

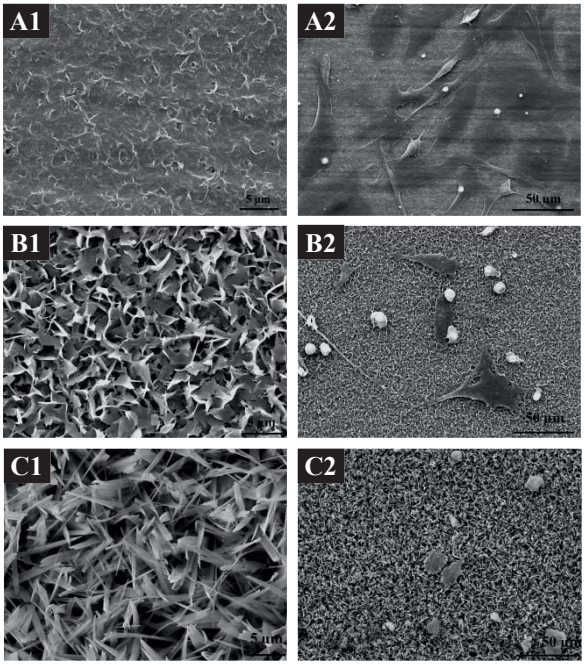

Fig. 1. SEM images of: hydroxyapatite coatings deposited at 1 min (A1), 3 min (B1), and 30 min (C1); adherent cells cultured for 2 days on hydroxyapatite coatings deposited at 1 min (A2), 3 min (B2), and 30 min (C2).

Conclusion: Hydroxyapatite coatings with different morphologies were achieved by altering the deposition time during electrochemical deposition. The most favourable surface for adhesion and growth of the cells is smooth surface with low roughness. As the roughness of the surface increased, cell adhesion, spreading and viability were compromised.

References: R. A. Surmenev, Acta Biomaterialia, 2014, 10.
M. Sadat-Shojai, Acta Biomaterialia, 2013, 9 (8).
D. Y. Lin, Surface and Coating Technology, 2010, 204(20).
D. Gopi, Surface and Coating Technology, 2012, 206(11-12).
H. Wang, Biomaterials, 2006, 27(23)

Development of Injectable BMP-2 Delivery Materials Using Collagen-I Based Recombinant Peptide

Didem Mumcuoglu[1,2], Laura de Miguel[1], Joachim Nickel[3], Johannes P.T.M. van Leeuwen[4], Gerjo J.V.M van Osch[2], Sebastiaan G.J.M. Kluijtmans[1]

[1]FUJIFILM Europe B.V., The Netherlands, [2]Department of Orthopaedics and Department of Otorhinolaryngology, Erasmus University Medical Center, The Netherlands, [3]Department for Tissue Engineering and Regenerative Medicine, University Hospital Wurzburg, Germany, [4]Department of Internal Medicine, Erasmus University Medical Center, The Netherlands

Introduction

Bone morphogenetic protein-2 (BMP-2) adsorbed to collagen sponge is used in clinics as a bone graft; however the supra-physiological amounts of protein used have been associated to adverse effects observed[1]. For a successful bone healing, it is important to provide sustained delivery of BMP-2 during the regeneration of the bone instead of a burst release of high amounts of protein. In this study, we have developed Collagen-I Based Recombinant Peptide (RCP) microparticles for delivery of BMP-2 and studied the effect of particle size, pore size and crosslinking on BMP-2 release. In addition, we have developed in-situ gelling hydrogel formulations with alginates and hyaluronic acid to deliver BMP-2 loaded RCP microspheres for bone regeneration.

Experimental Methods

Collagen-I Based Recombinant Peptide (RCP, commercial product of Fujifilm known as Cellnest™) micron-sized particles with different size and porosity were produced by emulsification and subsequently crosslinked either by hexamethylenediisocyanate (HMDIC) or by dehydrothermal treatment (DHT). Particles were characterized by SEM and degree of crosslinking. After overnight incubation of rhBMP-2 with particles, the release of BMP-2 was followed for 2 weeks and quantified by ELISA. The bioactivity of the released rhBMP-2 was analyzed by using C2C12 Bre-Luc reporter cell line. In situ gelling hydrogels were formed using SLM alginate, SLG alginate or thermosensitive hyaluronic acid[2]. Hydrogel mechanical properties were assessed by a Rheometer.

Results and Discussion

The release of BMP-2 from the microspheres revealed a two phase release kinetic which fits to the two phase exponential dissociation kinetic model curve with $p<0.001$. In the first 2 to 3 days BMP-2 release was fast, comprising up to 20% of the total, followed by a sustained release of BMP-2 for at least 2 weeks. Interestingly, after 2 weeks there was still at least 60% of BMP-2 that was not released yet. Upon degradation of the microparticles by collagenase, the remaining BMP-2 was liberated (Figure 1).

Particle size and crosslinking affected the BMP- 2 release. Particles having a smaller size released less protein than the bigger counterparts (both crosslinked in the same way), whereas a stronger chemical crosslinking also resulted in less BMP-2 release. Very importantly, the released BMP-2 was shown to be bioactive.

In situ gelling formulations of SLM alginate, SLG alginates or hyaluronic acid with RCP microspheres showed good mechanical properties and injectability. The release of BMP-2 from the composite hydrogel-microsphere system was slower than only microspheres or only hydrogels (Figure 2).

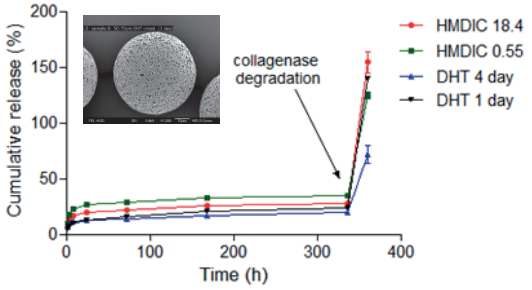

Figure 1. Cumulative release of rhBMP-2 from HMDIC and DHT crosslinked microspheres and release after collagenase degradation

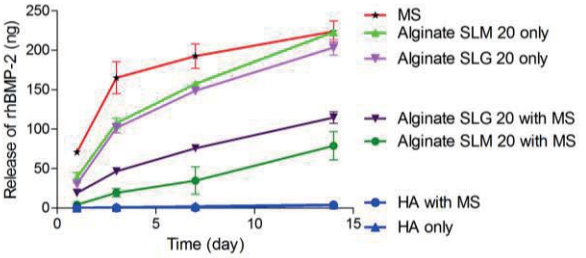

Figure 2. Release of BMP-2 from the microspheres (MS), only hydrogels (alginate SLM 20, alginate SLG 20 or hyaluronic acid) or from in-situ gelling hydrogel formulations comprising RCP microspheres and hydrogels

Conclusion

Novel BMP-2 loaded RCP particles demonstrated prolonged release of BMP-2 for at least 2 weeks in vitro. In-situ gelling hydrogels comprising these BMP-2 loaded microparticles retarded the release of BMP-2 even more. Owing to the desirable physical properties and release profile, this new RCP-based release system is a promising biomaterial to be used in a bone regeneration therapy.

References

1. Shields, L. B., *et al*., Spine 31(5): 542-547, 2006
2. D'Este, M., *et al.,* Carbohydr Polym 90 (3): 1378-85, 2012

Acknowledgments

The research leading to these results has received funding from the People Programme (Marie Curie Actions) of the European Union's Seventh Framework Programme FP7/2007-2013/ under REA grant agreement n° 607051. Thermosensitive hyaluronic acid was kindly provided by David Eglin from AO Research Institute, Switzerland.

didem_mumcuoglu@fujifilm.eu

Bone morphogenetic protein-2 release profile modulates bone formation in a novel phosphate modified oligo[(polyethylene glycol) fumarate] hydrogel

Maurits G.L. Olthof[1,3,4], Diederik H.R. Kempen[2], Mahrokh Dadsetan[1], Marianna A. Tryfonidou[3], Wouter J.A. Dhert[3], Michael J. Yaszemski[1], Lichun Lu[1]

[1]Department of Physiology and Biomedical Engineering and Department of Orthopedic Surgery, Mayo Clinic College of Medicine, 200 First Street SW, Rochester, MN 55905, United States of America
[2]Department of Orthopaedic Surgery, Onze Lieve Vrouwe Gasthuis, Oosterpark 9, 1090 HM Amsterdam, The Netherlands.
[3]Faculty of Veterinary Medicine, Utrecht University, P.O. Box 80154, 3508 TD Utrecht, The Netherlands
[4]Department of Orthopaedics, University Medical Center, Heidelberglaan 100, P.O. Box 85500, 3508 GA Utrecht, The Netherlands

Introduction: Bone morphogenetic protein-2 (BMP-2) is a potent osteoinductive growth factor, which has shown impressive results in many preclinical bone regeneration studies. Despite these results, clinical use of this growth factor is complicated by its short biological half-life and tissue selectivity. Therefore, local delivery of BMP-2 is essential for the effectiveness of the growth factor. Despite the extensive research on BMP-2 carrier development for bone regeneration, the optimal release profile for successful bone formation is not known. Therefore, in this study we aim to investigate the effect of differential BMP-2 release on bone formation in a novel biomaterial oligo[(polyethylene glycol) fumarate] bis[2-(methacryloyloxy) ethyl] phosphate hydrogel (OPF-BP) containing poly(lactic-co-glycolic acid) (PLGA) microspheres.
Materials and Methods: The composite implants all consisted of OPF-BP hydrogels containing PLGA microspheres. To vary the release in the composites, BMP-2 was loaded in the microspheres and/or adsorbed in the hydrogel. This resulted in 3 implants containing: 100% of BMP-2 encapsulated in microspheres (OPF-BP-MS: Microspheres), 50% of BMP-2 encapsulated in microspheres and 50% adsorbed on the hydrogel (OPF-BP-Cmb: Combined), and 100% of BMP-2 adsorbed on the hydrogel (OPF-BP-Ads: Adsorbed). To compare these composite designs to the clinically used BMP-2 carrier, Infuse® absorbable collagen sponge (ACS) was used as a control. BMP-2 release from the different composites was assessed in vitro and in vivo by employing BMP-2 radiolabeled with ^{125}I. The in vitro and in vivo bioactivity of the released BMP-2 was investigated by analyzing alkaline phosphatase activity in ATDC5 cells and bone formation after 9 weeks of subcutaneous implantation in rats, respectively.
Results: Bioactive BMP-2 was in vitro released in a differential profile by the composites during 9 weeks. In vivo, OPF-BP-Ads and control ACS generated a large BMP-2 burst release (>75%) within 3 days, while a more sustained release was seen for OPF-BP-MS and OPF-BP-Cmb with approximately 25% and 50% burst, respectively. OPF-BP-Ads generated significantly more bone compared to all other composite implants.
Conclusion: Overall, this study clearly shows that BMP-2 burst release generates more bone compared to sustained release in OPF-BP-microsphere composites. Furthermore, 12-fold more bone was formed compared to the clinically used ACS BMP-2 carrier emphasizing that composites should not only function as a delivery vehicle but also provide a proper framework to achieve appropriate bone formation.

Fabrication of porous poly(trimethylene carbonate) membranes for lungs-on-chips using phase separation techniques

T. Pasman, D.W. Grijpma, D. Stamatialis, A.A. Poot
University of Twente, Enschede, The Netherlands

E-mail: t.pasman@utwente.nl

Introduction *In vitro* models for lung research have improved much with the development of lung-on-a-chip technology. In these chips, a flat porous membrane gives support and allows for communication and nutrient transport between lung epithelial cells (epithelium) and blood vessel cells (endothelium) grown on opposite sides of the membrane. Stretch, microfluidics and air flow can be applied to mimic the alveoli, where gas exchange takes place in the lungs. However, unlike the flat membranes, often made of poly(dimethylsiloxane) (PDMS), alveoli are spherical structures. In this study, poly(trimethylene carbonate) (PTMC), a more biocompatible, biodegradable and mechanically favourable polymer was used. Two phase separation techniques were utilized to prepare porous membranes with microwells for use in transwell systems and ultimately a lung-on-a-chip.

Materials & methods Membranes were made of high molecular weight linear PTMC (300,000 g/mol) by casting a polymer solution, consisting of polymer, solvent and several additives, on a silicon wafer (with or without microstructures). Pores were fabricated by evaporation-induced or liquid-induced phase separation (EIPS and LIPS, respectively). Pores were temporarily stabilized by poly(ethylene oxide) (PEO) of 5,000,000 g/mol and afterwards permanently stabilized by treatment with UV-light, which initiates Irgacure 2959 to form a network of pentaerithrytol triacrylate (PETA) and PTMC. The membranes were then washed with distilled water and dried. Calu-3 (human airway epithelial) cells were seeded on the membranes to investigate the cell response to the materials.

Results and discussion Using EIPS and LIPS, porous PTMC membranes can be made with structures resembling the alveoli. The pores in general had a proper size for cell culturing (average pore diameter with both methods was below 10µm). However, LIPS resulted in membranes with higher pore numbers and larger pore size than membranes prepared by EIPS, which showed only a few micrometer-sized pores. LIPS, in general, resulted in thicker membranes and more superficial microstructures than EIPS, likely due to the fact that with EIPS the chloroform is removed rather than replaced by non-solvent, as is the case with LIPS. This decreases the porosity and pore size, but also results in thinner membranes that better follow the microstructures of the wafer. Hence, the microstructures were better replicated with EIPS, although some were damaged, perhaps due to the thin nature of the EIPS membranes. The EIPS membranes were also more transparent and showed less autofluorescence, which will enhance cell imaging. Again, this is most likely because there is a lower porosity in the EIPS membranes than the LIPS membranes. The gel content of EIPS membranes was also higher than that of LIPS membranes and had less variation (approximately 95-100% versus 5-35%, respectively). Most likely, a large amount of the crosslinking agents is lost from the membrane during phase separation in the coagulation bath in the case of LIPS. Calu-3 cells were cultured on non-porous PTMC membranes with shallow microstructures. The cells grew well and covered the entire membrane. In the future, Calu-3 and primary cells should also be cultured on membranes with the proper porosity and microstructures, since those features could change cell behaviour.

Both LIPS and EIPS have advantages. Especially EIPS is promising since only the pore size needs attention. In the future, pores will need to be more abundant and the shape and integrity of the microstructures improved, for instance by changing the non-solvent and casting thicker membranes.

Conclusion/summary Overall, the principles of LIPS and EIPS on flat and microstructured wafers yield membranes that have great potential for use in cell culturing and lungs-on-chips, as they provide an adaptable cell environment to more closely mimic the natural cell niche.

References:

1. Papenburg BJ, Schüller-Ravoo S, Bolhuis-Versteeg LA, Hartsuiker L, Grijpma DW, Feijen J, Wessling M, Stamatialis D. Designing porosity and topography of poly(1,3-trimethylene carbonate) scaffolds. Acta Biomater. 2009 Nov;5(9):3281-94.
2. Bat E, Kothman BH, Higuera GA, van Blitterswijk CA, Feijen J, Grijpma DW. Ultraviolet light crosslinking of poly(trimethylene carbonate) for elastomeric tissue engineering scaffolds. Biomaterials. 2010 Nov;31(33):8696-705.
3. Zhao J, Luo G, Wu J, Xia H. Preparation of microporous silicone rubber membrane with tunable pore size via solvent evaporation-induced phase separation. ACS Appl Mater Interfaces. 2013 Mar;5(6):2040-6.

Bone-like magnetic microspheres obtained by bio-inspired synthesis, for controlled release of BMP-2 in bone tissue engineering

T. M. Fernandes Patrício[1], D. Mumcuoglu[2], J. Nickel[3], M. Montesi[1], S. Panseri[1], M. Sandri[1], S. Kluijtmans[2], A. Tampieri[1] and S. Sprio[1]
(tatiana.patricio@istec.cnr.it)

[1] Institute of Science and Technology for Ceramics, National Research Council, Italy
[2] FUJIFILM Europe B.V., The Netherlands
[3] University Hospital Wurzburg, Department for Tissue Engineering and Regenerative Medicine, Germany

Introduction: The development of biomaterials enabling linking of bioactive molecules and characterized by stimuli-responsive release mechanisms is among the major research topics in biomaterial science. Bio-inspired synthesis processes can be applied to control the assembly of natural polymers and simultaneous mineralization with nano-apatites into hybrid gels that can be turned into biomimetic bone scaffolds [1] or, also, into carriers for controlled drug release *in vivo*, thanks to the high density of exposed charged sites. Bone morphogenetic proteins (BMPs) are the most studied growth factors in bone tissue engineering, due to their claimed osteoinductive effect. However, the delivery of supra-therapeutic doses can result in severely harmful side effects, therefore a major effort is in the development of innovative systems able to bind anabolic factors and to guarantee their controlled release *in vivo* [2,3]. Recently magnetic materials have risen the interest of scientists as they enable remote control by magnetic signalling; in particular the recent development of a biocompatible superparamagnetic nanophase made of iron-substituted apatite (Fe-HA) promises new safer approaches in the development of magnetic materials for controlled drug delivery [4].

Materials and Methods: Bio-inspired synthesis based on heterogeneous nucleation of Fe-HA on collagen [5] was translated to a different natural polymer, i.e. a recombinant peptide based on human collagen type I (RCP, commercially available as Cellnest™, by Fujifilm Manufacturing Europe B.V.), to generate mineralized hydrogels, then engineered into hybrid superparamagnetic microspheres proposed as smart carrier to control the BMP-2 release, by an oil-in-water emulsification process. A thorough investigation of chemical-physical composition, magnetic properties, cytocompatibility and expression of genes relevant in the bone regeneration cascade was investigated.

Results and Discussion: The new hybrid microspheres showed bone-like composition with intrinsic magnetic properties, and no toxic effect in presence of murine pre-osteoblasts (MC3T3-E1), up to 7 days of culture was detected. Preliminary investigation on BMP-2 release was carried out in cell culture media, under two conditions, static and pulsed electric magnetic field (PEMF). The effect of PEMF slightly increased the release of BMP-2 from hybrid magnetic microspheres.

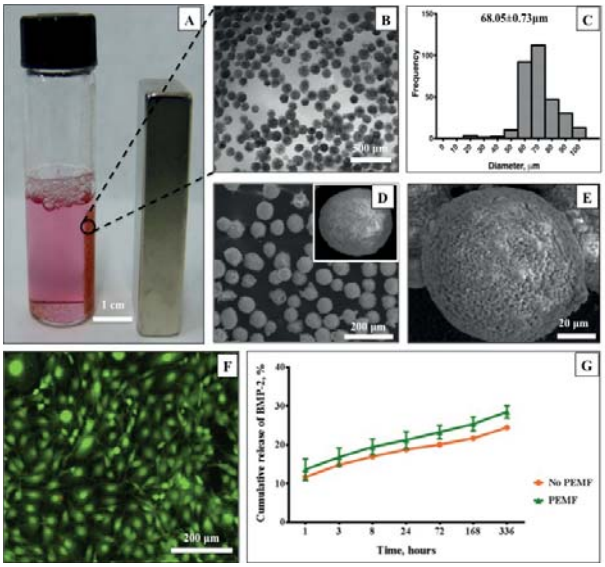

Fig. 1. Bone-like magnetic microspheres. A) Magnetic stimulation with 1.2 T neodymium magnet; B) Well dispersed microspheres in osteogenic cell medium; C) Microspheres size distribution, about 70µm; Dried microspheres before (D) and over the course of 28 days in osteogenic medium (E); F) MC3T3-E1 cell viability after 3 days in presence of magnetic microspheres; G) Cumulative release of BMP-2, up to 336 hours, under PEMF.

Conclusions: The peculiar properties of those bone-like magnetic microspheres can be tailored by means of external magnetic fields and applied as smart device to assist bone tissue regeneration.

References

[1] Tampieri et al. (2008) Biomaterials, 29(26), 3539-3546
[2] Kim, et al. (2016) Biomacromolecules, 17(5), 1633-1642
[3] Quinlan, et al. (2015) J. Cont. Release, 207, 112-119
[4] Tampieri, et al. (2012) Acta biomaterialia, 8(2), 843-851
[5] Tampieri, et al. (2014) ACS Ap. Mat. & interfaces, 6(18), 15697-15707
[6] Iafisco, et al. (2016) J. Mat. Ch. B, 4(1), 57-70

Funding

This work is supported by the European Union, Marie Curie Action, 7th Framework (FP7/2007-2013) under grant agreement N°607051, BIO-Inspire.

Evaluation of Silver Nanoparticles incorporated Chitosan-based Membranes as Antibacterial Wound Dressing

J Shao[1], B Wang[1], E Kolwijck[2], J Jansen[1], F Walboomers[1], F Yang[1*].

[1]Department of Biomaterials, Radboud university medical center, Nijmegen, the Netherlands

[2]Department of Medical Microbiology, Radboud University Medical Centre, Nijmegen, the Netherlands

*Correspondence to Fang Yang. Mailing: P.O. Box 9101, THK 309, 6500 HB, Nijmegen, the Netherlands; Email: fang.yang@radboudumc.nl

Introduction: Infection, usually secondary to the skin damage such as abrasions, punctures, burns, surgical wounds, and chronic wounds, can delay wound healing and tissue regeneration, and may result in death in severe conditions. For the prevention of the infection, wound dressings with incorporation of antibacterial agents have been investigated widely. Among those agents, silver nanoparticles gained considerable attention due to their superior antibacterial activity and, unlike the antibiotics, low chance of inducing resistance.[1] In our previous study, we developed a chitosan-based membrane incorporated with silver nanoparticles. The membrane facilitated sustained release of silver ions for at least 28 days and showed no cytotoxic effect on human fibroblasts.[2] In this study, we aimed to evaluate the antibacterial activity of this membrane and their effect on wound healing.

Materials and Methods: Chitosan-based membranes incorporated with 0, 1, or 5 wt.% $AgNO_3$ were fabricated by an electrospinning technique, and named as Ag0, Ag1, and Ag5, respectively. An agar diffusion test against *Staphylococcus aureus* (*S. aureus*) was conducted after the membrane immersion in PBS for 4, 7, 14, 21, and 28 days *in vitro*. The antibacterial efficacy of the membranes were further investigated *in vivo* in a rat subcutaneous animal model by challenging the wound with inoculation of 1×10^6 CFU of *S. aureus*. Moreover, the effect on wound healing was evaluated by a rat excisional wound splinting model using wounds without membranes as control. All the data were expressed as mean ± standard deviation.

Results and Discussion:

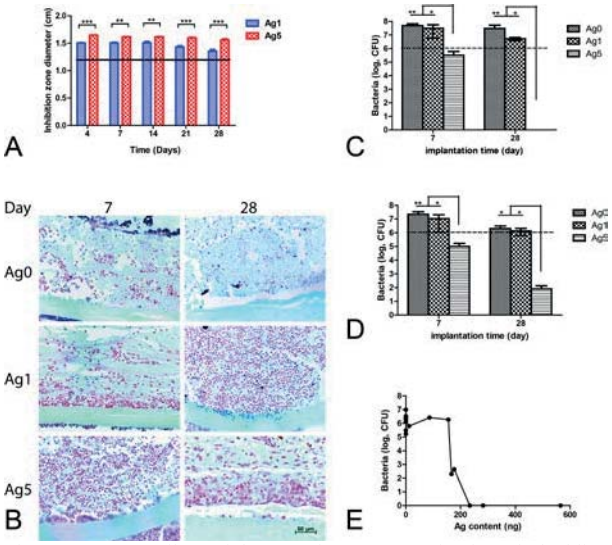

Figure 1 (A) Antibacterial test against S. aureus in vitro, dashed line represent the membranes' diameter. (B) Gram staining of explanted rat subcutaneous samples. Bacteria counting from (C) explanted membranes and (D) tissue, dashed line represent the original bacteria level. (E)Correlation between silver content and bacteria counting from explanted 28-day samples.

The *in vitro* antibacterial test showed that Ag1 and Ag5 had long-term antibacterial property for at least 28 days, and Ag5 had a significantly stronger antibacterial effect than Ag0 (Figure1.A). The following *in vivo* bacterial challenge model revealed that Ag5 killed the inoculated bacteria effectively while Ag0 and Ag1 had limited antibacterial effect (Figure1.C&D). This result was confirmed by Gram staining, where the tissues had a great number of bacteria in both Ag0 and Ag1 groups, but no bacteria in Ag5 samples (Figure1.B). A correlation between tissue bacteria counting and tissue silver content displayed that, silver can prevent bacterial infection effectively when the silver content was more than approximately 200μg in total (Figure1.E).

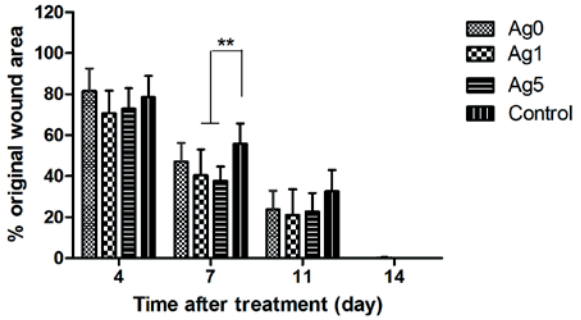

Figure 2 Quantitative measurement of wound size reduction in wound healing model.

For the rat excisional wound splinting model, the wound area was measured at day 4, 7, 11, 14 after surgery. All wounds were closed after 14 days. The membranes with silver, i.e. Ag1 and Ag5, showed a significant faster healing speed than control at day 7.

Conclusions / Summary: Silver nanoparticle incorporation enhanced the antibacterial property of the wound dressing, and a higher content (5wt.%) of silver nanoparticles was needed to prevent bacterial infection *in vivo* than *in vitro*. Furthermore, silver nanoparticle containing chitosan-based membranes promoted the wound healing, and has the potential to be used as an antibacterial wound dressing.

Acknowledgement: This work was supported by the NutsOhra Foundation (project no.: 1303-024) and the Chinese Scholarship Council (project number 201406220180). The authors would like to thank Carla J.M. Bartels and Natasja van Dijk for the help with the antibacterial test and histology, respectively.

Reference

1 Rai, M. *et al*. *Biotechnology advances* **27**, 76-83 (2009).

2 Song, J. *et al*. *Nanomedicine: Nanotechnology, Biology and Medicine* **12**, 1357-1364.

A novel real-time migration assay identifies stem cell migration in 3D matrices

K Sivasubramaniyan[1], GJ Kremers[2], ML Cruz[1], EC. Tanase[4], RE. Cameron[4], Martin van Royen[2], GJVM van Osch[1,3]

[1]Department of Orthopaedics, Erasmus MC, Rotterdam, The Netherlands. [2]Optical Imaging Center, Erasmus MC, Rotterdam, The Netherlands. [3]Department of Otorhinolaryngology, Erasmus MC, Rotterdam, The Netherlands. [4]Department of Materials Science and Metallurgy, University of Cambridge, Cambridge, UK.

Introduction: MSCs represent an important source of cells for the repair of a number of damaged tissues. The release of MSCs in vivo is likely to be followed by their active migration driven by multiple signals ranging from growth factors to chemokines secreted by injured cells and/or respondent immune cells. The soluble factors that induce stem cell migration are often identified in vitro using two-dimensional transwell and scratch assays. These assays have a major disadvantage that they grossly oversimplify the complex process of migration, thus lacking the structural architecture. Spheroid based assays, where cluster of cells are grown on gels on a 3-dimensional (3D) platform, are a more physiologically relevant method for studying migration and invasion. Further, the factors that stimulate MSC migration have not been extensively compared. In this study we developed a spheroid based migration assay and compared the effect of different factors on migration.

Methods: In brief, spheroids derived from Carboxyfluorescein labeled MSCs were seeded on collagen gel matrix in the presence or absence of factors. After 48 hours, 3D spheroid images in multiple stacks were obtained by confocal microscopy and a novel algorithm was applied to quantify migration (Fig. 1A, B). The advantage of this system is that the same spheroid can be tracked over time and hence the migration can be directly correlated with time.

Results: We first established a novel 3D real-time migration assay and developed an algorithm to quantify the migration (Fig. 1B). In the next part, we compared different concentrations of 13 commonly used cytokines, growth and chemotactic factors for their ability to stimulate the migration of bone marrow and synovial MSCs (BM-MSCs; SYN-MSCs). The migration of both BM- and SYN-MSCs was significantly stimulated in the presence of PDGF-BB, BMP2, NGFβ, SDF1α and CCL5. Inflammatory factors IL1β and TNFα stimulated the migration of BM-MSCs but not synovial MSCs. In contrast, MCP1 stimulated the migration of SYN-MSCs but not BM-MSCs.

Conclusion: This in vitro 3D system is a promising method for 3D screening to identify factors that stimulate stem cell migration in different 3D matrices. We have also adapted this system to study the migration of stem cells in different scaffolds (Fig. 1B).

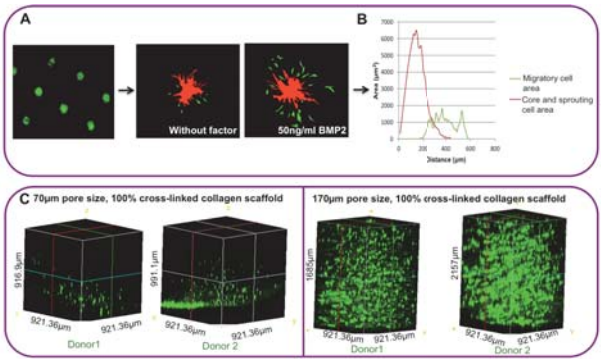

Figure 1. (A) Representative images of spheroid based 3D migration assay depicting the chemokinetic effects of BMP2 on BM-MSCs. Shown are fluorescently labeled spheroids embedded on collagen gel after 48h of culture with or without BMP2. Core of the spheroid with the sprouting cells are in red and detached migratory cells are in green. **(B)** The algorithm to quantify the migration is depicted in B. **(C)** Representative 3D images of collagen scaffolds with different pore sizes and cross-linking, showing the migration of human BM-MSCs into scaffold, 10-20 days after seeding

Catechol-functionalized UPy-based biomaterials improve cardiomyocyte progenitor cell adhesion

Sergio Spaans, Peter-Paul H.K. Fransen, Bastiaan D. Ippel, Henk M. Keizer, Carlijn V.C. Bouten, Patricia Y.W. Dankers

Department of Biomedical Engineering, Institute for Complex Molecular Systems, Eindhoven University of Technology, Eindhoven, Netherlands. s.spaans@tue.nl

The development of synthetic biomaterials that recapitulate the complete natural extracellular matrix is a well-established challenge in the field of regenerative medicine. Biomaterials that typically are used as natural extracellular matrix replacements are synthetic polymers, individual matrix components or bioactive sequences of a specific matrix component. Building the extracellular matrix using individual or a combination of components has proven to be difficult to completely mimic the natural extracellular matrix. Particularly, during heart disease where extracellular matrix becomes disfunctional, the use of synthetic biomaterials that mimics natural extracellular matrix could potentially improve functional matrix formation. For this reason, cardiomyocyte progenitor cells (CMPC) are used which have shown to produce cardiac specific extracellular matrix.[1] Here, the goal is to improve CMPC-biomaterial interactions using a completely synthetic precursor. To this end a supramolecular system was developed based on ureido-pyrimidinone (UPy) modified polymers modularly functionalized with UPy-modified catechol. CMPC were cultured on our catechol-functionalized supramolecular biomaterials and extracellular matrix production was studied at gene and protein level using quantitative PCR and immunohistochemistry.

Interestingly, adhesion, spreading and viability of cardiomyocyte progenitor cells were increased when the supramolecular materials were modified with the UPy-catechol molecules. Additionally, we managed to preserve cardiac specific extracellular matrix production by CMPC up to 7 days. In conclusion, this method shows the feasibility of UPy-catechol modified biomaterials to promote adhesion and preserve cardiac extracellular matrix formation by CMPC.

Modulating JAK-STAT Signaling Pathways in Macrophages to Improve Tissue Regeneration

M.A.M. Suijkerbuijk[1], S. Çapar[1], N. Kops[1], D.E. Meuffels[1], G.J.V.M. van Osch[1,2], Y.M. Bastiaansen-Jenniskens[1]
[1]Department of Orthopaedics, [2]Otorhinolaryngology, Erasmus MC, University Medical Center, Rotterdam, the Netherlands

Introduction – Macrophages, as specialized cells of the immune system, are present in many different tissues. Macrophages display remarkable plasticity, with phenotypes ranging from pro-inflammatory to anti-inflammatory/repair depending on the environmental cues they receive. The different macrophage subtypes can either positively or negatively affect surrounding tissues and influence regenerative processes. (1, 2) The current study aims to examine which intracellular JAK-STAT signaling pathway is responsible for which process in different macrophage subsets. Furthermore, the effect of STATs modulation on the behavior of the macrophage phenotypes is investigated and thereby their effect on surrounding tissues.

Materials and methods – Peripheral human monocytes were isolated from buffy coats using CD14+ selection and magnetic sorting. After seeding in 500.000 cells per cm^2, they were cultured in low glucose Dulbecco's modified Eagles medium (DMEM-LG) with 20% fetal calf serum (FCS) in the presence of either interferon (IFN) γ and tumor necrosis factor (TNF) α, Interleukin (IL) 4, or IL10 (all in 10 ng/ml) in order to obtain the macrophage phenotypes M(IFNγ/TNFα), M(IL4), or M(IL10). To examine STAT-1, STAT-6 and STAT-3 activation of different macrophage phenotypes on Western blot, cells were harvested after 30, 60, and 90 minutes. To determine the effect of STAT activation on protein production and gene expression, cells were harvested after 24 hours. To examine effect of STAT inhibition on macrophages, synovial tissue was obtained from osteoarthritic knees and cultured for 24 hours in DMEM-LG, 10% FCS with 50 μM STAT1-inhibitor NSC-118218(3) and 100 μM STAT-3 inhibitor S3I-201(4). After 24 hours, STAT activation was determined with Western blot, CCL18, IL6 and sCD163 production was analyzed with ELISA and *CCL18, CD163, CD206, IL6* and *TNFA* gene expression was determined in the tissue.

Results – Regardless of the timing of harvesting, STAT-1 was specifically phosphorylated in M(IFNγ/TNFα), STAT-6 in M(IL4) and STAT-3 in M(IL10), as detected by Western blot (Figure 1). Macrophage polarization was confirmed as M(IFNγ/TNFα) typically had high expression levels of IL6 and TNFA and high IL6 protein production. M(IL4) expressed high levels of CCL18 and CD206, and high CCL18 production, whereas M(IL10) had high expression of CD206 and high sCD163 production. (5)

When immediately obtained after surgery, STAT-1, STAT-3 and STAT-6 could be detected in osteoarthritic synovium. However, 24 hours after culturing synovial explants, only STAT-1 and STAT-3 could be detected. Treatment of synovial explants with NSC-118218 specifically decreased STAT-1 phosphorylation and downregulated *CD163* expression (Figure 2A) without affecting *TNFA* expression (Figure 2B). Treatment with S3I-201 decreased STAT-3 phosphorylation and increased *TNFA* expression (Figure 2B). STAT-1 and STAT-3 inhibition in synovial explants did not affect protein production.

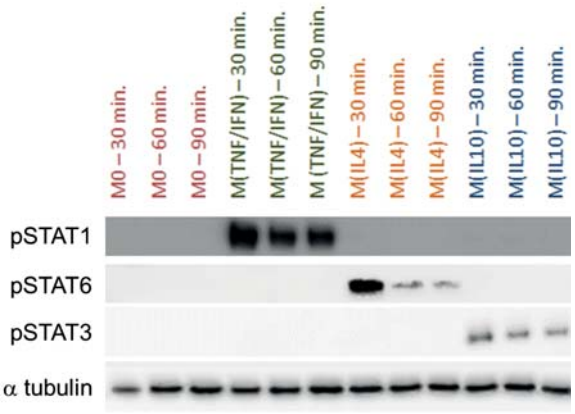

Figure 1: *STAT1, 6, and 3 are specifically activated (pSTAT) in different macrophage phenotypes. α-tubulin was used as control for equal loading.*

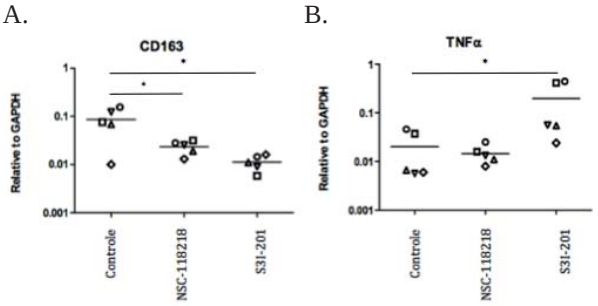

Figure 2: *Effect of NSC-11828 or S3I-201 treatment on A) CD163 expression and B) TNFA expression in synovial explants. *p < 0.05*

Discussion and Conclusion: Macrophage subsets obtained in this study have a specific pSTAT-1, pSTAT-6 or pSTAT-3 pattern. Inhibiting STAT-1 activation with NSC-118218 and STAT-3 activation with S3I-201, specifically affected gene expression patterns of synovium containing macrophages. Based on these results, targeting JAK-STAT signaling pathways seem promising to modulate macrophage behavior and may therefore be a potential target to induce tissue regeneration.

References

1. Fahy N et al. Osteoarthritis and cartilage. 2014
2.Utomo L et al.. Osteoarthritis and cartilage. 2016a
3.Frank D et al. Nature medicine. 1999
4.Barbieri et al. Cancer research. 2010
5.Utomo L et al. Osteoarthritis and cartilage. 2016b

Controlled release of celecoxib from polyesteramide microparticles in a canine pre-clinical intervertebral disc degeneration model

Anna R. Tellegen [1], Martijn Beukers [1], Imke Jansen [2], Guy C. M. Grinwis [3], Nina Woike [4], George Mihov [4], Björn P. Meij [1], Laura B. Creemers [2], Marianna A. Tryfonidou [1]

[1] Department of Clinical Sciences of Companion Animals, Faculty of Veterinary Medicine, Utrecht University, Utrecht, The Netherlands; [2] Department of Orthopedics, University Medical Centre, Utrecht, The Netherlands; [3] Department of Pathobiology, Faculty of Veterinary Medicine, Utrecht University, The Netherlands; [4] DSM Biomedical, Geleen, The Netherlands

Introduction: Low back pain affects 80% of the people worldwide at least once in their lives. It is a major cause of sickness related work absence and poses a high financial burden on societies. In a large part of the affected population, low back pain is related to degeneration of the intervertebral disc (IVD). The process of IVD degeneration and its clinical representation in dogs resembles the human situation and therefore, dogs are a suitable large animal model to study IVD disease and develop novel treatments. Pro-inflammatory mediators such as the COX-2 mediated prostaglandin E2 play an important role in both catabolic at the molecular level and the sensitization to pain at the clinical level. Clinical studies have already shown that oral COX-2 inhibitors are effective reducing in low back pain, although they are associated with gastro-intestinal or cardiovascular side effects. Moreover, it is not known how much of the orally administered drug reaches the avascular IVD. Therefore, local delivery of anti-inflammatory and analgesic drugs directly into the IVD could be a suitable treatment strategy for back and neck pain. We have previously demonstrated safety of intradiscally injected Poly-Ester-Amide Microparticles (PEAMs) in a canine model with long term follow up of 6 months at the radiological, biochemical, and histological level. The aim of the present study was to find the optimal loading dose of locally administered celecoxib in a controlled release system based on PEAMs, in a canine model with induced IVD degeneration as a first step towards clinical translation.

Methods: The animal experiment described in the current study was performed with prior approval of the ethics committee for laboratory animal use of Utrecht University (protocol # 2015.II.813.025). IVD degeneration was induced in 5 lumbar IVDs of 3 beagle dogs by puncture with an 18G needle and partial nuclectomy by aspiration. IVDs that were not punctured served as controls. Four weeks later, degeneration was confirmed by MRI. Thereafter, the dogs received intradiscal injections with PEAMs, loaded with 0.2 3mg/mL or 7 mg/mL celecoxib or unloaded microparticles (sham), with n=6 discs per treatment group. Insertion of the needle for induction of IVD degeneration and intradiscal injection with celecoxib were guided by fluoroscopy in two directions. After the 16 week follow-up period, the MRI was repeated and dogs were sacrificed. Post mortem, a CT scan of the spinal column was performed and IVDs were harvested for macroscopic and histopathological evaluation and biochemical analyses (DNA-, collagen-, and glycosaminoglycan content). All data were examined for normal distribution (Shapiro Wilks test). Kruskal Wallis and Mann-Whitney U tests were performed on non-normally distributed data, whereas general linear regression models based on ANOVA were used for normally distributed data. $P < 0.05$ was considered significant after correcting for multiple testing with Benjamini & Hochberg False Discovery Rate *post-hoc* tests.

Preliminary results: Recovery from induction of IVD degeneration was uneventful. Four weeks after induction of degeneration, MRI showed mild IVD degeneration (Pfirrmann grade II – III). At the end of the experiment, 16 weeks after intradiscal injection with 40µL unloaded PEAMs (sham), low (0.23 mg/mL) or high (7 mg/mL) dose celecoxib, no adverse effects were visible on imaging modalities (MRI, CT) or macroscopic evaluation. The macroscopic and MRI scores were significantly higher in the IVDs where degeneration was induced compared to control IVDs. The IVDs treated with the PEAMs containing low and high dose CXB did not statistically differ from either non-induced and sham groups. Total and PGE2/DNA levels were significantly increased in both the NP and AF of the control IVDs, compared to non-induced IVDs. PGE2 decreased after treatment with both the low and high dose of celecoxib. Sustained release of celecoxib, regardless of the dose, resulted in a significantly increased glycosaminoglycan content of the nucleus pulposus. Intradiscal injection of PEAMs had no effect on glycosaminoglycan-, total collagen- or DNA content of the annulus fibrosus.

Discussion & conclusions: Celecoxib incorporated in PEAMs were safely administered intradiscally in experimental beagle dogs. Ongoing histological analyses will shed light on changes at the biochemical and histological level. Follow up studies in a large animal model with naturally occurring clinical IVD disease as a preclinical model for translation to humans is warranted to determine the efficacy of celecoxib loaded PEAMs in inhibiting low back pain.

3D-printed Injectable Poly- ε-caprolactone Molds for Ear Cartilage Tissue Engineering

D.O. Visscher[1,2], A. Gleadall[3], J.K. Buskermolen[4], M.N. Helder[5], J. Segal[3], P.P.M van Zuijlen[1,6]

[1] Department of Plastic, Reconstructive and Hand Surgery, VU University Medical Center, Amsterdam, the Netherlands, MOVE Research Institute Amsterdam, Amsterdam, The Netherlands
[2] 3D InnovationLab, Amsterdam, The Netherlands
[3] Manufacturing and Process Technologies, Faculty of Engineering, University of Nottingham, University Park, Nottingham, UK
[4] Department of Dermatology, VU University Medical Center, MOVE Research Institute Amsterdam, Amsterdam, The Netherlands
[5] Department of Oral and Maxillofacial Surgery/Oral Pathology, VU University Medical Center, MOVE Research Institute Amsterdam, Amsterdam, The Netherlands
[6] Burn Center, Red Cross Hospital, Beverwijk, the Netherlands

3-dimensional (3D) printing technology can be used to produce scaffolds with complex architectures for tissue engineering. Here, a 3D bioprinting device was used to manufacture 3D-printed injectable poly- ε-caprolactone molds for ear cartilage tissue engineering.

The printing accuracy and mechanical properties of 3D-printed poly-ε-caprolactone (PCL) scaffolds with varying porosities were first determined to assess the overall structure properties. These same porosities were used to construct injectable 3D-printed PCL cube molds and an ear mold. The molds were then injected with chondrocyte-filled collagen I/fibrin hydrogel to engineer an implantable ear construct for *in vitro* tissue maturation.

Analysis revealed that smaller pore width correlated with increased mechanical properties of 3D-printed PCL scaffolds. Optical microscopy showed that scaffolds with smaller pore widths exhibited better printing accuracy. In addition, the screw-based extruder of the bioprinter produced filaments with variable strand diameters that lead to a range of pore sizes. Chondrocyte slurry injected into a 3D-printed PCL mold displayed excellent cell survival. Proof-of-concept injection of collagen hydrogel into a 3D-printed ear mold showed high accuracy.

The presented 3D-printed scaffold construct may be an adequate model for ear cartilage tissue engineering and provides a novel approach to ear regeneration by enabling *in vitro* tissue maturation.

Geometry-guided cell migration on competing length scales

M. Werner, N.A. Kurniawan, A. Petersen, C.V.C. Bouten

[1]*Soft Tissue Biomechanics and Tissue Engineering, Department of Biomedical Engineering, Eindhoven University of Technology, Netherlands.*
[2]*Julius Wolff Institut and Berlin-Brandenburger Centrum für Regenerative Therapien, Charité - Universitätsmedizin Berlin, Germany.*
Contact: M.Werner@tue.nl

Introduction

Cell migration plays a critical role in a large number of physiological and pathological processes in the body, such as tissue development and wound healing. Moreover, cell migration is essential in scaffold-based tissue engineering applications to allow sufficient cell colonization throughout the whole scaffold. It is well known that cell migration can be triggered and directed by changes in the mechanical properties of the cell's microenvironment[1,2]. However, knowledge on how cell migration is influenced by the geometrical properties of the cell's environment remain mostly limited to 2D surfaces. A deeper insight in how cells migrate in response to 3D geometrical cues of different length scales is therefore needed to understand the role of the architecture of the extracellular environment as a cell-instructive parameter in health and disease.

Methods

In this study we explored the impact of geometry on cell migration on 2 competing length scales. We developed a method to deposit isotropic and anisotropic fibrillar collagen networks on cylindrical substrates with diameters of 250–5000 μm created in PDMS via a molding process. Using this method, we systematically varied the mesoscale curvature of the substrate in combination with nanoscale geometrical cues provided by the collagen fibers. We monitored the migration of human mesenchymal stem cells (hMSCs) on these structures over 24 hours using confocal time-lapse imaging and analysed the migration speed, migration direction and persistence length.

Results and Discussion

Our data reveals that at high surface curvatures (on small radius cylinders) cells preferentially align and migrate along the longitudinal axis of the cylindrical structures. This effect is pronounced at cylindrical structures with diameters 2-3x the cell size, and thereafter decreases with decreasing substrate curvature. On cylindrical structures with an isotropic fibrillar collagen network, this leads to an increasingly random cell migration on large-diameter cylinders. However, on cylindrical substrates with an anisotropic collagen network, cells align and migrate along the direction of the collagen fibers. These results suggest that the guidance effect of the mesoscale geometrical cues dominate the contact guidance cues from the nanoscale collagen fibers on small diameter cylinders ($\varnothing \approx$ 2-3x cell size).

Conclusion

The results indicate that cell migration is controlled by the combined, and sometimes competing, effects of contact guidance by the nanoscale, aligned collagen fibrils and the surface-curvature guidance by structures much larger than the cell size. Further study is directed at elucidating the specific roles of the cytoskeleton and nucleus on this geometry-guided cellular orientation and migration. Ultimately, the knowledge gained from this study could be of relevance for the design of cell-instructive biomaterials, e.g. in the field of tissue engineering, but also for a better understanding of organogenesis and disease pathogenesis.

Acknowledgements

We acknowledge the support from the Netherlands Cardio Vascular Research Initiative: The Dutch Heart Foundation, Dutch Federation of University Medical Centres, the Netherlands Organisation for Health Research and Development and the Royal Netherlands Academy of Sciences.

References

[1] C. M. Lo, H. B. Wang, M. Dembo, Y. L. Wang, *Biophys. J.* **2000**, *79*, 144.
[2] M. Ehrbar, a Sala, P. Lienemann, a Ranga, K. Mosiewicz, a Bittermann, S. C. Rizzi, F. E. Weber, M. P. Lutolf, *Biophys. J.* **2011**, *100*, 284.

Type VII Collagen in the Human Accommodation System: Expression in Ciliary Body, Zonules and Lens Capsule

B Wullink[1], co-authors (HH Pas[2], RJ van der Worp[1], R. Kuijer[3], LI Los1)
University of Groningen, University Medical Center Groningen, Dept. of [1]Ophthalmology, [2]Dermatology, and [3]Biomedical Engineering, Hanzeplein 1, 9700 RB, Groningen, The Netherlands. Email: b.wullink@umcg.nl

Introduction: The accommodation system transfers mechanical forces from the ciliary muscles to the lens capsule, via the zonules, adjusting the lens refraction power. The tissues of this system must therefore endure considerable mechanical stress throughout our lives. Recently, type VII collagen (Col VII) was discovered in the inner eye. This anchoring fibril forming protein is thought to aid tissues in resisting mechanical stress. By immunohistochemistry, we investigated if Col VII might support the attachment of accommodation system tissues.

Materials: Nineteen human donor eyes (mean age 65 years) without known ophthalmic disorders were processed within 48 hours post mortem.

Methods: Eyes were embedded in paraffin or Technovit resin, sectioned and immunostained using polyclonal and monoclonal antibodies against Col VII. Analysis was done by light- and transmission electron microscopy. Ciliary body, iris and lens capsular tissue (including zonules) substrates were immuno-blotted.

Results: Col VII was demonstrated in most substructures. The unpigmented epithelium of the ciliary body, the basement membrane zone of the pigmented epithelium and the zonules expressed Col VII profoundly. Both epithelial layers expressed higher collagen concentrations at the bases of the ciliary processes. The iris expressed Col VII underneath the pigmented posterior epithelium, especially at the pupillary constrictor muscle. The ciliary stroma and muscle had low and moderate levels of expression, respectively. The zonular lamella of the lens capsule and the lens fibers did not express Col VII. By immunoelectron microscopy, additional specific Col VII expressing structures were found within the lens capsule. Western blot confirmed Col VII expression in the various substructures.

Discussion

The accommodation system tissues express Col VII at their basement membranes. At sites of (expected) high degrees of mechanical stress, the expression appears the most profound. The zonular fibers are most immunoreactive, as are their attachments to the ciliary body and lens capsule. The pupillary constrictor muscle has a moderate level of expression. All in all, the data of this investigation suggests an increase of Col VII expression at sites where mechanical stress, thus the need of an anchoring protein, is high.

Surface Modification of 3D-Printed Polycaprolactone Scaffolds by Functional Carboxyl and Hydroxyl Groups Enhances MC3T3-E1 Pre-osteoblast Proliferation and Matrix Production

Y. Zamani[1,2,3], G. Amoabediny[2,4], M.N. Helder[5], B. Zandieh-Doulabi[2], J. Klein-Nulend[2]
[1]Dept Biomed Engin, Faculty of New Sciences and Technologies, University of Tehran, North Kargar Street, Tehran, Iran
[2]Dept Biomed Engin, Research Center for New Technologies in Life Science Engineering, University of Tehran, 16 Azar Street, Tehran, Iran
[3]Dept Oral Cell Biology, Academic Centre for Dentistry Amsterdam, University of Amsterdam and VU University Amsterdam, MOVE Research Institute Amsterdam, Gustav Mahlerlaan 3004, 1081 LA Amsterdam, NL
[4]Faculty of Chemical Engineering, College of Engineering, University of Tehran, 16 Azar Street, Tehran, Iran
[5]Dept Oral & Maxillofacial Surgery, VU University Medical Center, MOVE Research Institute Amsterdam, P.O. Box 7057, 1007 MB Amsterdam, NL

Introduction: The polymer polycaprolactone (PCL; FDA approved) is often used as a scaffold in bone tissue engineering because of its high stiffness and long degradation time. Unfortunately PCL is not suitable for cell adhesion since it is hydrophobic. Cell adhesion to the scaffold surface is a critical factor since adhesion occurs before other biological events such as cell proliferation, differentiation and matrix production. Therefore PCL surface modification can be used to improve cellular activity.

Aim: To study the effect of surface modification of 3D-printed PCL scaffolds by functional carboxyl and hydroxyl groups on MC3T3-E1 pre-osteoblast proliferation and matrix production.

Methods: PCL scaffold was fabricated using a 3D-bioprinter device (RegenHU; CH). Cubic scaffolds (0.5×0.5×0.5 cm) were plotted layer-by-layer with a layer deposition angle of 90°. The pore size was ~300 µm. Surface modification was performed by treatment with 1, 3, and 5 M NaOH for 24 h, followed by 24 h immersion in simulated body fluid. MC3T3-E1 pre-osteoblasts were seeded on PCL scaffolds, and cell metabolic activity (proliferation marker) was quantified using Alamar Blue staining up to 8 days of culture. Scaffolds were cut longitudinally to show cell activity in the center of the scaffold. Cell nuclei were visualized by DAPI and extracellular matrix by Pico Sirius Red staining.

Results: Surface modification of 3D-printed PCL scaffolds with 1, 3, or 5 M NaOH enhanced MC3T3-E1 pre-osteoblast metabolic activity compared to unmodified scaffolds at all time points. Cell metabolic activity was increased from day 1-8 on scaffolds treated with 1 M NaOH (by 5.6 fold), 3 M NaOH (4.8 fold), and 5 M NaOH (3.6 fold; Fig. 1). Cells were present in the scaffold center and produced their own matrix (Fig. 2). Surface modification using 3 M NaOH resulted in visibly more extracellular matrix filling the scaffold pores compared to 1 or 5 M NaOH (Fig. 3).

Discussion and conclusion: Surface modification of 3D-printed PCL scaffold by introducing functional carboxyl and hydroxyl groups enhanced MC3T3-E1 pre-osteoblast metabolic activity independent of the NaOH concentration used. Most matrix produced by cells was observed in scaffolds treated with 3 M NaOH. In conclusion, our data suggest that surface modification of 3D-printed PCL scaffold by introducing functional carboxyl and hydroxyl groups is highly suitable for use in bone tissue engineering.

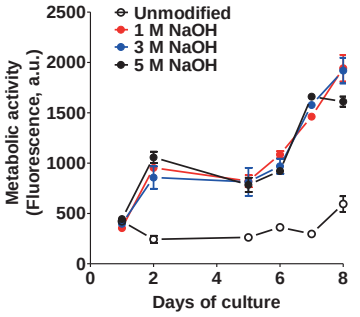

Fig. 1. Increased metabolic activity of MC3T3-E1 pre-osteoblasts on surface-modified (1,3,5 M NaOH-treated) 3D-printed PCL scaffolds up to 8 days.

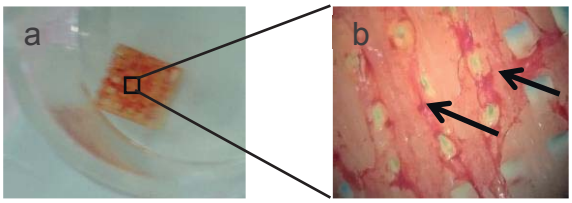

Fig. 2. Sirius Red-stained matrix produced by MC3T3-E1 pre-osteoblasts on 3D printed PCL scaffolds treated with 3 M NaOH at day 8. (a) Scaffold. (b) Magnification of area indicated in (a). Black arrows: Sirius Red-stained matrix deposition.

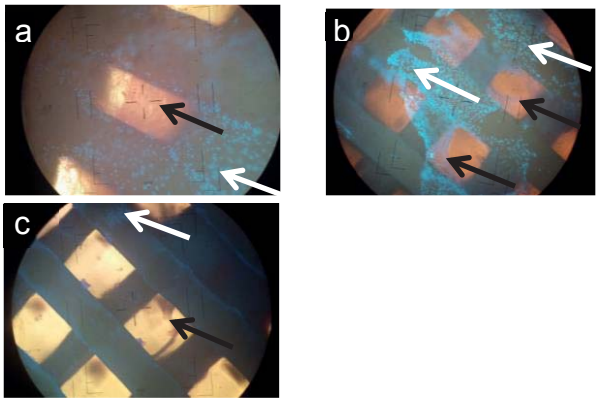

Fig. 3. Difference in DAPI-stained cell nuclei and Sirius Red-stained matrix produced by MC3T3-E1 pre-osteoblasts on surface modified 3D printed PCL scaffolds. a) 1 M NaOH, b) 3 M NaOH, and c) 5 M NaOH treated scaffolds. White arrows (blue dots): DAPI-stained cell nuclei. Black arrows: Sirius Red-stained matrix deposition.

High-throughput Screening of Cell Contact Guidance on Directional Micro/nanotopographical Gradients

Q. Zhou, P.T. Kühn, T.G. van Kooten, P. van Rijn*
Department of Biomedical Engineering-FB40, W. J. Kolff Institute for Biomedical Engineering and Materials Science, University of Groningen, University Medical Center Groningen, A. Deusinglaan 1, 9713, AV, Groningen, The Netherlands.

Introduction

It has been well-demonstrated that surface topography and chemistry of biomaterials can mediate cell behavior, such as cell adhesion, morphology, orientation, differentiation, etc [1][2][3]. The relationship between the topography and cell response depends on the pattern and dimensions, among other factors, which are critical issues to be clarified. However, most of these studies focused on independent substrates with various and randomly selected degrees of topography which provided only limited information and lacked in identifying optimal condition that regulate cell response. Surface topographic gradients offer an ideal platform for the high-throughput screening of cell-surface interactions [4]. Using gradients saves time and resources, maximum data output with minimal number of experiments is obtained and variations due to systematic errors minimized. Most studies focused on the microscale alignment gradients or non-directional nanotopographic surfaces and did not contrast cell behavior on topographic gradients in the range between 0-1000 nm including a surface directionality. Here, we developed biomimetic wrinkle gradients with amplitudes ranging from 49 to 2561 nm and wavelengths between 464 and 7121 nm for the analysis of cell-substrate interactions, which have been translated to clinically relevant biomaterials (**Fig.1**).

Materials and Methods

The PDMS (polydimethylsiloxane) substrate was stretched uniaxial to a strain of 30% of its original length. Stretched PDMS was partly covered with a mask and oxidized with air plasma. Subsequently, the strain was released which induced the wrinkled gradient. To expand the platform to various clinically relevant biomaterials, we deposited different metals (Ti, Cr and Al) on PDMS wrinkled gradient surfaces by metal evaporation. Exposure of the different metal coatings to air, the respective oxides are rapidly formed. SaOs (human osteosarcoma cell line) were used for the cell response study for 2 days culturing.

Results and Discussion

A 2-day *in vitro* assessment of SaOs cultured on wrinkle gradients showed that cellular responses were closely correlated to the wrinkle amplitude and wavelength (**Fig.1B**). Less focal adhesion area per cell with increasing wrinkle amplitude and wavelength was found, while focal adhesion and cell orientation initially increased with increasing wrinkle features and subsequently decreased again. It was identified that wrinkles with 130-180 nm amplitude and 550-730 nm wavelength are the most favorable topography for improving the osteoblast alignment while amplitudes of 15-45 nm and wavelengths of 400-520 nm are required to have an optimal combined parameter response to direct osteoblast behavior (**Fig.1B**).

The platform was expanded to various clinically relevant inorganic biomaterials (i.e., SiO_2 as a bioglass,TiO_2 and CrO_3 for biometal oxides, Al_2O_3 as bioceramic) generally used in orthopedics, orthodontic and dentistry, without affecting wrinkle dimensions (**Fig.1C**). It was found that mesenchymal stem cells display altered behavior on the wrinkle gradients when different biomaterials are used.

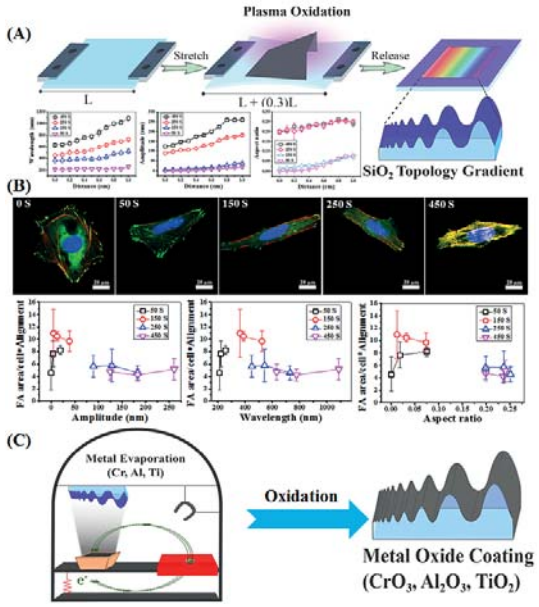

Figure 1. (A) Schematic diagram for wrinkle gradient formation by air plasma oxidation. (B) Fluorescent staining of single osteoblast for different wrinkles prepared by varied plasma oxidation times. Dependence of the values of FA/cell * alignment on amplitude, wavelength and aspect ratio. (n = ~100 cells). (C) Schematic illustration of wrinkle gradients translation to other inorganic biomaterials.

Conclusions

The novel strategy of using PDMS-based topography gradient platforms enables us to screen efficiently for optimum cell behavior *via* low-cost approaches. Additionally, we show that topography response greatly depends on the type of biomaterial used and the novel biomaterial interfaces allows us to study this in a clinically relevant fashion.

References

[1] R. Langer, D. a Tirrell, *Nature* **2004**, *428*, 487.
[2] Q. Zhou, P. Wünnemann, P. T. Kühn, J. de Vries, M. Helmin, A. Böker, T. G. van Kooten, P. van Rijn, *Adv. Mater. Interfaces* **2016**, 10.1002/admi.201600275.
[3] Q. Zhou, J. Xie, M. Bao, H. Yuan, Z. Ye, X. Lou, Y. Zhang, *J. Mater. Chem. B* **2015**, *3*, 4439.
[4] Q. Zhou, P. T. Kuhn, T. Huisman, E. Nieboer, C. van Zwol, T. G. van Kooten, P. van Rijn, *Sci. Rep.* **2015**, *5*, 16240.

NBTE
Netherlands society for
Biomaterials and Tissue Engineering

Poster Abstracts

(Alphabetical order)

S53P4 bioactive glass is clinical effective in one-stage surgery in treatment of chronic osteomyelitis

T.A.G. van Vugt[1], J.J.C. Arts[1-2], Jan A. Geurts[1]
[1]Department of Orthopaedic Surgery, Researchschool CAPHRI, Maastricht University Medical Centre, the Netherlands
[2] Department Orthopaedic Biomechanics, Eindhoven University of Technology, the Netherlands

Introduction: Chronic osteomyelitis is historically treated in a two-stage fashion with debridement and placement of antibiotic-loaded polymethylmethacrylate (PMMA) beads as local antibacterial therapy. However, two-stage surgeries are associated with high morbidity, long hospitalization and high treatment costs. In recent years new biomaterials were developed that allow to change this treatment algorithm. S53P4 bioactive glass is such a novel biodegradable antibacterial bone graft substitute that enables a one-stage surgery in local treatment of chronic osteomyelitis. After implantation of BonAlive (S53P4) bioactive glass surface reactions ensure deposition of a calcium phosphate layer when it gets in contact with (body) fluid. Sodium, silica, calcium and phosphate ions are released from the surface and increase the local pH and osmotic pressure creating a local bactericidal environment. Thereafter, a silica gel layer is formed on the glass surface, and amorphous calcium phosphates precipitate on this layer. These amorphous structures then crystalize to natural hydroxyapatite, which starts the activation of osteoblasts for the formation of new bone This study aimed to explore the eradication of infection and bone healing capacities of S53P4 bioactive glass in clinical practice.

Methods: In this prospective longitudinal outcome study, clinical applicability of S53P4 bioactive glass in treatment of patients with chronic osteomyelitis was assessed. All patients with clinically, haematologically and radiologically evident chronic osteomyelitis were included. All patients were treated with an extensive debridement surgery, S53P4 bioactive glass implantation and systemic antibiotic administration. Primary endpoint of this study is eradication of infection. During follow-up eradication was analysed based on clinical outcomes, blood samples (inflammatory parameters) and radiological outcomes. The secondary endpoint, bone healing, is assessed using conventional radiographic images of the treated region. This study was approved by the ethical committee of Maastricht University and informed consent was obtained form all patients.

Results: Between 2011 and 2016, 25 patients were included in this study, with a mean follow-up of 23 months (range 4 – 57). Hospital stay was short with a mean of 18 days (range 4 – 40) and patients required an average of 1,4 surgeries (range 1 – 4). The inflammatory parameter C-reactive protein (CRP) showed normalization after a mean duration of 46 days (range 0 – 211).

At the end of follow-up haematological and clinical outcomes showed eradication of infection in 24 (96%) of all patients. Radiological assessment showed that none of all patients exhibited persisting signs of infection and bone healing was observed in 22 (88%) patients based on changes on conventional radiographic images. One patient had a persistent infection without any bone healing; this patient had an infected non-union prior to surgery. There were two other patients with an initial infected non-union fracture that was not consolidated at last follow-up, although they had successful infection treatment. Another patient had a femoral fracture after surgery that needed additional surgery, which did not interfere with eradication of infection. Four (16%) of all patients had initial wound healing problems related to compromised skin and/or soft tissue prior to surgery.

Discussion: Based on the results of our clinical experience, S53P4 bioactive glass can successfully be used in a one-stage procedure for treatment of chronic osteomyelitis. Eradication of infection was successful in almost all patients and so far no patients required a second surgery due to infection recurrence. Bone healing (incorporation of the bioactive glass) was seen in all patients except for the patients with an initial infected non-union fracture. A limitation of this study is the small patient group but this is primarily due to the incidence of osteomyelitis in the general population and the relatively high hospital density in the Netherlands. As a consequence of these results, we changed our institutional protocol for treatment of chronic osteomyelitis from a two-step approach with introduction of antibiotic loaded PMMA beads to a one-stage approach using S53P4 bioactive glass.

Significance: Based on the results of our clinical experience, S53P4 bioactive glass can successfully be used in a one-stage procedure for treatment of chronic osteomyelitis

Optimisation of a shear stress free microfluidic device for large gradient profiles of soluble species and cell culture: a modelling study

D. BARATA, C.A. VAN BLITTERSWIJK, P. HABIBOVIC

Department of Instructive Biomaterials Engineering, MERLN Institute for Technology Inspired Regenerative Medicine, Maastricht University, The Netherlands (d.barata@maastrichtuniversity.nl)

Introduction

Microfluidics has enabled technological developments and enhancement of knowledge in various scientific fields including, but not restricted to, medical diagnostics, biology and ecology [1].

Geometrical arrangements of microscale systems and associated tridimensional (3D) spatial configuration enable compartmentalization and generation of complex microenvironments. In such systems, physico-chemical parameters like volume, flow speed, shear stress, hydrophobicity, surface-bound and soluble compounds chemistry, can easily be decoupled and arranged in a combinatorial manner, making them suitable for numerous applications. One important feature of microfluidic devices is the possibility to create and sustain gradients of diluted species, surface-bound materials, electric field, flow rate, etc.

In this work, a finite element model was employed to perform 3D modelling [2] of gradients of diluted species in a microfluidic system.

Materials and Methods

A 3D model was built based on three major compartments; two independent inflow boundaries and two subsequent outflow boundaries, corresponding to feeding side-channels (each actuated by independent longitudinal flow, at same speed) of the intermediate planar compartment (Figure 1).

This model simulates a microreactor, within which unbalanced species concentrations will generate a gradient. The model was defined using the Transport of Diluted Species interface (describing Fick's law), coupled to Laminar Flow interface (governed by Navier-Stokes equations) of COMSOL Multiphysics software 4.3.

Geometry nodes were built using design tools of the software (Figure 1).

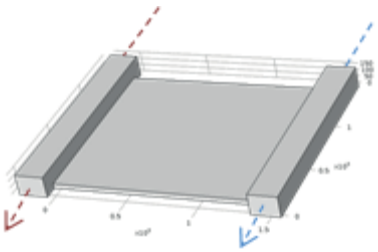

Figure 1 – 3D representation of the microfluidic reactor. Dashed arrows represent flow direction.

MG-63 osteosarcoma cells were seeded in the device and cultured in basic culture medium, the flow of which was kept constant through the side-channels, and incubated at 37 °C and 5% CO_2.

Results and Discussion

The model demonstrated a displacement of shear focus into the side-channels, leaving the intermediate compartment practically free of flow (Figure 2).

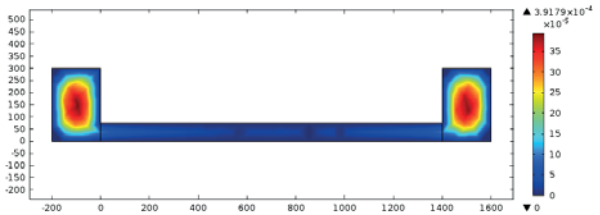

Figure 2 – Fluid flow surface plot for Velocity field. Units are in $m.s^{-1}$.

Regarding the concentration distribution over the volumetric capacity of the central intermediate compartment, located in the core of the microfluidic reactor, the simulation showed the formation of a gradient profile of concentration of the species of interest. A source-sink mechanism was reflected in an unbalance of concentrations, which may stay stable over time. Cross-section of the structure, showing narrow spectral distribution of the gradient is depicted in Figure 3A. The

respective concentration profile is plotted in Figure 3B, where the slope characterizes the microenvironment at a specific position on the compartment length.

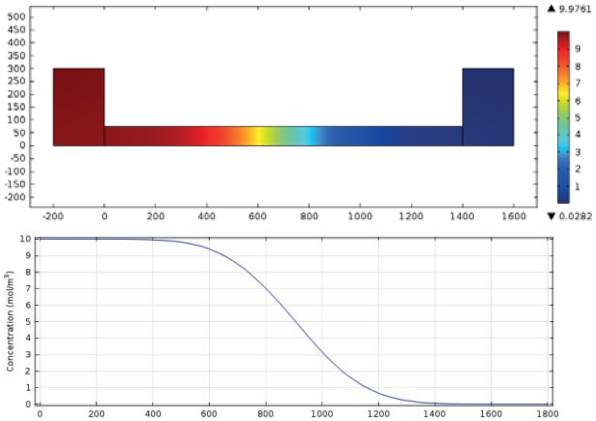

Figure 3 – Concentration gradient surface plot (top) and gradient profile of concentration (down). Units are in mol.m^{-3}.

Computational results showed the possibility to simultaneously simulate fluid flow and soluble compounds diffusion, providing an approximation of expected profiles of speed and concentration levels. Other geometries can now be proposed and simulated in order to further optimize the gradients in multiparametric microfluidic reactors. The microfluidic device was successfully tested for generating a gradient of a soluble dye and no shear stress was observed. Furthermore, MG-63 cells were successfully cultured in the device as was shown by the fluorescent live staining (Figure 4).

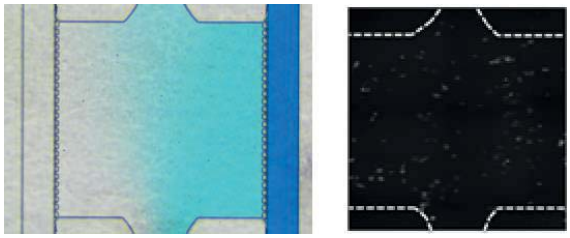

Figure 4 – Brightfield image of a culture chamber of the microfluidic device showing a blue dye gradient (left), and fluorescence image of cultured MG-63 cells (right).

References

[1] Mark, D. et al. Microfluidic lab-on-a-chip platforms: requirements, characteristics and applications. Chem. Soc. Rev., 2010,39, 1153-1182

[2] COMSOL Inc. website support information and models. Available at: http://www.comsol.com/models (2013)

Human Osteoblast-derived Extracellular Matrix with High Homology to Human Bone Proteome Enhances the Osteogenic Potential of Mesenchymal Stromal Cells

M. Baroncelli[1], S. Chatterji[1], E. Rull Trinidad[3], R.D Alves[1], J.A Demmers[2], J. van de Peppel[1], J.P.T.M van Leeuven[1]
[1] Department of Internal Medicine, [2] Proteomic Center, Erasmus Medical Center, Wytemaweg 80, Rotterdam, The Netherlands; [3]Department of Precision and Microsystem Engineering, Technical University of Delft, The Netherlands

Introduction: Efficient osteogenic differentiation of mesenchymal stem cells (MSCs) is crucial to accelerate bone formation. However MSC osteogenic potential decreases during *ex-vivo* expansion for bone tissue engineering applications. The extracellular matrix (ECM) represents a natural 3D-framework that actively modulates stem cell properties. Strategies combining cell-derived ECMs and MSCs have been proposed to improve MSC properties and culture conditions for bone tissue engineering applications.
The aim of this study was to generate a devitalized human MSC-derived ECM and to investigate its impact on osteoblast differentiation of MSCs, to improve MSC properties for bone regeneration.

Materials and Methods: Human MSCs were cultured in osteogenic conditions and devitalized by freeze/thaw cycles to produce the ECM. The proteomic composition was analyzed by mass spectrometry. Fresh MSCs were seeded on the ECM and monitored for cell adhesion, proliferation and osteoblast differentiation.

Results and Discussion: The devitalized ECM exhibited a rough surface and significantly enhanced MSC adhesion ($P<0.01$). A significantly higher percentage of proliferating cells was detected on the ECM than in control conditions after 1 day of culture ($P<0.001$). The osteogenic differentiation and mineralization of MSCs on the devitalized ECM were faster than in standard culture conditions ($P<0.001$) (Figure 1A and 1B). We detected 846 proteins in the devitalized ECM. Of these, 473 proteins were shared with a human bone proteome that we previously described[1], demonstrating that the devitalized ECM was comparable to an *in vivo* microenvironment. Bioinformatic analysis of the 846 proteins showed involvement in adhesion and matrix vesicle production (Figure 1C), confirming the ECM composition as key modulator of MSC behaviour.

Conclusions: This study provides a simplified method to obtain an *in vitro* MSC-derived ECM that enhances MSC osteogenic differentiation, and could be applied as natural biomaterial to accelerate bone regeneration.

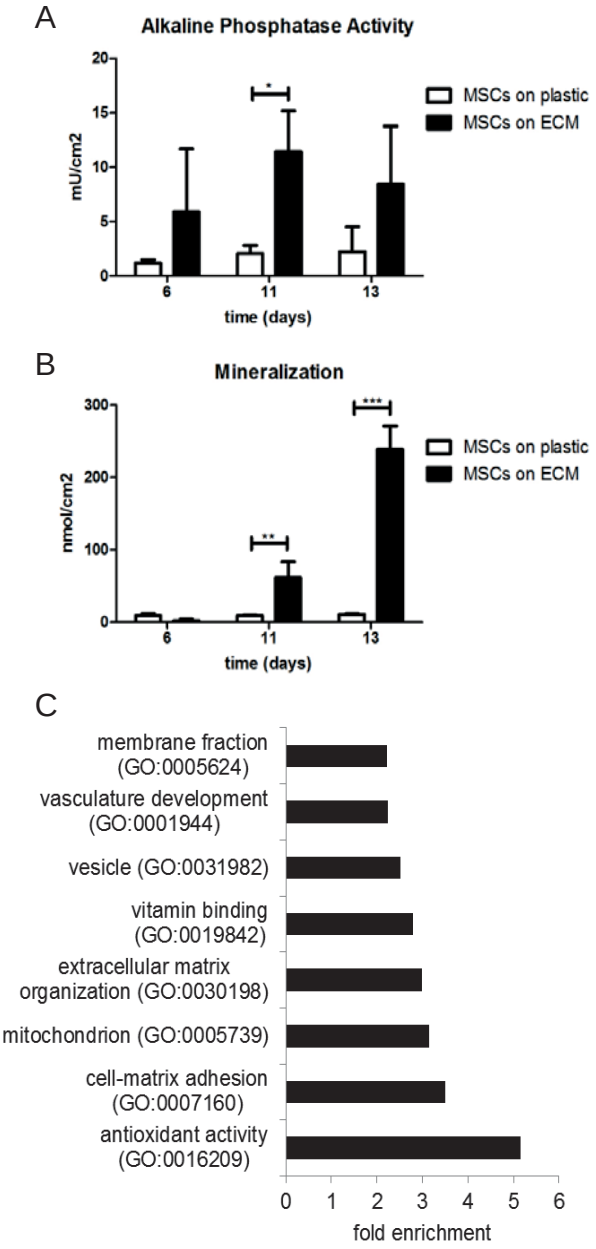

Figure 1: A) Alkaline phosphatase activity in cell extracts of MSCs on ECM and plastic. B) Deposition of calcium in cell extracts of MSCs cultured on ECM and on plastic. In A and B the values of MSCs on ECM were subtracted by the ECM contribution. (*, $P<0.01$; **, $P<0.05$; ***, $P<0.001$). C) Gene ontology (GO) analysis of all the 846 proteins detected in the devitalized ECM. Only significantly enriched GO terms are shown ($P<0.01$).

[1] Alves R.D., J Proteome Res, 2011. 10 (10): p.4725-33

m.baroncelli@erasmusmc.nl

IL-4 functionalized supramolecular materials for *in situ* vascular regeneration

V. Bonito[1,2], *A. Driessen-Mol*[1,2], *T.J.A.G. Münker*,[1,2], *O. J.G.M. Goor*[1,2], *A.W. Bosman*[3], *T. Mes*[3], *P.Y.W. Dankers*[1,2], *A. I.P.M. Smits*[1,2], *C.V.C. Bouten*,[1,2]

[1]Dept. of Biomedical Engineering, Eindhoven University of Technology, The Netherlands
[2] Institute for Complex Molecular Systems, Eindhoven University of Technology, The Netherlands
[3] SupraPolix BV., Eindhoven, The Netherlands

Objective:

Over the last decade, acellular synthetic grafts homing bioactive compounds have been proposed as a promising, off-the-shelf solution to accelerate cellular infiltration, promote selective recruitment and enhance functional tissue regeneration *in situ*. Along this line, much research was devoted to the modulation of the inflammatory response via the polarization of macrophages[1-4], which are believed to determine the outcome of the implantation procedure depending on their phenotype [5]. In this respect, functional bone[2,3] and nerve regeneration[1] were proven *in vitro* and *in vivo* for synthetic materials functionalized with interleukin 4 (IL-4)[1-4], a cytokine responsible, amongst others, of the activation of the wound healing M2 macrophage phenotype. The proposed approaches are based either on pre-mixing of the IL-4 into hydrogels, and consequent burst release within few hours[1,4], or on biotin-streptavidin interaction, with an IL-4 gradual release within a few days[2].
Here, we propose a new, non-covalent method for IL-4 functionalization and release over a more prolonged period of time, based on a supramolecular approach. Supramolecular materials can assemble via their repeating units, i.e. 2-ureido-4[H], UPy moieties, resulting in modular and reversible structures that can be easily bioactivated with UPy-modified biolecules[8]. Particularly, a bioactive UPy-modified peptide, i.e. the UPy-heparin binding peptide (UPy-HBP), is mixed in and matched to UPy–modified polymers via dimerization of self-complementary quadruple hydrogen bondings[8]. The UPy-HBP modified supramolecular polymer is further functionalized with a solution of heparin, which can click to the UPy-HBP, and IL-4, which is known to bind to heparin via its heparin binding domain[6].

Material and Methods:

Chain-extended ureido-pyrimidinone (UPy) modified polycaprolactone (CE-UPy-PCL) was used as a base material to design 2D and 3D structures, and further modified with UPy-HBP, as previously described[9]. The nanostructure of the dropcast films was evaluated via atomic force microscopy (AFM), and the wettability levels measured via water contact angle experiments (WCA). For the functionalization with IL-4, dropcast films were incubated overnight with different concentrations of IL-4 in heparin, i.e. 20 ng/mL and 0.2 ng/mL. Monocytes isolated from human peripheral blood mononuclear cells (hPBMCs) were seeded on dropcast films, further stimulated towards non-polarized macrophages with macrophage colony stimulating factor (MCSF) and cultured for 7 days. At day 3 and day 7, cell morphology was observed with light microscopy and via actin staining. Also, cell phenotype was assessed via immunostainings with markers specific for M1 and M2 macrophages. Furthermore, the extent of the inflammatory response was evaluated via quantification of a panel of pro- and anti- inflammatory cytokines (MCP-1, IL-6, TNFα, IL10, MMP9, TGFβ) via Multiplex ELISA.
For electrospinning, CE-UPy-PCL and CE-UPy-PCL+UPy-HBP were dissolved in chloroform ($CHCl_3$) and hexafluoro-2-propanol (HFIP) and fibrous sheets fabricated. Heparin complexation to the CE-UPy-PCL+UPy-HBP was assessed via fluorescence analysis of heparin-FITC incubated onto the dropcast films. Subsequently, scaffolds were incubated with IL-4 pre-complexed with heparin, and the IL-4 release was measured via an IL-4 specific enzyme linked-immune-sorbent assay (ELISA) over time. The experiment was performed in static conditions and under a flow regime mimicking the physiological hemodynamic environment of small diameter arteries.

Results:

AFM micrographs of dropcast CE-UPy-PCL showed large PCL crystalline domains, and the lack of a well-defined fibrous morphology, while, upon addition of UPy-HBP, phase separation occurred, next to the self-assembly of UPy-HBP into small nanofibers. WCA measurements did not show significant differences in the wettability levels of pristine CE-UPy-PCL and CE-UPy-PCL+UPy-HBP (data not shown) .

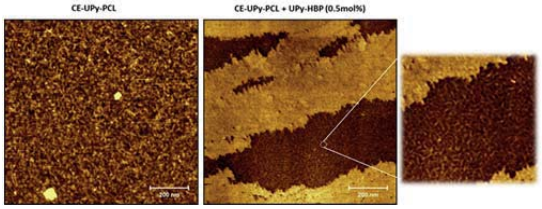

Figure 1: Fig1. Atomic force microscopy phase images of pristine CE-UPy-PCL, and UPy-HBP modified CE-UPy-PCL (0.5mol%) drop cast surfaces. CE-UPy-PCL showed large PCL crystalline domains, and the lack of a well-defined fibrous morphology (left). Upon introduction of 0.5mol% of UPy-HBP in CE-UPy-PCL, small nanofibers were observed (right), due to co-assembly of the two polymers or phase separation and subsequent assembly of UPy-HBP only in small nanofibers.

In 2D cultures, differences in cell morphology were observed at day 3 and day 7, with elongated M2-type macrophages[6] displayed on IL4 functionalized CE-UPy-PCL+UPy-HBP films, and rounded M1-type macrophages on CE-UPy-PCL films (Fig.2.), regardless of the MCSF treatment (data not shown). Multiplex ELISA results revealed immunomodulatory properties of the IL-4 functionalized material. At day 3, regardless of the functionalization, inhibition of IL-6, MCP-1, was noticed, which is in line with the dampening of the M1 polarization shown by the immunohistochemistry results. Remarkably, at day 7, next to the decrease in secretion levels of some pro-inflammatory cytokines, e.g. IL-6 and TNF-α, an IL-4 induced significant increase in production of all the anti-inflammatory cytokines was detected, possibly mirrored in the switch in macrophage polarization towards the anti-inflammatory phenotype M2 revealed by the immunohistochemistry results at day 7 (data not shown). Also, within the functionalized films, no significant differences were detected for different concentrations of IL-4 (Fig.3). Therefore the lowest concentration of IL-4, i.e. 0.2 ng/mL, was preferred to functionalize the electrospun scaffolds in 3D.

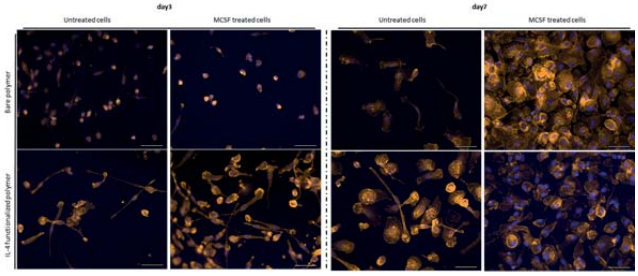

Figure 2: Phalloidin staining of monocyte-derived macrophages on dropcast CE-UPy-PCL (top row) and IL-4 functionalized CE-UPy-PCL-HBP (bottom row) films after 3 days (left) and 7 days (right) of culture (scale bar 50μm). Cells cultured on IL-4 functionalized films showed a spindle-shaped morphology, typical of the wound healing macrophage phenotype M2, either with or without treatment with MCSF.

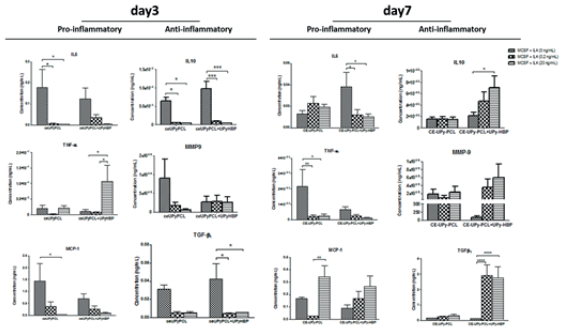

Figure 3: Secretion levels of pro- and anti- inflammatory cytokines quantified via MULTIPLEX ELISA on the supernatants of CE-UPyPCL and IL-4 functionalized CE-UPy-PCLHBP. Dropcast films were incubated with different concentrations of IL-4 (0, 0.2, 20ng/mL). Cells for all the group were treated with MCSF (100ng/mL). IL-4 functionalized films are proven to be immunomodulatory, inducing the inhibition of pro-inflammatory cytokines production and the promotion of anti-inflammatory cytokines secretion at day7.

As a first step toward the development of synthetic vascular grafts for in vivo implantation, electrospun meshes with an average fiber diameter of 10.31±1.02 μm and 10.06±2.11 μm were obtained for CE-UPy-PCL and CE-UPy-PCL+UPy-HBP, respectively (Fig.4A). Successful adsorption of heparin on the UPy-HBP activated scaffold (Fig.4B) was demonstrated, together with biofunctionalization with IL-4 for both static and flow regimes (Fig.4C).

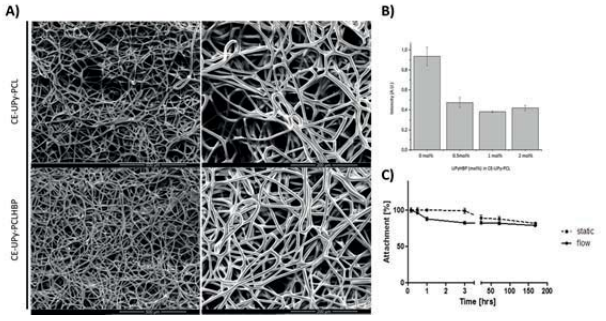

Figure 4: A) Electrospun CE-UPy-PCL (top) and CE-UPy-PCL+UPy-HBP (bottom) (100X, left; 250X, right), with average fiber diameters of 10.31±1.02 μm and 10.06±2.11 μm, respectively. B) Heparin binding assay on the supernatant of CE-UPy-PCL and CE-UPy-PCL+UPy-HBP electrospun scaffolds incubated with 50 μg/mL heparin-FITC, showing a drastic reduction in signal intensity for CE-UPy-PCL+UPy-HBP with increasing concentrations of UPy-HBP, therefore successful heparin immobilization. C) ELISA assay on the supernatant of CE-UPy-PCL+UPy-HBP electrospun scaffolds incubated with 0.2 ng/mL of IL-4 in heparin, with attachments of 81.6% and 78.81% at 1 week for static and flow regime, respectively.

Conclusions:

We developed an IL4-functionalized supramolecular material showing immunomodulatory properties which relies on the possibility to bias macrophage polarization over time. Moreover, we proved that the IL4 immobilization via heparin approach can be translated to 3D electrospun scaffolds. These bioactivated systems hold a great deal of promise for the development of truly 'smart', cell-responsive scaffolds which can interact with their environment and mediate a favorable host response to the implanted vascular graft in vivo.

[1] Mokarram N, Merchant A, Mukhatyar V, Patel G, Bellamkonda R V. Effect of modulating macrophage phenotype on peripheral nerve repair. Biomaterials. (2012)
[2] Spiller KL, Nassiri S, Witherel CE, et al. Sequential delivery of immunomodulatory cytokines to facilitate the M1-to-M2 transition of macrophages and enhance vascularization of bone scaffolds. Biomaterials. (2015)
[3] Reeves ARD, Spiller KL, Freytes DO, Vunjak-Novakovic G, Kaplan DL. Controlled release of cytokines using silk-biomaterials for macrophage polarization. Biomaterials. (2015)
[4] Kumar VA, Taylor NL, Shi S, Wickremasinghe NC, D'Souza RN, Hartgerink JD. Self-assembling multidomain peptides tailor biological responses through biphasic release. Biomaterials. (2015)
[5] Badylak, S.F. et al. Macrophage phenotype as a determinant of biologic scaffold remodeling. *Tissue Engineering*. Part A (2007)
[6] McWhorter, F.Y. et al. Modulation of macrophage phenotype by cell shape. *Proc.Natl.Acad.Sci.U.S.A.* (2013)
[7] Lortat-Jacob, H., Garrone, P., Banchereau, J., & Grimaud, J. a. Human interleukin 4 is a glycosaminoglycan-binding protein. Cytokine (1996)
[8] P. Y. W. Dankers, M. C. Harmsen, L. A. Brouwer, M. J. A.Van Luyn, E. W. Meijer. A modular and supramoleuclar approach to bioactive scaffolds for tissue engineering. Nat. Mater. (2005).
[9] V.Bonito et al., IL-4 functionalized vascular grafts for in situ vascular tissue regeneration, *In preparation*

Bacterial antigens for bone regeneration

M. Croes, M. Kruyt, W. Boot, B. Pouran, W.J.A. Dhert, F.C. Oner, J. Alblas
University Medical Center Utrecht, Department of Orthopedics

Introduction

It has become increasingly clear that the immune system has a profound interaction with the cells of the skeletal system. In a pathological context, inflammatory reactions can induce excessive new bone formation in patients, suggesting that inflammation-associated pathways may be harnessed to promote new bone formation. Here, we investigated whether the immuno reaction to bacteria can potentially be used in bone regenerative therapies.

Materials and Methods

In an orthotopic study, 10^9 gamma-irradiated (γi) bacteria were inoculated in the medullary cavity of the tibia in rabbits. The contralateral tibia served as a control. The bone changes were quantified by micro-CT. Fluorochrome markers were injected at different time points to determine the onset and progression of new bone depositon. *S. aureus, E. coli* and *M. marinum* were investigated. The tibial bone volume after 4 weeks was the main outcome parameter.

In an ectopic study, porous biphasic calcium phospate (BCP) scaffolds were loaded with different γi bacteria (*S. aureus, B. cereus, E. coli, H. influenzae* and *M. marinum)* in a low to high concentration (10^5-10^9/ml). Half of these samples were-co loaded with a minimal amount of bone morphogenetic protein (BMP)-2 to mimick an osteogenic environment. These constructs were implanted in intramuscular and subcutaneous pockets in the dorsum of rabbits, respectively, and bone volume in the contructs was assessed by histomorphometry. The bone volume (bone area%) after 8 weeks was the main outcome parameter.

Results and Discussion

The inoculation of γi *S. aureus* or γi *E. coli* in the medullary cavity induced similar periosteal new bone formation in the tibia compared to that observed during an implant infection. Also osteolytic bone changes were observed, however these were less profound compared to virulent bacterial strains. The analysis of fluorochrome incorporation showed that new bone formation started within 3 days and continued for at least 4 weeks. This new bone formation resulted in a significant increase in the bone volume compared to untreated tibiae. The bone volume, together with its enhanced porosity, largely restored to normal between week 4 and 8. These data suggest that the inflammatory reponse to bacterial cell wall components stimulates bone anabolic pathways.

To assess whether the pro-osteogenic effect of bacterial antigens was limited to the periosteum, we investigated the effects of whole inactivated bacteria on the ectopic bone formation within BCP constructs. The results showed that these constructs were not bone inductive, irrespective of the presence of γi bacteria. In the context of BMP-2 however, a mild response to γi *S. aureus*, *M. marinum* or *H. influenzae* resulted in a significant increase in the bone volume. In the optimal condition, a two-fold increase in bone area% was seen. No significant differences were found for the other γi bacteria. A severe inflammatory response, i.e. loading of a high concentration of γi bacteria, was always associated with an inhibitory effect on BMP-2-induced bone formation. These data suggest that the inflammatory response to bacterial cell wall antigens can be beneficial for the formation of osteoblasts in an ectopic location.

Conclusion

Inactivated bacteria elicit an inflammatory response that activates both bone anabolic and catabolic pathways, in a concentration dependent manner. When loaded onto calcium phosphate carriers in bone tissue engineering contructs, they profoundly affect the ectopic bone formation, while acting in synergy with the bone-associated growth factor BMP-2. This study identifies a novel role for bacterial antigens in skeletal tissue regeneration.

Biphasic calcium phosphate with crystalline surface microstructure as bone graft substitute in *Ovine* model of maxillary sinus floor augmentation

Luuk van Dijk[a,b*], Nard Janssen[b], Rob Bakker[b], Alessia Longoni[b], Debby Gawlitta[b], Antoine Rosenberg[b], Joost D. de Bruijn[a,c], Florence Barrere-de Groot[b]

[a] Xpand Biotechnology BV, Bilthoven, The Netherlands; [b] Department of Oral and Maxillofacial Surgery, University Medical Centre Utrecht, Utrecht, The Netherlands; [c] MIRA Institute, University of Twente, Enschede, The Netherlands

* Corresponding author: luuk.van.dijk@xpand-biotech.com

INTRODUCTION

In maxillofacial surgery, autogenous bone grafts are frequently employed in the reconstruction of bone defects or deformations. Calcium phosphate (CaP) ceramics have been developed as synthetic bone graft substitutes that eliminate the need for autogenous bone harvesting. A distinct set of CaP ceramics holds the capacity to induce *de novo* bone formation, therefore termed osteoinductive CaPs. The osteoinductive capacity of these CaPs is attributed to microstructural surface features [1]. The current study investigates a biphasic CaP (BCP) ceramic with crystalline surface microstructure as bone graft substitute in a pre-clinical model of maxillary sinus floor augmentation in sheep.

METHODS

Material production: Porous biphasic CaP (BCP) blocks were prepared by use of H_2O_2 and were sintered at 1125ºC to produce surface micropores and –grains. The blocks were crushed in order to obtain granules of 0.25 – 1 mm in size. Granules then underwent a hydrothermal treatment inducing the formation of epitaxial polygon crystals on the material surface (Figure 1). Material composition and surface structure were assessed by X-ray diffractometry and scanning electron microscopy (SEM). The material was sterilized by gamma radiation (25 kGy).

In vivo study: 24 Swifter sheep underwent bilateral maxillary sinus floor augmentation with microstructured BCP granules as test treatment and autogenous cristae illiaca bone particles as control treatment. Access to the maxillary sinus was obtained through the facial antral wall. A bony window was created in the lateral wall after which the Schneiderian membrane was carefully elevated and 1.5-2cc of graft material was implanted on the sinus floor. After healing periods of 3, 6 and 12 weeks, animals were sacrificed by an injection of barbiturate. A polychrome sequential fluorescent labelling method was applied on the animals in the group of 12 weeks, by injection of distinct fluorochrome labels at 3, 6 and 9 weeks post-surgery.

Histology and μCT: After sacrifice, samples were harvested by en-bloc resection of maxillary sinuses. After fixation, samples were processed for undecalcified histology by graded ethanol dehydration series and embedded in polymethyl methacrylate (PMMA). Before sectioning, samples in PMMA blocks were imaged by μCT to determine graft volume. Histology sections were stained with basic fuschin and methylene blue to visualize bone tissue in grafted region. Histomorphometric analysis was performed by pseudo-coloring pixels representing bone, bone marrow and remaining material in a region of interest in order to determine bone and material percentage. Unstained sections were analysed by fluorescence microscopy to visualize temporal fluorochrome label deposition in newly formed bone.

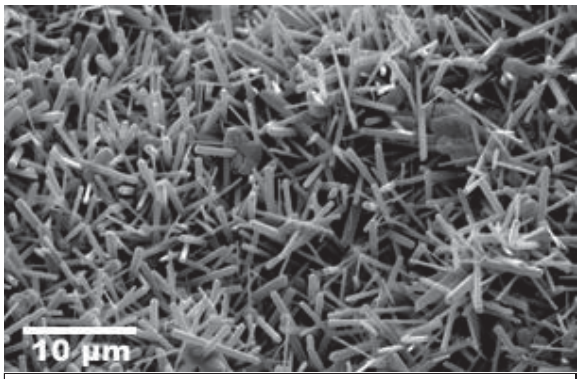

Figure 1. SEM image of sintered BCP granule surface with crystalline microstructure.

RESULTS

All surgeries and recovery were uneventful.
Post-mortem radiography of maxillary sinuses indicated good retention of BCP granules for up to 12 weeks. First results indicate considerably less graft resorption in sinus augmentation with microstructured BCP granules as compared to autogenous bone particles. Histological and histomorphometric data will be presented at NBTE conference 2016.

DISCUSSION AND CONCLUSION

Preliminary results suggest microstructured BCP granules are a suitable bone graft substitute for maxillary sinus floor augmentation.

REFERENCES

1. Yuan *et al*., PNAS 107:13614-19, 2010.

ACKNOWLEDGMENTS

The authors would like to thank the European Union's Horizon 2020 research and innovation program for the financial support to this project (grant agreement no. 674282).

Tuning the resorption and bone regeneration potential of β-tricalcium phosphate ceramics via the dimension of their surface microstructure

Rongquan Duan[1,2,#], Davide Barbieri[2,#], Florence de Groot[2], Joost D. de Bruijn[1,2], Huipin Yuan[2,3,*]
[1]Biomaterial Science and Technology, MIRA, University of Twente, Enschede, the Netherlands;
[2]Xpand Biotechnology BV, Bilthoven, the Netherlands;
[3] CTR&IBE, MERLN Institute, Maastricht University, Maastricht, the Netherlands
[#] These authors contributed equally to this work; * Corresponding author: h.yuan@maastrichtuniversity.nl

INTRODUCTION

Calcium phosphate (CaP) ceramics are widely used in clinics as bone void fillers, and their bone forming capacity depends on their physicochemical properties.[1] In particular, reducing the dimension of the grain surface structure of CaP ceramics was already shown to enhance their resorption and bone formation potential in spinal site.[2] In this study, we aimed at further exploring the performance of three CaP ceramics with various surface grain dimensions in a well-established rabbit condyle bone defect model.[3]

EXPERIMENTAL METHODS

Three CaP ceramics were used in this study: Chronos (Synthes, 1.4-2.8mm) and Osferion (Olympus, 1-3mm) were used as purchased, while TCP-S (1-2mm) was prepared as described previously.[2] They were characterized with XRD (chemistry), SEM (surface structure), mercury intrusion (microporosity and surface area). Calcium ion release, protein adsorption and bioactivity (formation of apatite layer in simulated body fluid) were evaluated *in vitro*. Each material (0.3cc, n=8) was implanted in lateral femoral condyle defects (Ø6×10mm) of New Zealand white rabbits (≥3 kg). At each end point (4, 12 and 26 weeks), animals were sacrificed and the explants were subjected to radiological and histological evaluations (non-decalcified; methylene blue/basic fuchsin). Histomorphometric analysis was done to quantitatively determine the bone formation and material resorption.

RESULTS AND DISCUSSION

XRD (Fig. 1A) confirmed that the three materials have identical chemistry (β-tricalcium phosphate, β-TCP). Quantitative measurements from SEM imaging shows that, despite their similar grain-like texture (Fig. 1B), the three materials had different grain size (Table 1). Mercury intrusion revealed that TCP-S has submicron-sized pores (Fig. 2A), which increased its surface area. This led to more protein adsorption (Fig. 2B), faster release of calcium ions (Fig. 2C) and better surface mineralization (Fig. 2D) of TCP-S compared to the other two ceramics.

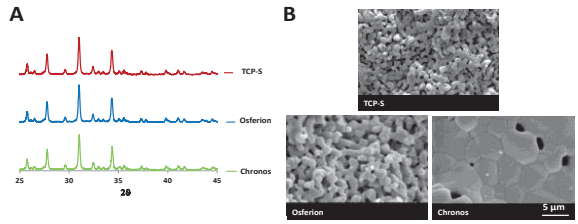

Figure 1. *(A) XRD showing the chemistry of the three ceramics; (B) SEM images showing the different surface structure of the ceramics.*

Table 1. *Grain size of the three ceramics.*

	TCP-S	Osferion	Chronos
Grain size (μm)	0.77±0.21	1.21±0.35	4.87±1.24

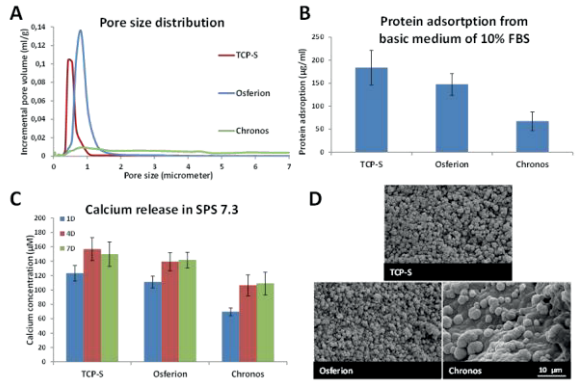

Figure 2. *(A) distribution of the surface pore dimension; (B) amount of proteins adsorbed into implants (1 ml) from basic medium after 4-day incubation; (C) calcium ion release from the materials into SPS at day 1, day 4 and day 7; (D) apatite formation on the surface of three CaP ceramics after soaking in SBF for 1 day.*

As shown in Figure 3, bone formation and ceramic resorption occurred in all the three materials. However, quantitatively, TCP-S implants formed most bone tissue and underwent most resorption, followed by Osferion and Chronos. This indicates a close relationship between the materials' performance and their surface grain size.

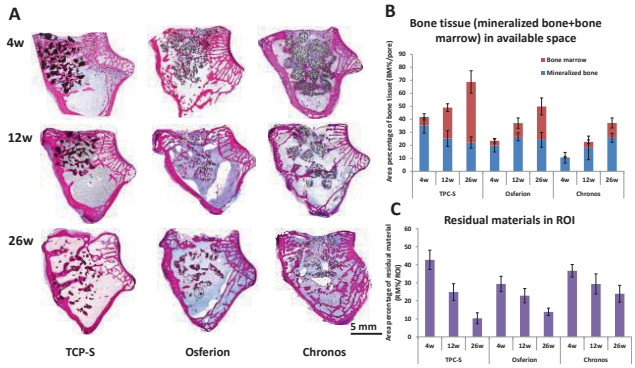

Figure 3. *Bone regeneration of histological overview (A); the area percentage of bone tissue (mineralized bone + bone marrow) (B) and residual materials (C) in the available spaces of the CaP material implants.*

DISCUSSION AND CONCLUSION

Our results suggest that tuning the dimension of the surface structure of CaP ceramics is a promising method to regulate not only the bone regeneration but also the resorption of the materials.

REFERENCES

1. Yuan *et al.*, PNAS 107:13614-19, 2010.
2. Duan *et al.*, J Orthop Res. 2016. DOI: 10.1002/jor.23201.
3. Chen *et al.*, Biomedical Engineering 24: 537-548, 2012.

ACKNOWLEDGMENTS

The authors would like to thank the Netherlands Institute for Regenerative Medicine (NIRM) and Rapid Prototyping of Custom-Made Bone-Forming Tissue Engineering Constructs (Rapidos) projects for their financial support to this project.

Size-Controlled Nanogels for Drug Delivery and Imaging

M.R. Elzes, A.C.A Doensen, J.M.J. Paulusse
Department of Biomaterials Science and Technology, MIRA Institute for Biomedical Technology and Technical Medicine, Faculty of Science and Technology, University of Twente, P.O. Box 217, 7500 AE Enschede, The Netherlands

Introduction

The size of nanoparticles is known to dramatically affect biological processes such as cellular uptake, tissue/tumor penetration and immune response.[1,2] For example, nanogels of 30 nm are frequently reported as optimally-sized nanogels for tumoral drug delivery.[3] In order to take full advantage of this effect, nanogels between 10 and 100 nm should be prepared and evaluated, however these sizes remain a challenge using conventional preparation techniques such as emulsion polymerization. We use the approach outlined in Fig. 1; by performing controlled radical polymerization using a monomer and crosslinker, nanogels with various sizes are formed after different reaction times.

Results and discussion

Using our aggregation polymerization approach, nanogels sized between 10 and 120 nm were obtained, growing exponentially with monomer conversion (see Fig. 2). Various monomers were employed to achieve different properties, such as 2-(dimethylamino)ethyl methacrylate (DMAEMA) for cationic nanogels, and polyethylene glycol methacrylate (PEGMA) for high biocompatibility. Other monomers like the temperature responsive *N*-isopropylacrylamide (NIPAM) can also readily be polymerized to form nanogels.

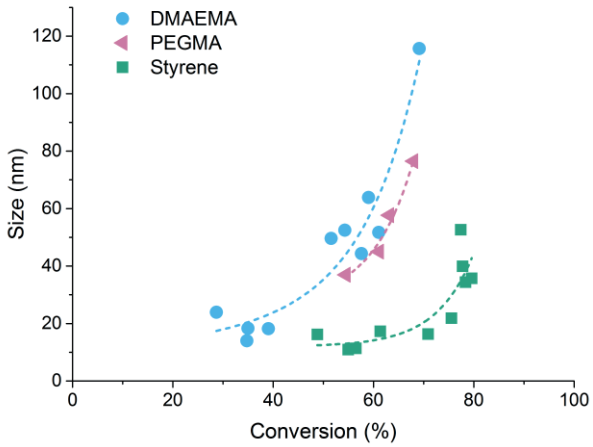

Figure 2. *Size vs. conversion plot using three monomers.*

Conclusions

A method to prepare nanoparticles with good control over particle size has been successfully developed and used to obtain nanogels with different properties. This approach is highly versatile and can be used in combination with almost any vinyl monomer.

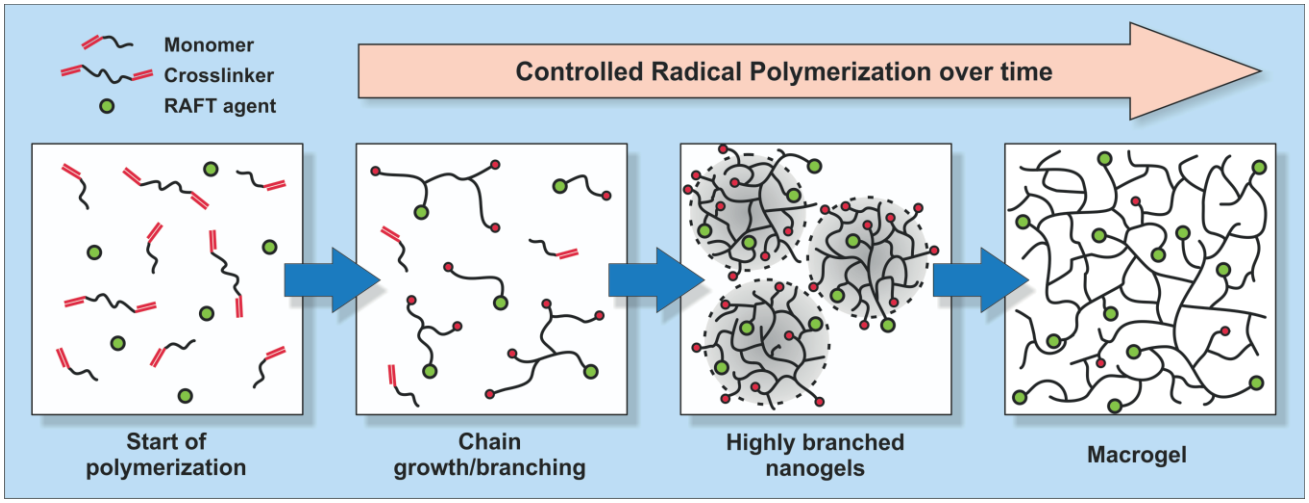

Figure 1. *Aggregation polymerization approach to prepare size-controlled nanogels, by controlled radical copolymerization of monofunctional vinyl monomer and difunctional crosslinker. Quenching the polymerization at different timepoints yields nanogels with various sizes.*

References

(1) Zhang, S.; Gao, H.; Bao, G. *ACS Nano* **2015**, *9*, 8655.
(2) Kiessling, F.; Mertens, M. E.; Grimm, J.; Lammers, T. *Radiology* **2014**, *273*, 10.
(3) Cabral, H.; Matsumoto, Y.; Mizuno, K.; Chen, Q.; Murakami, M.; Kimura, M.; Terada, Y.; Kano, M. R.; Miyazono, K.; Uesaka, M.; Nishiyama, N.; Kataoka, K. *Nat. Nanotechnol.* **2011**, *6*, 815.

Injectable hydrogels comprising collagen I based recombinant peptide microspheres loaded with BMP2 promote ectopic bone formation

S. Fahmy-Garcia[1,2]; D. Mumcuoglu [1,3]; L. de Miguel [3]; V. D. Dieleman [4]; B.C.J van der Eerden [2]; D. Eglin [5]; S.G.J.M. Kluijtmans [3]; G.J.V.M van Osch [1,6] and E. Farrell [4]
[1]Department of Orthopaedics, [2]Department of Internal Medicine, Erasmus MC, Rotterdam, The Netherlands.
[3]Fujifilm Manufacturing Europe B.V, Tilburg, The Netherlands.
[4]Department of Oral and Maxillofacial Surgery, Special Dental Care and Orthodontics, Erasmus MC.
[5]AO Research Institute Davos, Davos, Platz, Switzerland.
[6]Department of Otorhinolaryngology, Head and Neck Surgery, Erasmus MC.

Introduction: The goal of bone tissue engineering is to use biomaterials, cells and signaling molecules capable of inducing bone formation. Systems derived from polysaccharides and natural proteins are ideal scaffolds for tissue engineering since they mimic the extracellular matrices. In this study, we used Collagen type-I Based Recombinant Peptide (RCP) microspheres developed by Fujifilm loaded with rhBMP-2, a well-known growth factor involved in bone regeneration, and included them in various hydrogels to generate an injectable rhBMP-2 delivery system. The used hydrogels were thermoresponsive hyaluronic acid (HA) and two alginate types with different physicochemical characteristics (sterile lyophilized high mannuronate (SLM) alginate and sterile lyophilized high guluronate (SLG) alginate). The goal of this study was to determine the most biocompatible injectable microsphere/hydrogel system in terms of host reaction, vascularization and bone formation in a cell-free system.

Methods: Twenty four 10-week-old male Sprague Dawley rats were used. Alginate SLG, Alginate SLM (Novamatrix, Sandvika, NO) or poly(*N*-isopropylacrylamide) hyaluronic acid hydrogels (kindly provided by D. Eglin, AO Research Institute Davos, CH) containing RCP microspheres (Fujifilm, Tilburg, NL) loaded with a constant concentration of rhBMP-2 (3.5 µg per injection) were subcutaneously injected (n=6 per condition). At the end of week 1, 4 and 10, eight animals were euthanised using CO_2. All implants were harvested and scanned using micro-CT to evaluate the formation of mineralised tissue. Implants were paraffin embedded and processed. Blood vessels, TRAP-positive cells and CD68-positive cells were counted in a blinded fashion.

Results: Both injectable alginate gels with microspheres containing rhBMP-2 promoted ectopic bone formation, but the thermoresponsive HA did not. More than 95% of the injected formulations were retrieved at each time point. At week 1, cellular infiltration was visible in all the implanted formulations, even though the hydrogels were not degraded yet. At 4 weeks mineralised tissue was observed by micro-CT in most of the implants, especially at the edges or the areas where the hydrogel started to break down. At 10 weeks, bone formation was assessed in all of the alginates by histology. However, in the HA formulations, although calcified tissue was detected on the micro-CT scans, no bone structure was observed by histology. Moreover, it is important to highlight that although no major differences in calcified tissue volume were observed between 4 and 10 week scans in the alginate SLM formulation, alginate SLG showed a 5 fold increase in the amount of calcified tissue from 4 week scans to 10 weeks ($p < 0.05$). In addition, bone marrow was observed and neovascularisation within the formulations increased over time. The number of CD68 positive cells decreased over time in the alginate implants. However, when thermoresponsive HA was used as hydrogel, a delay in macrophages recruitment was observed, showing the peak in CD68 positive cells infiltration at 10 weeks ($p < 0.01$ compared to the infiltration observed at both, 1 and 4 week.

Discussion & Conclusions: This work has shown that the use of rhBMP-2 loaded RCP microspheres contained within alginate hydrogels promotes subcutaneous ectopic bone formation. However, when HA was used as hydrogel, most gel had disappeared within the first weeks and no bone formation was observed. Furthermore, for these HA formulations, macrophage-osteoclast cell lineage infiltration increased over time, contrary to what happened with alginate formulations. The physical-chemical properties of the HA implant may have perturbed the natural cascade of key events needed for bone formation. Previous studies used hydrogel-microspheres combination with the addition of osteoprogenitor cells to trigger bone formation [1-2]. In accordance with these studies, bone formation had been achieved using alginate formulations implanted in a subcutaneous environment without further need of adding cells.

A major limitation of the commonly used release systems is the difficulty to modulate the release of the growth factors or signaling molecules to maintain their actions for a long time period. A combination of alginate hydrogels and collagen I based recombinant peptide beads might help to overcome this problem. Our data further demonstrate the importance of the choice of gel in this composite system.

References: 1 He, X., Dziak, R., et al (2013). Tissue Eng Part A 19(3-4): 508-518.
2 Moshaverinia, A., Ansari S., Chen C., et al (2013). Biomaterials 34(28): 6572-6579.

Acknowledgments: BioInspire Marie Curie Action (FP7/2007-2013, grant agreement n° 607051).

Using the high throughput generated micro-aggregates as a model to investigate the underlying mechanisms of cartilage matrix formation

Y. Fu, S.J.Henke, S.K. Both, H.B.J. Karperien.
Developmental Bioengineering, University of Twente, Enschede, the Netherlands

Introduction

Cell-based cartilage repair strategies such as matrix-induced autologous chondrocyte implantation (MACI) could be improved by enhancing cell performance. Aggregation of chondrocytes is a well-studied phenomenon that enhances the chondrogenic phenotype. The traditional way of aggregation is generate a micromass. More recently, highly controlled micro-aggregates that induce maximal cartilaginous matrix deposition per chondrocyte are formed by using a platform. Compared to the transitional pellet, cells in the micro-aggregates can communicate with each other in different ways. To determine the cell activation and communication method, we introduce the micro-aggregates to the co-culture system and use it as a model to investigate the underlying mechanisms of cartilage matrix formation.

Materials and methods

Human bone marrow mesenchymal stem cells (hMSCs) and bovine primary chondrocytes (bPCs) were isolated as previously reported. We then formed micro-aggregates of 100 cells with highly controlled size, stability and viability. Different micro-aggregates were generated with mixed hMSCs and bPCs at the ratio of 80/20 or pure cells separately. These three kind of micro-aggregates were then cultured in 3D after encapsulation in agarose *in vitro*. Single cells in same conditions also seeded in agarose. For each group, different series of cell concentrations were set for 1, 3, 10, 20 million cells/mL in agarose. With the different cell concentrations, we can investigate the methods different cells communicate with each other.

To tracking the cell assembly, different cells were labeled with fluorescence dyes. EdU and TUNEL staining were then evaluated and quantified for the positive cells. Histology staining and gene expression were analyzed to investigate the matrix formation and underlying biomolecular mechanisms.

Results and discussion

Histological and biochemical analysis demonstrated enhanced matrix deposition in constructs seeded with micro-aggregates, compared to single-cell seeded constructs. Compared to the pure cells group, the mixed cell groups produced similar matrix with less amount of chondrocytes which is corresponding with pellet co-culture system. The histological analysis showed pure hMSCs samples from single cells group reveal the formation of cartilage matrix while the cells in the micro-aggregates samples were dead and no sign of matrix formation. In 3D pellet co-culture system, the MSCs dead while the matrix produced from chondrocytes were promoted. The further step for this study is to determine the cells status and underlying mechanisms in the micro-aggregates model.

Currently EdU/TUNEL staining and gene expression analysis of samples are performed which will be reported upon during the meeting.

Conclusion

This research revealed that high throughout generated micro-aggregates can effectively accelerate hyaline cartilage formation and act as a model to investigate the underlying mechanisms.

Key words

Micro-aggregates, matrix formation, biomolecular mechansim

Development of a Human Reporter Cell Line for Medium-throughput Evaluation of Chondrogenic Activity

João Pedro Garcia[1], Luca Braccioli[2], Laura Creemers[1]
[1]Department of Orthopedics, UMC Utrecht, The Netherlands
[2]Department of Cell Biology, UMC Utrecht, The Netherlands

Introduction. Affecting more up to 30 % of the world's population, musculoskeletal diseases such as chronic low back pain (CLBP) and Osteoarthritis (OA), are the leading causes of morbidity and a major economic burden in the Western world[1]. While the specific mechanisms are not known yet, it is widely accepted that CLBP and OA are caused by degeneration of the intervertebral disc and articular cartilage, respectively. Systemic administration of drugs proves to be ineffective due to rapid clearance and low vascularization of both tissues, and local administration is also known to be suboptimal due to fast clearance[2]. Hence, there is an increasing interest in the development of liposome- and polymer-derived delivery platforms that allow for sustained release of drugs and prolonged therapeutic effect, allowing for lower drug concentrations and less frequent administrations[2].

The development of proper *in vitro* models for drug testing is critical for the translation of new therapies from bench to the bedside. *In vitro* assays capable of characterization of the biological response are of great use for medium- to high-throughput screening of such delivery systems[3].

Here we describe a reporter cell line based on the C-28/I2 chondrocytic cell line[4] harboring a luciferase gene under control of a sequence containing four tandem 48-bp chondrocyte-specific enhancer segments of type II collagen α1 (4Col2E)[5], which is one of the main matrix components of both cartilage and IVD. This cell line can be used to easily and rapidly measure regenerative effects of chondrogenic inducers through luciferase activity. In future studies, this reporter cell line will be incorporated in bioactivity assays for medium-throughput evaluation of different drug delivery systems for further tailoring and optimization of their properties.

Materials and Methods. *Generation of the 4Col2E-Luc C-28/I2 reporter cell line.* The human chondrocytic cell line C-28/I2 was a generous gift from Mary B. Goldring (Hospital for Special Surgery, New York, USA). The 4Col2E-Luc construct was a generous gift from Shuki Muramatsu (Asahi Kasei Pharma Corporation, Fuji, Japan). The 4Col2E-Luc fragment cloned into a pLenti X1 Puro (Addgene) destination vector using Gateway Cloning (Invitrogen) and the primers described in Table 1. Along the process, correct insertion and orientation of the fragment was confirmed by sequencing (Macrogen Inc., The Netherlands). Subsequently, 5 µg of the resulting vector were mixed with the packaging vectors psPax2 and pMD2.G (Addgene) and transfected into HEK293T cells using PEI. Medium was harvested 24 hours after transfection, filtered using a 0.2 µm membrane, diluted in DMEM (1:1), supplemented with 8 µg/mL Polybrene, and added to C-28/I2 cells. Fresh medium was added to the HEK293T cells and 24 hours after the conditioned medium was added to the C-28/I2 cells. 72 hours post transfection, puromycin-resistant C-28/I2 cells were expanded and selected for 4 passages in DMEM/F-12 medium, supplemented with 10% FBS, 1% Pen/Strep, 1% ASAP and 1 µg/mL Puromycin (Invivogen).

TGF-β induction of Luciferase activity. As proof of concept, 4Col2E-Luc C-28/I2 cells were plated in 48-well plates at a density of 15000 cells/well and cultured in DMEM medium supplemented with 1% P/S for 24 hours. Subsequently medium was replaced by DMEM 1% P/S supplemented with increasing concentrations of TGF-β (0, 0.01, 0.1, 1, 10 ng/mL). Cells were harvested at 24, 48 and 72h and luciferase activity was measured using the Luciferase Assay System (Promega) according to the manufacturer's instructions. Luciferase activity was normalized to DNA content measured using the Quant-iT Picogreen assay (Invitrogen).

Statistical analysis. All data are presented as mean ± standard deviation. Statistical analysis was performed using SPSS 21 software (SPSS Inc., USA). Significant differences between the concentration groups were assessed by one-way analysis of variance followed by Tukey's post-hoc test for multiple comparisons. Normal distribution and homogeneity of variances were also verified. The level of significance was set at $p < 0.05$.

Table 1. Primers used for PCR of the 4Col2E-Luc fragment

Primers	Tm (ºC)
5' GGGGACAAGTTTGTACAAAAAAGCAGGCTTC**CTAGCTCGA GATCCTGTG** 3' (Forward)	59º
5' GGGGACCACTTTGTACAAGAAAGCTGGGTCTTA**CACGGC GATCTT TCC** 3' (Reverse)	60º

Results. The 4Col2E-Luc was successfully incorporated into C-28/I2 cells by lentiviral transduction, with 90% of the cells surviving after being selected in puromycin-supplemented DMEM. Preliminary tests with TGF-β show that the reporter cell line is responsive to growth factors. Figure 1 shows more than 1.5 fold increase in luciferase activity of TGF-β-treated cells over non-treated cells. A significant increase is seen for the first two time points (24 and 48 hours) between concentrations 0.01 and 10 ng/mL, and for 72 hours a significant difference is observed between groups 0.01/0.1 and 1/10.

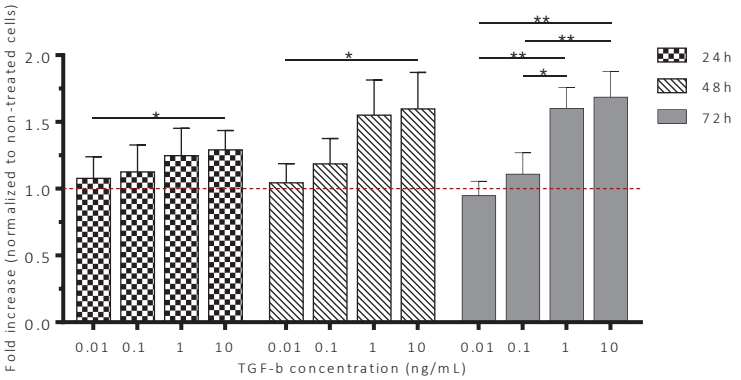

Figure 1. Luciferase activity of the 4Col2E-Luc C-28/I2 cell line upon TGF-β treatment. Fold increase in luciferase activity of TGF-β treated cells over non-treated cells at 24, 48 and 72 hours (n=3). Luciferase activity was normalized to DNA content. Dotted line represents the basal activity for non-treated cells. (* - $p < 0.05$; ** $p < 0.01$).

Conclusion and further studies. Here we describe the generation of a chondrocyte cell line responsive to chondrogenic stimuli, showing an enhanced luciferase activity with increasing TGF-β concentrations. Particularly, the cell line shows to be more responsive to prolonged exposure since differences between concentrations tend to me more significant at later time points (72 hrs). Further studies will focus on the characterization of the cell line by measuring gene expression levels and, most importantly, in increasing the sensitivity of the cell line to growth factors by modifying culture conditions. Moreover, other growth factors (i.e. BMPs) and cytokines (i.e. IL-1) will be studied for their capacity to enhance and inhibit luciferase activity, respectively. As ultimate goal we aim to determine chondrogenic bioactivity of drug-loaded nanoparticles by relating drug release with luciferase activity.

References.

1. Woolf, A. D. *et al. Bulletin of the World Health Organization* **81**, 646-656, (2003).
2. Evans, C. H. *et al. Nat Rev Rheumatol* **10**, 11-22, (2014).
3. Yang, H.-y. *et al. Pharmaceutical Research* **32**, 680-690, (2014).
4. Goldring, M. B. *et al. The Journal of Clinical Investigation* **94**, 2307-2316, (1994).
5. Lefebvre, V. *et al. Molecular and cellular biology* **16**, 4512-4523, (1996).

Design and fabrication of patient-specific osteoconductive orbital floor implants by stereolithography

M.A. Geven[1*], V. Varjas[2], D. Eglin[2], D.W. Grijpma[1,3]
[1]Department of Biomaterials Science and Technology, University of Twente, 7522 NB Enschede, The Netherlands
[2]AO Research Institute, 7270 Davos, Switzerland
[3]Department of Biomedical Engineering, University Medical Center Groningen, 7600 AD Groningen, The Netherlands
*Presenting author's e-mail address: m.a.geven@utwente.nl

Introduction.

Blow-out fractures of the orbital floor do not heal spontaneously and are still challenging to restore. The current gold standard, autograft implantation, suffers from drawbacks such as donor site morbidity and limited availability of tissue.

Synthetic implants offer an appealing alternative. Ideally these restore the orbital volume, reposition the globe accurately and allow for bone ingrowth whilst degrading over time. This requires the implant to be shaped according to the orbital floor defect, to have an interconnected porosity and to be osteoconductive.

Previously we have shown that composites of photo-crosslinked poly(trimethylene carbonate) containing nano-hydroxyapatite are promising materials for bone tissue engineering[1,2].

Here we report on the design of patient-specific orbital floor implants that precisely fit the defects and possess an interconnected porosity. These implants were subsequently fabricated by stereolithography using photo-crosslinkable poly(trimethylene carbonate) and nano-hydroxyapatite resins.

Methods.

Implant models were designed according to CT scans of orbital floor fractures. Using a semi-automated process, implant model shapes were defined according to landmarks placed around the fracture. Then, by Boolean intersection and splitting operations a supporting structure was generated for the implant model. A porosity was based on triply periodic minimal surfaces and defined mathematically. Overlap of the implant with the porosity design and subsequent Boolean intersection operations yielded a porous and supported implant model suitable for fabrication by stereolithography.

Three-armed poly(trimethylene carbonate) (PTMC) was synthesized by ring opening polymerization and was functionalized with methacrylic anhydride to yield a photo-crosslinkable macromer (PTMC-MA). This macromer was mixed with nano-hydroxyapatite, Omnirad TPO-L photo-initiator and Orasol Orange G dye into propylene carbonate to prepare a resin for stereolithography.

Stereolithography was done using an Envisiontec Perfactory$^{3®}$ SXGA^{+} Standard UV system.

Results.

The method used here to design implants allows for patient specific modification of implant structures. The semi-automated process can generate an implant shape based on a specific orbital floor defect. It furthermore allows for modifications based on the surrounding bony tissue, such as the addition of a connector which allows for immobilization of the implant on the infraorbital rim. The use of a mathematically defined model of the pore structure furthermore allows for the design of a fully interconnected pore network in the implant model, leaving a solid connector for stability. An overview of these modifications of the implant model is given in Figure 1.

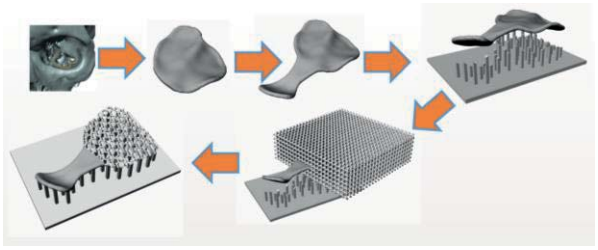

Figure 1. *Flow diagram of implant model design showing (starting from the top-left) a CT reconstruction of a patient's orbit, the generated implant, modified implant model with a solid connector, supporting structure generation, overlap with the pore structure and the porous supported implant model.*

The designed implant models could be accurately fabricated by stereolithography as shown in Figure 2.

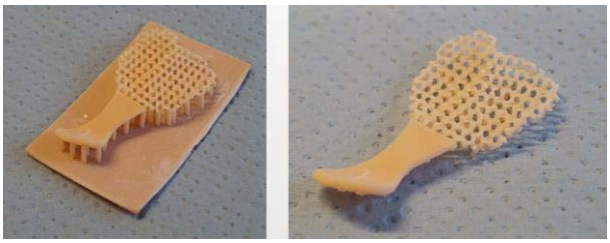

Figure 1. *Fabricated implant containing 40 wt.% nano-hydroxyapatite (left) and implant structure after support removal (right).*

Conclusions.

It was shown that models of porous and patient specific orbital floor implants can be designed to allow for fabrication by stereolithography. The designed porosity allows for bone ingrowth and was readily reproduced using a composite resin of PTMC-MA and nano-hydroxyapatite.

References.

1) Geven, M.A. et al., Polymers for Advanced Technologies, 2015, DOI: 10.1002/pat.3589
2) Guillaume, O. et al., Polymers for Advanced Technologies, 2016, DOI: 10.1002/pat.3892

Acknowledgements.

Huizhou Foryou Medical Devices Co. Ltd. provided trimethylene carbonate. XPand Biotechnology BV provided nano-hydroxyapatite. This project is funded by the FP7 EU-China RAPIDOS grant, project number 604517.

Interaction Between Mechanical Deformation and Substrate Properties on *in vitro* Cell Differentiation

H.I. Güngördü[1,2], S. Leeuwenburgh[1,2], X.F. Walboomers[1,2], J.A. Jansen[1,2]
[1] Department of Biomaterials, Radboud University Medical Center, [2]Radboud Nanomedicine Alliance, Nijmegen, The Netherlands

Introduction: Various cellular processes, like cell attachment, proliferation and differentiation can be maintained by the mechanical properties of the cell microenvironment. The extra-cellular matrix (ECM) is a dynamic factor and has a determining role in the final cell fate. Guiding cellular differentiation through modulation of the substrate stiffness was proven to be an effective method to change the stem cell fate towards osteogenesis. Moreover, mechanical loading is known to be a strong catalyst for osteogenic differentiation while tissue is being structured under physiological conditions.
Objective: In this study, we aimed to design a multifactorial system that will use mechanical loading, by substrate deformation, together with altered substrate elasticity properties. We would like to understand whether the combination of an appropriate substrate elasticity with the presence of mechanical loading could have a synergistic effect on stem cell differentiation, or otherwise what is the over-ruling mechanism that determines the in vitro cell differentiation for hard tissue regeneration.
Materials and Methods: Poly-dimethylsiloxane (PDMS, 1.5 MPa) elastomer dishes were fabricated by mixing the monomer and catalyst components in 10:1 ratio and cured overnight at RT. Poly-acrylamide (PAAm, 123 kPa) hydrogels were synthesized according to previous protocol. Following the Ar-plasma treatment and silanization of PDMS surface, PAAm hydrogel films were attached on half of the PDMS dishes and incubated overnight at 37°C. Both types of dishes were coated with collagen (50µg/ml) monomer to obtain cell attachment (Fig. 1).

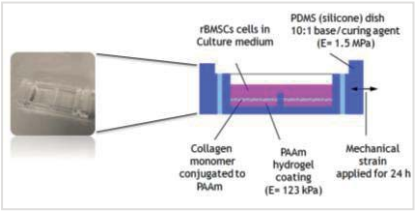

Figure 1. Illustration of the substrate preparation for stretch experiment.

Rat bone marrow-derived stem cells (BMSCs) of early passage numbers (<5) were used for all experiments. $1x10^4$ cells/cm^2 were seeded on each dish. Following 8 hours rest after the medium change uniaxial stretch was applied with the magnitude of 8% and a constant frequency of 1 Hz for 16 hours intermittently (Fig. 2).

Figure 2. Custom-made uniaxial stretch machine.

Results: Samples were collected 3 days after the mechanical loading protocol was stopped and cell nuclei and actin filaments of the cytoskeleton were visualized by DAPI and Phalloidin, respectively and imaged by CLSM (Fig. 3).

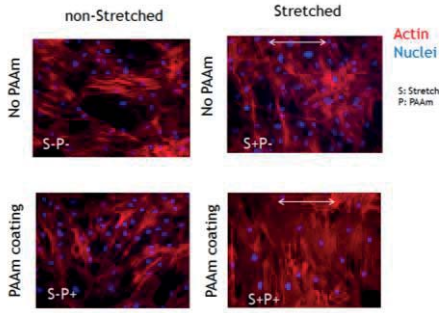

Figure 3. Fluorescent images of rBMSCs collected after mechanical deformation.

We observed higher number of cells on PDMS surface than PAAm coated substrates. Our findings show that cells were perpendicularly aligned to the stretch direction (Fig. 4).

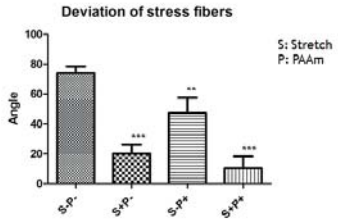

Figure 4. Deviation of stress fibers from the center.

Furthermore, the expression of the genes of interest for osteogenic, chondrogenic and adipogenic lineages as RUNX-2, ACAN and LPL was analyzed by RT-PCR. According to the RT-PCR results the expression of early osteogenic marker RUNX2 was upregulated for stretched samples without PAAm coating. Whereas no significant difference was observed between groups for chondrogenic differentiation. Lastly, PAAm coated samples with mechanical loading showed significantly different results for LPL expression (Fig. 5).

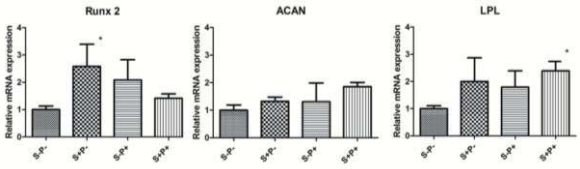

Figure 5. RT-PCR results for the samples that are collected 3 days after the finalization of stretch.

Conclusion: In conclusion, we observed that cells responded to uniaxial strain on both substrates and the strain loads were transferable to PAAm in order to align the cells towards a specific direction. Additionally, mechanical loading overruled the stiffness sensing during in vitro osteogenic differentiation of mesenchymal stem cells.

Preparation and characterization of reduced graphene oxide and poly (trimethylene carbonate) composites for nerve regeneration

Z. Guo, S. G. Rotman, D. W. Grijpma, A. A. Poot
Biomaterials Science and Technology, University of Twente, Enschede, The Netherlands.

Introduction

Although peripheral nerves are known to have some regenerative abilities, completely separated nerve ends are rarely known to restore function without medical intervention. The main scientific focus for novel treatments of peripheral nerve injury lies with a biodegradable nerve guide channel (NGC) that promotes and guides axonal regrowth, while shielding it from scar tissue ingrowth. Because electrically conductive NGCs promote axon regeneration [1], a composite material is proposed with poly (trimethylene carbonate) (PTMC) and reduced graphene oxide (rGO) as a conductive filler.

Materials and Methods

3-armed PTMC was synthesized by ring-opening polymerization of trimethylene carbonate (TMC) and subsequently functionalized with methacrylic anhydride (MA). rGO was prepared by oxidizing graphite flakes following a modified Hummer's method, exfoliated using ultrasound and finally reduced with hydrazine monohydrate. The oxidation and exfoliation to graphene oxide (GO) and the reduction to rGO was assessed by Fourier transformed infrared spectroscopy (FTIR), X-ray photoelectron spectroscopy (XPS) and atomic force microscopy (AFM). Methacrylate-functionalized 3-armed PTMC (PTMC-MA) of 20,000 g/mol were dissolved in rGO dispersions in dimethylformamide (DMF). After precipitation and re-dissolving in chloroform, PTMC-MA/rGO composites with 0, 0.5, 1, 2 and 4 wt% rGO contents were solvent cast and UV-crosslinked after evaporation of the solvent. The conductivity of the PTMC-MA/rGO composite was determined using four-probe Van der Pauw measurements. The tensile mechanical properties of PTMC-MA-/rGO composite were tested in this research. PC-12 cell was cultured on PTMC-MA/rGO composite films for checking its biocompatibility.

Results and Discussion

After exfoliation, bi- and few-layer GO was observed by AFM height profiling. FTIR and XPS results indicated a successful removal of functional oxygen groups during chemical reduction of GO to rGO. The gel content of the crosslinked PTMC-MA/rGO composites was determined to be over 84%. Water-uptake and contact angle measurements confirmed the hydrophobic nature of the PTMC chains. With increasing rGO content the contact angle of water on the film surface increased. For PTMC-MA with 2 wt% rGO content, the conductivity was determined to be 6.88×10^{-2} S/cm. These values are up to par with the work of other groups like Sayyar et al., also reaching conductivity values in the range of 10^{-2} S/cm with rGO contents up to 10 wt% [2]. The PTMC-MA/rGO films proved to be biocompatible as adhesion and proliferation of PC-12 cells was shown by CyQUANT® cell proliferation assay. The E-modulus and maximum tensile strength of PTMC-MA films with 0.5% rGO, 1%rGO and 2%rGO were close each other and all of their corresponding values were higher than PTMC-MA film. The E-modulus, maximum tensile strength and elongation at break of PTMC/r-GO film with 2% rGO was 10.2 MPa, 3.4 MPa and 96.5 %, respectively.

Conclusion

PTMC-MA/rGO composites show promise as a conductive material that has potential as a NGC material. The next step would be to develop a porous NGC using the PTMC-MA/rGO material for further in vitro and especially in vivo characterization in small animal models.

REFERENCES:

[1] Chiono, V. and C. Tonda-Turo, Trends in the design of nerve guidance channels in peripheral nerve tissue engineering. Progress in Neurobiology 2015, 131, 87-104.
[2] Sepidar Sayyar, Eoin Murray, Brianna C. Thompson, Sanjeev Gambhir, David L. Officer, Gordon G. Wallace. Covalently linked biocompatible graphene/polycaprolactone composites for tissue engineering. Carbon 2013, 52, 296–304.

cBiT - The Compendium for Biomaterial Transcriptomics

Dennie G.A.J. Hebels, Aurélie Carlier, Víctor Galván Chacón, Pamela Habibović, Jan de Boer
Department of Cell Biology-Inspired Tissue Engineering (cBITE), MERLN Institute, Maastricht University, Universiteitssingel 40, 6229ER Maastricht, The Netherlands

Introduction: Despite its great clinical success, the development of new biomaterials for clinical application is hampered by a lack of understanding the precise interaction between a cell and the surface it grows on. This surface communication can strongly impact cell shape, proliferation and differentiation which are usually key to a successful integration of a material into the host tissue. While transcriptomics-based analysis of cells grown on biomaterials can be very beneficial for understanding important signaling mechanisms, this technique is still relatively underused within biomaterial research. Moreover, linking material-specific topographical and chemical properties to gene expression data could really push the biomaterial field forward by enabling the selection of material properties with desirable biological effects. Such an interdisciplinary approach could provide a major contribution to a more efficient development of new and better materials that show an improved integration in the human body. We propose to systematically collect all data from biomaterial-based transcriptomics studies so far available together with measurements of biomaterial properties. Next, we will deposit all generated data in our Compendium for Biomaterial Transcriptomics (cBiT), a repository which will be the first specialized biomaterial-related transcriptomics database that also offers other relevant data on cell responses and biomaterial characteristics and will provide scientists with a powerful tool to improve their research.
Methods: cBiT is being developed as a publically accessible data portal where users can browse through the available studies. All study details, including material properties and culturing conditions will be indexed, enabling the use of a search engine to find specific samples matching the user's search query. Samples of interest can be marked for download and will contain the gene expression data and any measurements on associated biomaterial properties. cBiT will be able to accommodate both microarray and RNAseq data and any format of material property measurements.

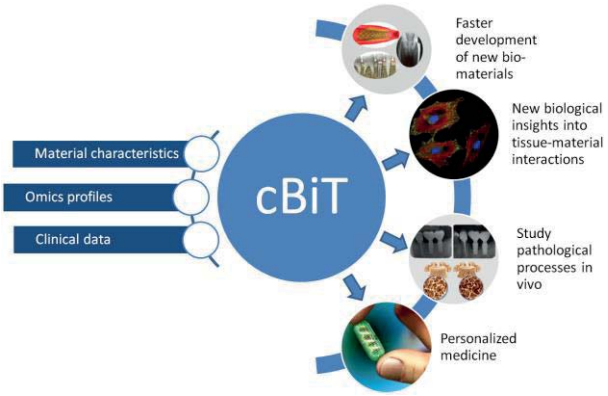

Results: So far, cBiT contains 9 microarray-based transcriptomics studies covering approximately 25 different biomaterials, several cell types (including mesenchymal stem cells and MG-63), and two species (mouse and human). cBiT is expected to go online in January 2017 and will continue to be updated with new transcriptomics-based biomaterial studies.
Conclusion: cBiT represents a new tool for material scientists and biologist that wish to use an interdisciplinary approach encompassing cell biology, transcriptomics, micro-fabrication, materials science and computational sciences. cBiT is expected to continue to grow and cover an increasing number of biomaterials and cell types. With the accumulation of data we aim to ultimately be able to predict cell responses to biomaterials which will aid in a more efficient development of new biomaterials with clinical potential.

Cell Viability in Bioprinting with Spray Deposition: Influence of the Cell Type

J. Hendriks[1], C. W. Visser[2], D.B.F. Saris[3,4], H.B.J. Karperien[1]

1 Department of Developmental BioEngineering, MIRA Institute for Biomedical Technology and Technical Medicine, University of Twente
2 Physics of Fluids Group, MIRA institute for Biomedical Technology & Technical Medicine, University of Twente, The Netherlands.
3 Department of Orthopedics, UMC Utrecht, The Netherlands.
4 Department of Reconstructive Medicine, MIRA, Faculty of Science and Technology, University of Twente, The Netherlands

Spray deposition of cell-containing liquids is a common method for the treatment of burn wounds and an upcoming technology for direct deposition of live cells for tissue regeneration. In particular, cell spraying offers a novel high-throughput method allowing for contact-free deposition of both high-viscosity liquids and hydrogels. The potential of the method was recently illustrated by construction of multi-cell tissues and layer-by-layer structures.

In cell spraying, pressurized gas and a cell-containing liquid or gel are mixed inside a nozzle, forming a cell-containing spray. However, spraying with a high input gas pressure can negatively influence cell viability after spraying. Previously, we developed and validated a quantitative model to predict the influence of the spray control parameters (liquid flow rate, liquid viscosity, and gas pressure), the nozzle-substrate distance and the substrate stiffness on cell survival. While highly predictive, these experiments were performed on a single cell type and therefore the effect of the cellular properties was not investigated. A better understanding of the effect of these properties on survival will help in a broader application of the technology.

Therefore, we investigated cell survival after spraying with 8 cell types originating from a broad range of tissues. We discovered that the cell type has a large influence on the cell survival, ranging from 40% viability in fibroblasts, to up to 90% in chondrocytes. We subsequently applied our quantitative model to explain which cellular properties could be responsible for this observed effect. In the model three important parameters were considered specific for the cell type: The cellular diameter, the apparent viscosity and the membrane expansion at which rupture occurs (critical membrane expansion). Applying these parameters to our survival data could explain the difference between the cell types.

With this in mind, we performed subsequent experiments in which the cellular properties of a fibroblast cell line (3T3) were carefully by adjusting osmolality and membrane cholesterol content. The results confirm that the cellular properties can strongly influence the cell survival after spraying. Also, it shows that these properties can be adjusted allowing for exiting possibilities to improve cell spraying applications.

In conclusion, we show the influence of both spray control parameters and the cell type on survival after spraying. Using our model we were able to predict which cell properties were responsible for the cell dependent effect. We subsequently show that we can adjust these properties leading improved survival outcomes. Our approach allows to rationally optimize both spray control parameters and cellular properties for tissue regeneration purposes and provide practical suggestions to improve the cell viability in cell spraying.

Supramolecular functionalization of thermoplastic elastomers for tissue engineering

B.D. Ippel[1,2], E.E. van Haaften[1,2], C.V.C. Bouten[1,2], P.Y.W. Dankers[1,2]
1 Laboratory for Cell and Tisuse Engineering, Departement of Biomedical Engineering, Eindhoven University of Technology, PO Box 513, 5600 MB, Netherlands
2 Institute for Complex Molecular Systems, Eindhoven University of Technology, PO Box 513, 5600 MB, Netherlands

Introduction

Materials used for *in-situ* tissue engineering require easy tunability. Cellular response to these materials and mechanical properties are key in developing new biomaterials. Here, biodegradable polycarbonate (PC-BU) and polycaprolactone (PCL-BU) based thermoplastic elastomers containing a supramolecular bisurea motif are functionalized in a modular fashion. Incorporation of additives occurs through strong and directional non-covalent interactions between matching bisurea motifs[1]. In the studies described here, two types of additives are studied for their supramolecular **incorporation** and **functionality**:
For 1. Modulation of cell adhesive properties
and 2. Tuning mechanical properties.

1. Modulation of cell adhesive properties

Three designs of molecules containing poly (ethylene glycol) (PEG) chains and bisurea motifs, where the ratio of bisurea to PEG differs were studied to modulate cell adhesion on our elastomeric materials.

Incorporation: AFM analysis

Supramolecular incorporation of the PEG-additives was investigated using tapping mode atomic force microscopy. In the phase images, the self-assembling fibrous structure of defined bisurea containing polymers can be observed. Upon incorporation of 2 mol% PEG-additives, the morphology of these nanofibers changes, but is not lost. Evidence for PEG-rich domains within the fibrous surface is also present.

Functionality: Reducing cell adhesion

Human venous saphena cells (HVSC) were cultured on dropcast films of PCL-BU and PC-BU with increasing concentrations of PEG-additives for 24 hours. The additives with more PEG inhibited cell adhesion allready at 2 mol%, for the additive with the least amount of PEG, cells did not adhere when 4 mol% was incorporated.

2. Tuning mechanical properties

Increasing the hard-block (*i.e.* bisurea) to soft-block (*i.e.* backbone polymer) ratio in thermoplastic elastomers will increase stiffness. In our materials this can be achieved without changing the M_w of the soft-block and withouth introducing an extra crystalline phase using a small bisurea filler molecule[2].

Incorporation: DSC analysis

Supramolecular incorporation of the filler molecule was investigated using differential scanning calorimetry. A single melting peak for the hard-phase in the material indicates a single hard-phase and therefore intimate incorporation of the filler molecule in the stacks of the base material.

Functionality: Increasing Young's modulus

The Young's modulus of dropcast films of PCL-BU and PC-BU with and without 15 mol% bisurea-filler, was investigated using uniaxial tensile testing, where digital image correlation techniques were employed to characterize the true strain in the material. The Young's modulus increased significantly upon incorporation of the bisurea-filler molecule.

Conclusion

Both the PEG-bisurea additives and the bisurea-filler molecule are shown to be incorporated in the material through supramolecular interactions. Using the PEG-additives, non-cell adheisve properties can be added to bisurea containing thermoplastic elastomers and with incorporation of the bisurea-filler molecule, the stiffness of the bulk material can be increased significantly.

References

(1) Koevoets, R. a.; Versteegen, R. M.; Kooijman, H.; Spek, A. L.; Sijbesma, R. P.; Meijer, E. W. Molecular Recognition in a Thermoplastic Elastomer. *J. Am. Chem. Soc.* **2005**, *127* (9), 2999–3003.

(2) Wisse, E.; Govaert, L. E.; Meijer, H. E. H.; Meijer, E. W. Unusual Tuning of Mechanical Properties of Thermoplastic Elastomers Using Supramolecular Fillers. *Macromolecules* **2006**, *39* (21), 7425–7432.

High throughput production of cell laden microgels using in-air microfluidics

L.P. Karbaat, T. Kamperman, C.W. Visser*, S.K. Both, P.J. Dijkstra, M. Karperien
Department of Development BioEngineering, University of Twente, Drienerlolaan 5, 7522 NB Enschede

Introduction

Microfluidic chips can be used to produce hydrogel droplets. They are versatile, can be used with many different materials and offer a precise control over the shape and size of the produced gels. However, their low throughput and clogging problems make them unsuitable for the production of large amounts of gels for use in clinical practice.
In-air microfluidics (IAMF) is a novel technique offering the versatility of microfluidic chips, without wielding their disadvantages. In IAMF two reacting liquid jets are merged in air to produce fibres or droplets (see figure 1).

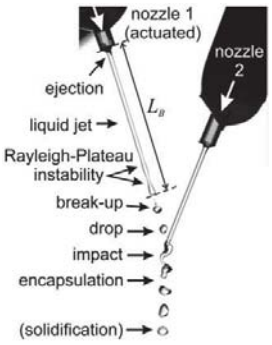

Figure 1, the principle of IAMF. Jet 1 is actuated by a piezo element, resulting in uniform breakup of the jet. The droplets merge in air with jet 2 containing a solidifier. Due to the difference in surface tension between them, jet 2 encapsulates the droplets from jet one (Marangoni effect) and solidifies the droplets in air.

The production speed of gels is 100x higher than that of microfluidic chips, while it still offers control over the shape and size of the particles. Additionally, since all solidification reactions occur in air, clogging does not occur. IAMF, with its high throughput and precise control, offers the possibility to produce a large amount of cell laden microgels for use in clinical practice.
In this work we show that cell laden alginate and calcium chloride precursor solutions can successfully be used for the fabrication of cell laden microgels using IAMF.

Materials and methods

Cell culture

3T3 cells are kept in culture medium (DMEM, 10% FBS, 100U/ml penicillin, 1mg/ml streptomycin)

IAMF

Jet 1; 0.5 w/v% sodium alginate, 5 or 10 w/v % dextran in culture medium
Jet 2; 0.1M CaCl in 10 v/v% ethanol

Results

The production of cell laden microgels using alignate/CaCl precursor solutions is possible. Uniform droplets are formed with concentrations up to 1 million cells per ml gel precursor (see figure 2 and 3). These gels contain on average 2-3 cells/gel. Above 1 million cells/ml the droplet this number rises, but the breakup is disturbed and non-uniform droplets are formed, resulting in an increase in size variation.

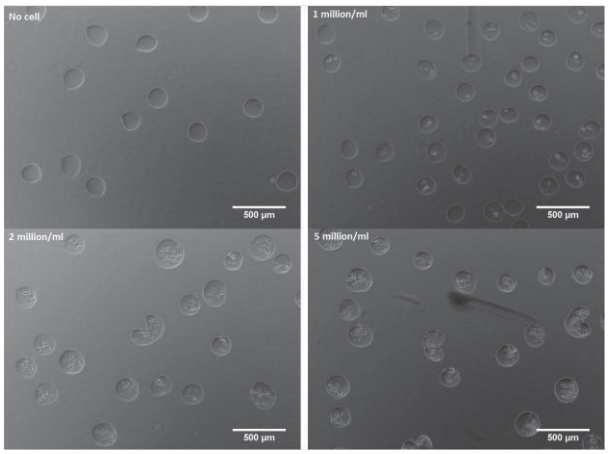

Figure 2, alginate/dextran cell laden microgels with differing cell concentrations.

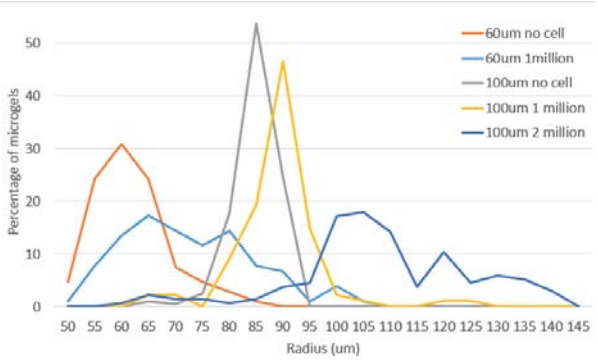

Figure 3, size distribution of cell laden microgels.

Discussion

The production of large quantities of cell laden microgels for clinical applications is possible using IAMF. Using concentrations up to 1 million cells/ml it is possible to create microgels of a uniform size and shape. Above this number, the hetreogenicity of the microgels increases due to a disturbed jet breakup. Although the exact mechanism is unknown, the presence of the cells hinders the actuation of the jet, thereby preventing a uniform breakup. Other factors influencing the properties of cell laden microgels are the size of the nozzle, the jet impact angle.

Conclusion

IAMF is a fast technique for production of cell laden microgels. Up to 1 million cells/ml we can successfully produce uniform alignate/dextran microgels containing 2-3 cells/gel.

Outlook

Since in clinical applications the treatment volumes are often limited, optimization of the cell/gel ratio is crucial. Increasing the amount of cells while keeping the result reproducible opens the way for IAMF to be used in clinical practise.

* Lewis Lab, Harvard School of Engineering and Applied Sciences, 29 Oxford Street, Cambridge, MA 02138

Allogeneic chondrogenically differentiated human bone marrow stromal cells do not induce complete dendritic cell maturation *in vitro*

C.H. Kiernan[1, 3], A. Kleinjan[2], M. Peeters[3], E.B. Wolvius[3], P.A.J. Brama[1], E. Farrell[3]

[1] Veterinary Clinical Sciences, School of Veterinary Medicine, University College Dublin, Dublin, Ireland, [2] Department of Pulmonary Medicine and [3]Department of Oral and Maxillofacial Surgery, Erasmus MC, University Medical Centre, Rotterdam, Netherlands

Introduction

Bone marrow stromal cell (BMSC) mediated endochondral bone formation may be a promising alternative to the current gold standards of autologous bone transplantation, in the development of novel methods for bone repair. Our group has previously shown that implantation of chondrogenically differentiated BMSCs, leads to bone formation *in vivo* [1]. The success of this bone formation in an allogeneic system relies on the host's endogenous cells, however, little is known about the specific immune cells involved in this process. We have shown that allogeneic chondrogenically differentiated BMSCs do not induce T cell responses *in vitro* [2]. Dendritic cells (DCs) are highly specialised antigen presenting cells with a fundamental role in priming T cell responses [3]. We hypothesised that T cells might ultimately be indirectly activated by DCs that have encountered allogeneic chondrogenic BMSCs. Therefore, the aim of the current research was to access the effect of chondrogenically differentiated BMSCs on the maturation and function of DCs.

Methods

Human BMSCs were differentiated in chondrogenic medium supplemented with TGFβ3 for 10 days. DCs were isolated from the CD14+ population of peripheral blood mononuclear cells and cultured in medium containing GM-CSF (50ng/ml) and interleukin-4 (10ng/ml) for 5 days. DCs were matured using lipopolysaccharide (100ng/ml) for 24 hours. Immature DCs were maintained for a further 24 hours in culture medium without LPS. Immature and LPS-matured DCs (1 x 10^6) were co-cultured with chondrogenic hBMSCs (0.2 x 10^6) for 24, 48 and 72 hours. The DCs were characterised by flow cytometry for CD80, CD86 and HLADR. The mean fluorescence intensity (MFI) of FITC-dextran was measured to quantify antigen uptake capacity. DC migration to CCL21 was performed in transwells. IL-6 and IL-12 ELISA was performed on supernatants. CD11c immunostaining was performed on chondrogenic hMSCs pellets. All data was analysed using a linear mixed model with Bonferroni post-test or an unpaired t-test. $P<0.05$ was considered to be statistically significant.

Results

Following 24 hours in co-culture, the levels of CD80, CD86 and HLADR were mildly but significantly increased in immature DCs cultured with allogeneic chondrogenic hBMSC pellets. This trend was maintained for at least 48 hours in co-culture. This minor increase represented about 10-40% of the LPS-induced response. The expression of CD80, CD86 and HLADR was unaffected in LPS-matured DCs cultured with chondrogenic hBMSC pellets over time. Allogeneic chondrogenic hBMSC pellets again mildly but significantly induced FITC-dextran uptake in immature DCs following 24 hours in co-culture and no difference between conditions was observed at 48 hours. Allogeneic chondrogenic hBMSC pellets had no significant effect on LPS-matured DC antigen uptake. DC migration was unaffected by allogeneic chondrogenic hBMSC pellets over time (both immature and LPS-matured DCs). IL-6 was significantly secreted in supernatants from cultures of LPS-matured DCs and allogenic chondrogenic hBMSC pellets after 24 hours in co-culture and this continued over 48 and 72 hours of co-culture. At mRNA level, IL-6 expression was found to be significantly expressed by allogeneic chondrogenic hBMSC pellets from the culture with LPS-matured DCs. IL-12 was secreted at higher levels in supernatants from co-cultured LPS-matured DCs and chondrogenic hBMSC pellets following 48 and 72 hours.

Discussion and conclusion

The characteristics of a fully mature DC are defined as cell surface expression of maturation markers, presentation of antigen and induced migration. While allogeneic chondrogenic BMSC pellets mildly but significantly affected maturation and antigen uptake after 24 hours in co-culture, this mild induction of activation was largely inferior to LPS-induced maturation, and no migration was induced. Therefore, complete maturation of immature DCs was not influenced by allogeneic chondrogenic hBMSC pellets. IL-6 appears to be an important cytokine secreted by allogeneic chondrogenic hBMSC pellets in response to LPS-matured DCs. Overall, This study demonstrated that allogeneic chondrogenic hBMSC pellets do not induce DC maturation *in vitro*. Due to the small but very reproducible responses from the DCs following 24 hours in co-culture, further studies are required to investigate whether these DCs exposed to the chondrogenically primed BMSCs will activate third party cells and how this would affect BMSC-mediated endochondral bone formation.

References

1. Farrell, E, et al., *BMC Musculoskeletal Disorders*, 12(31), 2011.
2. Kiernan, CH, et al., *Cytotherapy*, 18(8):957-969, 2016
3. Rossi, M & Young, JW, *J Immunology*, 175(3): 1373-81, 2005

Bottom-Up Tissue Engineering as an *in vitro* Vascularization Strategy

A. M. Leferink[a], M. P. Tibbe[a], E. G. B. M. Bossink[a], L. E. de Heus[a], L. I. Segerink[a], R. K. Truckenmüller[b], A. van den Berg[a], L. Moroni[b]

a The BIOS Lab-on-a-Chip Group, MESA+ Institute for Nanotechnology and MIRA Institute for Biomedical Technology and Technical Medicine, University of Twente, Enschede, The Netherlands

b Department of Complex Tissue Regeneration, MERLN Institute for Technology-Inspired Regenerative Medicine, Maastricht University, Maastricht, The Netherlands.

Corresponding Author: a.m.leferink@utwente.nl

Introduction

Angiogenesis remains a challenge of vital importance in *in vitro* tissue- and tumor engineering (TE) approaches [1]. Till date, artificial non-vascularized 3D *in vitro* cultured tissues are reported to retain their viability for constructs up to 600 µm in diameter. Recently, we have shown a novel bottom-up approach to overcome this limitation [2]. By combining SU-8 based engineered micro-objects with bone marrow stromal cells (hMSCs) *in vitro*, mm-sized viable tissue constructs were obtained with a shown homogenous distribution of the cells throughout the construct.

Method

Here, we report a novel method to fabricate micro-objects with several well-defined shapes (e.g. cubes, donuts) based on medical-grade poly (D,L-lactic acid) (PDLLA) to allow for clinical translation in a later phase. Hot embossing technology and oxygen etching are applied to obtain an array of free-standing objects (in the size range of 20-100 µm). The objects act both as spacer and as scaffolding material for cells without limiting the remodeling capacity while simultaneously lowering the required number of cells to obtain constructs of clinically relevant size (>600 µm). Although we have observed high viability in large aggregates in previous work, the need for vascularization remains in approaches to further scale-up the size of cultured tissues.

Results

Human umbilical vein endothelial cells (HUVECs) were added to multiple small aggregates of hMSCs and PDLLA-based micro-objects. The effect of the ratio of cells to objects on cell viability and aggregation behavior was studied. The cellular distribution was monitored by applying cell tracker dyes during 14 days. Histological analysis revealed that the aggregates showed a homogeneous distribution of cells between the micro-objects without indications of a necrotic core. By fluorescence microscopy, some alignment of HUVECs could be observed on the surface and through the cultured tissue construct.

Conclusion

Although no lumen is yet observed, the self-organized alignment of HUVECs on and in between hMSCs-based aggregates could be considered a first step towards vascularization.

References

[1] S. Almubarak, H. Nethercott, M. Freeberg, C. Beaudon, A. Jha, W. Jackson, *et al.*, "Tissue engineering strategies for promoting vascularized bone regeneration," *Bone,* vol. 83, pp. 197-209, Feb 2016.

[2] A. Leferink, D. Schipper, E. Arts, E. Vrij, N. Rivron, M. Karperien, *et al.*, "Engineered micro-objects as scaffolding elements in cellular building blocks for bottom-up tissue engineering approaches," *Adv Mater,* vol. 26, pp. 2592-9, Apr 23 2014.

Design of Polyisocyanopeptide (PIC) Hydrogels with Biomimetic Mechanics for 3D In-Vitro Stem Cell Culture

K. Liu[1,2], S. M. Mihaila[2], E. Oosterwijk[2], P. H. J. Kouwer[1] and A. E. Rowan[1,3]

1. Institute for Molecules and Materials, Radboud University, Nijmegen, The Netherlands

2. Department of Urology, Radboud Institute for Molecular Life Sciences, Nijmegen, The Netherlands

3. Australian Institute for Bioengineering and Nanotechnology (AIBN), The University of Queensland, Brisbane, Australia

Email: k.liu@science.ru.nl, kaizheng.liu@radboudumc.nl

Fully synthetic hydrogels have emerged as a type of materials highly promising for tissue engineering. Recently, a new hydrogel was reported, which is fully synthetic, but closely mimics the architecture and nonlinear mechanical properties of biogels, which is known as stress stiffening. Stem cell studies showed differentiation into different lineages, dependent on the structure of the PIC polymer. In this research, PIC hydrogel was synthesized and functionalized with GRGDS(Gly-Arg-Gly-Asp-Ser), a cell-adhesion promotive peptide. Human adipo-derived stem cells (hASCs) were subsequently encapsulated in order to create a 3D in-vitro stem cell culture model, followed by a series of biological characterizations. Rheological tests show that polymers of different lengths result in gels of different stiffness, whilst conjugation of peptide induces a decrease in bulk matrix stiffness. Preliminary cellular outcome indicates that GRGDS-functionalized PIC gel promotes cell adhesion to the matrix, and gel stiffness has a crucial impact on morphology of cells. Our results highlight the suitability of PIC gel as artificial extracellular matrix (aECM) for tissue engineering.

Strategies for Chondrogenic Differentiation of Dental Pulp Stem Cells

A.Longoni, I.E.M. van Hooijdonk, G.K.P. Bittermann, A.J.W.P. Rosenberg, D. Gawlitta

Department of Oral and Maxillofacial Surgery & Special Dental Care, University Medical Center Utrecht, Heidelberglaan 100, 3508 GA, Utrecht, The Netherlands

Introduction: Craniofacial bones, similarly to other skeletal elements, possess an intrinsic capability to regenerate upon injuries. However, in case of critical size defects, this regenerative potential is not sufficient, and a clinical intervention is required.
Endochondral bone regeneration based on a chondrogenic template from mesenchymal stromal cells (MSCs) has been demonstrated to be a promising approach to develop bone substitutes[1]. However, MSCs present some limitations, including an invasive procedure to obtain them, a low stem cell yield, a limited *in vitro* expansion potential and a heterogeneous differentiation potential. Thus, an alternative cell source is desirable.
Because of their neural crest origin, dental pulp stem cells (DPSCs) represent an interesting alternative cell source. It has been proven that neural crest-derived bones remodel and heal through recruitment of progenitor cells of the same embryonic origin[2]. Further, DPSCs are harvested from permanent teeth with a minimally invasive procedure, display a high proliferation rate and are capable of undergoing multilineage differentiation[3]. However, the chondrogenic differentiation capacity of DPSCs has not been extensively studied. Therefore, the aim of this study is to test several strategies to differentiate DPSCs chondrogenically. Once a protocol for chondrogenic differentiation of DPSCs is established, the potential for endochondral bone regeneration can be evaluated.
Material and Methods: Human DPSCs from the pulp tissue of third molars were isolated from five different, otherwise healthy patients following informed consent.
I) First, a chondrogenic differentiation strategy based on MSC differentiation, was evaluated. Briefly, a total amount of $2*10^5$ cells per pellet were suspended in 0.2 mL of chondroinductive medium (CM) supplemented with 10 ng/ml of TGFβ1. After 3 weeks of culture, chondrogenic differentiation was evaluated by a Safranin-O and collagen types I and II (immuno)staining.
II) Next, the seeding density in the pellet culture model was optimized. Four seeding densities, namely $2*10^5$, $5*10^5$, $1*10^6$ and $1.5*10^6$ cells per pellet were compared. After 4 weeks of culture in the pellet model, glycosaminoglycan (GAG) content was evaluated both quantitatively by the DMMB assay and qualitatively by toluidine blue staining.
III) Third, the optimized cell number was used to perform a screening of several candidate growth factors (GFs) associated with chondrogenesis. In particular, BMP2, 6 and 7 and IGF-1 (100ng/ml) were added to the CM alone or in combination with TGFβ3 (10ng/ml). In the combination groups, the TGFβ3 was administered following two different patterns: a continuous or an alternating combination of the two GFs. After 4 weeks of culture, chondrogenesis was assessed.

Results and Discussion: I) After three weeks of culture, in all chondrogenically differentiated DPSCs it was possible to observe GAG deposition, in a donor dependent manner. However, pellets were small (<1mm) and showed a fibrous morphology, as they deposited more collagen type I than II.
II) The two highest cell densities, $1*10^6$ and $1.5*10^6$, did not display any GAG deposition in histological sections. The pellets formed by the lowest amount of cells, displayed the highest GAG/DNA. However, pellets from $5*10^5$ cells exhibited the highest absolute amount of GAGs. Therefore, $5*10^5$ cell was selected as the optimal cell number for aggregation.
III) In general, no condition where the GFs were supplemented outperformed the CM control. Comparable results where observed when BMP 2,6 or 7 were supplemented alone or in an alternating pattern with TGFβ3. Interestingly, when the members of the BMP family were administered continuously with TGFβ3, no synergistic effect was observed. Moreover, the pellets showed a lower GAG/DNA compared to the other conditions. On the contrary, no differences in GAG/DNA ratios between conditions were observed when IGF-1 was supplemented alone or in the continuous or alternating pattern with TGFβ3.
Conclusions: DPSCs do undergo inferior chondrogenesis compared to MSCs, when subjected to chondrogenic conditions that are common for MSCs. Embryologically, this may be attributed to the DPSC origin, which may favour fibrocartilaginous tissue formation. On the other hand, DPSC differentiation may require a protocol completely different from MSCs. It is suggested that further tailoring of DPSC chondrogenic protocols, while taking their embryological development into account, may overcome this. Once chondrogenesis of DPSCs is established, hypertrophy could be stimulated to identify their potential in endochondral bone regeneration.

[1] van der Stok J et al, *Eur Cell Mater*. 2014
[2] Leucht P et al, *Development* 2008
[3] Zhang W, *Tissue Eng*. 2006
[4] Hui T, *Biomaterials*, 2008

XS-Graft: Design Requirements And Electrospinning Parameters

G. Marchioli[(1)], J.J. van Gorp[(2)], P. Sawo[(3)], S. Quicken[(3)], G.C. van Almen[(1)], C.V.C. Bouten[(1)], P.Y.W. Dankers[(1)]

(1) Eindhoven University of Technology, Institute for Complex Molecular Systems, and Department of Biomedical Engineering, De Rondom 70, 5612 AP Eindhoven, Eindhoven, The Netherlands
(2) DSM, Urmonderbaan 22, 6167 RD Geleen, The Netherlands
(3) Maastricht University, P. Debyelaan 25, 6229 HX Maastricht, The Netherlands

Introduction

End-stage renal disease (ESRD) is a major complication that arises as a consequence of common diseases such as diabetes and hypertension and that can lead to death. In these patients, renal functionality is below 10% of the normal capacity. In these circumstances, renal replacement therapies, such as kidney transplantation or hemodialysis (HD), are required to increase their life expectancy. For an efficient hemodialysis to occur, a proper access to blood flow is needed to provide sufficient flow rate. In most cases, this is achieved by surgically connecting an autologous artery and a vein (arteriovenous fistula (AVF). However, creating an AVF is not always possible for every patient, because of previously failed fistulae, co-morbidities or lack of a suitable artery [1]. For these patients an artificial vascular access graft (AVG) is used as a valid alternative to AVF. Grafts need to assure good long term patency rates, be anti-thrombogenic, have good resealing properties after puncturing and prevent grafts infections. The most used material for arteriovenous grafts is ePTFE, but thrombosis of the graft and intimal hyperplasia at the venous anastomosis is the most common complication and most common cause of graft failure

Aim of the project

This project aims at fabricating a medical-grade, polyurethane-based, graft for HD access by using electrospinning technique. Electrospinning is a valuable technique for producing non-woven, fibrous structures in a shape of sheets or tubes. The resulting mechanical properties of the graft can be tuned by varying spinning parameters, in order to produce electrospun meshes with different fiber diameter, fiber alignment, and tube thickness. These same parameters can influence also biological behavior of the construct, haemocompatibilty and a non-thrombogenicity. Additives can play an important role in influencing the spinning behavior of the polymer. In addition, anti-microbial moieties can be immobilized on the construct with the aim to prevent peri-implant infections. First results in spinning optimization show that medical-grade polyurethanes are suitable polymers for electrospinning and that the material can be processed in a tubular graft with suitable dimensions to be used as vascular access grafts.

Figure 1: prototype of an electrspun polyurethane graft.

References

[1] Moist et al. Optimal Vascular Access in the Elderly Patient Semin Dial. 2012 ; 25(6): 640

This work was performed under the framework of Chemelot InSciTe

Behavioural characterization of Polyisocyanopeptide (PIC) hydrogel wound dressings

Roel C. op 't Veld[1], Frank A.D.T.G. Wagener[2], X. Frank Walboomers[1], Lieke Joosten[3], Otto C. Boerman[3], Onno van den Boomen[4], John A. Jansen[1]

Department of Biomaterials[1], Orthodontics and Craniofacial Biology[2], and Nuclear Medicine[3] (Radboudumc, 6500 HB Nijmegen, the Netherlands) and the Department of Molecular Materials[4] (Radboud University, 6525 HP, Nijmegen, the Netherlands)

Introduction

Hydrogels are formed when water is retained by a polymer network. The type and composition of these polymers is determinative for the final characteristics of these gels. Previously, it has been shown that polyisocyanopeptide (PIC) based hydrogels that are functionalized with polyethylene glycol (PEG) side chains possess multiple beneficial characteristics. In short, hydrogels based on these polymers are strain-stiffening, can be formed at very low weight percentages, and are readily modified with different molecules. Here, we present the potential for PIC hydrogels as a new type of wound dressing. The high water content of the gels can keep wounds moist, the small pore size provides protection against bacteria, and therapeutic drugs may easily be delivered. PIC gels may thus offer some improvements over current wound dressing techniques, as those often have problematic side effects. Therefore, we have tracked the behaviour of PIC gel in murine full thickness wounds for up to 7 days using both histology and SPECT imaging. In addition, the quality of wound healing was compared for wounds treated with PIC gel, RGD-peptide conjugated PIC gel, and an untreated control.

Objective

Assess the biocompatibility and suitability of PIC gels as wound dressings, while simultaneously confirming if the gels can have a direct influence on wound healing.

Materials and Methods

Hydrogels were produced at 4 mg/ml in saline or 2-(N-morpholino)ethanesulfonic acid (MES) buffer using PIC polymer functionalized with three PEG molecules per side chain. For the RGD-conjugated PIC polymers, GRGD peptides were covalently bound to the side chains of the PIC polymer at random intervals. For SPECT imaging, a Dibenzocyclooctyne –Pentetic acid (DBCO-DTPA) conjugate was covalently bound in a similar fashion, which was later labelled with In-111. Two studies were performed using mice (6 weeks old, n = 36 and n = 12). Two full thickness wounds were applied using a biopsy punch (Ø4 mm) through a fold of dorsal skin, which were treated with a PIC gel product or left untreated. For the SPECT imaging study, 18 of 24 wounds were splinted with a silicone ring and then a sheet of Tegaderm™ and a bandage were applied. SPECT images were obtained immediately, as well as 1, 3 and 7 days after wounding. Histological sections were obtained at 3 and 7 days after wounding. Sections were stained with general stainings (H&E and AZAN) as well as immuno stainings (alpha smooth muscle actin (αSMA), granulocytic marker GR-1, and macrophage marker F4/80).

Results and Discussion

Histological sections of unsplinted wounds show that no elevated immune response is present at day 3 and 7 post wounding for both PIC and PIC-RGD gels (fig. 1). This is made evident by the lack of giant cells as well as similar macrophage infiltration between groups. Remarkably, granulocyte (GR-1) infiltration is significantly lower at 7 days in both the PIC and PIC-RGD groups. We speculate the immune response is attenuated as a result of the PIC gels preventing the infiltration of bacteria. No conclusions on wound contraction rate could be made, as unsplinted wounds are contracted by muscles. No significant influence on the number of myofibroblasts or blood vessels was found.

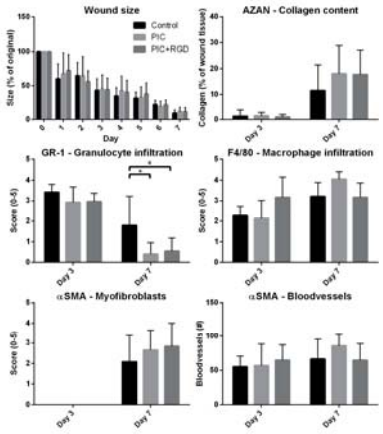

Figure 1: The status of wound healing up to 7 days post wounding. No significant differences were found between treatment groups, with the exception of granulocyte infiltration which was lower in gel treated wounds.

The SPECT images below (fig. 2) show that gel is stable within the wound bed for at least 7 days. Contamination is spotted on local areas on the dorsal skin. It is assumed pressure on the skin created by the bandage causes gel to migrate underneath the Tegaderm™ sheet. Furthermore, it was discovered that if the wound is shielded with a secondary dressing, mice are unable to remove the gel. Consequently, gel appears to become encapsulated in pockets within the regrowing skin. This illustrates cells are incapable of infiltrating the dense polymer network.

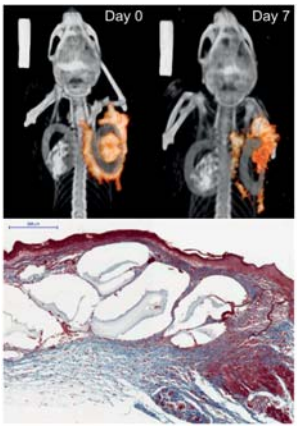

Figure 2: In wounds treated with secondary dressings gel can be seen for at least 7 days on both SPECT images and histological sections. Scale bar = 200 μm.

Conclusion

PIC gels show good biocompatibility. No convincing evidence was found for a direct influence of PIC or RGD conjugated PIC gels on unimpaired wound healing. Lastly, even though PIC gel can be stable in wounds for up to a week, its encapsulation in the skin can be problematic.

Contact: Roel.optVeld@Radboudumc.nl

Bioinspired Engineering of Multi-layered Electrospun Blood Vessels

I. Pennings[1], T. Jungst[2], J. Groll[2], A.J.W.P. Rosenberg[1], D. Gawlitta[1]

[1] Department of Oral and Maxillofacial Surgery & Special Dental Care, Regenerative Medicine Center Utrecht, UMC Utrecht, Uppsalalaan 8, 3584CT Utrecht, The Netherlands
[2] Department for Functional Materials in Medicine and Dentistry, University Hospital Würzburg, Pleicherwall 2, 97070 Würzburg, Germany

Introduction

In the field of maxillofacial surgery, autologous bone grafting (*e.g.* iliac crest or free fibula flaps) is regarded as the gold standard treatment option to restore bone defects[1]. Nevertheless, the use of autologous bone grafts is associated with drawbacks such as shape mismatch, limited availability and the necessity for a second operation site[1]. Future therapies must therefore exceed the successes of autologous grafting and moreover, evade donor site morbidity. Regenerative techniques hold the promise to develop bioengineered osteogenic constructs with functional vasculature, that can be transplanted into the site of defect. Functional vasculature is desired for nutrient and oxygen supply of the developing bone tissue as well as for anastomosis[2]. All natural blood vessels share a similar basic structure, comprised of a single intimal layer of endothelial cells and a secondary medial layer containing smooth muscle cells[3]. A confluent endothelium is required for anti-thrombogenic purposes and inhibiting intimal hyperplasia. The layer of smooth muscle cells is essential for the vasoconstriction and relaxation of arteries[4].

The present study aimed to engineer a small diameter vascular construct, inspired by the native microenvironments of the different layers of a blood vessel. By means of a technique capable of creating the desired structures, electrospinning, a multi-layered scaffold was designed that fosters the infiltration of the smooth muscle cells while also supporting endothelialisation.

Material and Methods

The bi-layered electrospun scaffolds were fabricated using two fabrication processes. Solution electrospinning that enables the generation of nonwovens and melt electrospinning to generate constructs with oriented fibers. One type of polymer was used to create both layers: poly-ε-caprolactone (PCL), either dissolved in hexafluoroisopropanol (HFIP) for fabrication of the inner layer, or melted at 90 degrees Celsius for the outer layer.

Endothelial Colony Forming Cells (ECFCs) were isolated from human cord blood and Multipotent Mesenchymal Stromal Cells (MSCs) were derived from human bone marrow, upon informed consent of the donors. ECFCs were seeded on the inside of the scaffold and MSCs on the outer layer, respectively. Samples were cultured for 7 days in 1:1 mixed Endothelial and MSC expansion medium.

Samples were analysed by immunofluorescent labelling of the endothelial markers VE-cadherin and Von Willebrand Factor (vWF) and the smooth muscle marker α-smooth muscle actin (α-SMA). Confocal microscopy was used to visualize the fluorescently labelled markers and the cellular orientations.

Results and discussion

Multi-layered cylindrical scaffolds were electrospun, adhering to the design criteria. First a solution electrospun nonwoven was deposited onto a 3 mm diameter grounded collector. The same collector was used for melt electrospinning where fiber orientation could be controlled by varying the collector rotation and translation velocity[5,6]. The inner layer (diameter 3 mm) was composed of fibers with a random orientation (fiber thickness ~1-1.5 µm). The outer layer consisted of orientated fibers with winding angles between 35 and 70° (fiber thickness 20-30 µm). Overall, the feasibility of combining melt and solution electrospinning techniques in engineering of one construct was demonstrated.

The multi-layered electrospun scaffold resembled the dimensions and spatial organization of the intimal and medial layers of a native vessel. After a culture period of 7 days, a confluent monolayer of VE-cadherin and vWF positive ECFCs was found on the luminal side of the scaffold. The characteristics of the electrospun intimal layer was therefore shown to be sufficient in steering the process of endothelialisation.

On the outer layer, a circumferential layer of α-SMA-positive cells was found throughout the thickness of the electrospun medial layer. The orientation of the α-SMA cells was resembling the situation in native vessel, essential to provide the vessel with mechanical strength necessary to withstand the circulatory pressures when moving to *in vivo* conditions.

Conclusion

In the present study, the combination of two different electrospinning methods in one construct was proven to be a successful approach for vascular tissue engineering. With the bioinspired, multi-layer approach for scaffold design, the vascular construct provided a suitable substrate to the different cell types.

Future directions are aimed at applying fluid shear stress at the luminal side of the vascular scaffold, via a flow-perfusion bioreactor.

[1] Dimitriou *et al.,* Injury, Int. J. Care Injured (2011)
[2] Costello *et al.,* J Oral Maxillofac. Surg (2015)
[3] Glynn *et al.,* Tiss Eng B (2014)
[4] Prichard *et al.,* J. of Cardiovasc. Trans. Res. (2011)
[5] Jungst *et al.,* Polym. Int. (2015)
[6] Brown *et al.,* Biointerphases (2012)

Calcium-binding Polyester Fibers Designed for Reinforcement of Calcium Phosphate Cements

DG Petre[1], A Abbadessa[2], T Vermonden[2], A Polini[1], SCG Leeuwenburgh[1]
[1] Department of Biomaterials, Radboud University Medical Center, Philips van Leydenlaan 25, 6525 EX Nijmegen, The Netherlands. [2] Department of Pharmaceutics, Utrecht University, Universiteitsweg 99, 3584 CG Utrecht, The Netherlands.

Introduction: Calcium phosphate cements (CPC) have been extensively researched over the past two decades due to their excellent osteocompatibility, injectability and/or moldability into bone defects of various sizes and geometries. However, these ceramics are brittle and can only be used in non-load bearing sites. A common method to overcome this weakness is to incorporate fibers [1]. Fibers that are currently used for reinforcement of calcium phosphate ceramics are generally hydrophobic, which results into poor adhesion between the fibers and the ceramic matrix. The strength of the interface bonding between the fiber and the matrix is crucial for a successful reinforcement. To improve this adhesion, bisphosphonates (BP) can be instrumental since they bind strongly to calcium ions in hydroxyapatite and are already being used for the treatment of osteoporosis. Herein, we present a novel method to functionalize commonly used polymeric fibers with these calcium-binding BP groups.

Materials and Methods: Sub-micron fibers were produced by electrospinning a 4 wt% solution of poly-L-lactic acid (PLLA) in hexafluoro-2-propanol at a voltage of 20 kV, an air gap of 20 cm and a flow rate of 5 µL/min. The prepared meshes were chemically cut through aminolysis [2] in a solution of 5 wt% ethylenediamine in isopropyl alcohol at 37°C for different time periods, then freeze dried. By using different aminolysis time, the fiber meshes were chemically fragmented and functionalized with amine groups. The morphology of electrospun nanofibers before and after aminolysis was investigated using scanning electron microscopy (SEM).
Trinitrobenzenesulfonic acid was used to quantify the amine groups linked to the surface of the fibers after the aminolysis procedure.

Subsequently, we investigated if the aminolyzed polyester fibers could be further functionalized with BP groups through a Michael addition reaction. For this purpose, the Michael acceptor, acrylamidoalkylmethylene bisphosphonate (AcrBP), was synthesized by acrylating alendronate using acryloil chloride in aqueous NaOH [3]. Briefly, the reaction took place between the newly synthesized AcrBP and the –NH2 groups present on the sub-micron fibers, in HEPES buffer at pH 7. The amount of covalently linked AcrBP was quantified by determining the phosphorous amount using ICP-OES.

Results: SEM revealed that the length of the aminolysed fibers could be adjusted to few micrometers by increasing the aminolysis time from 2 to 6 hours (Fig. 1).

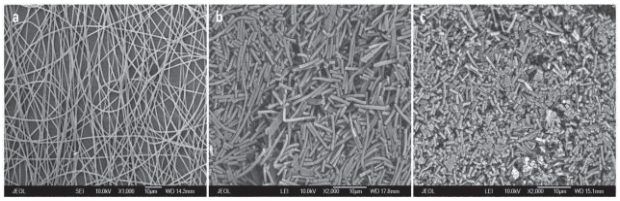

Fig. 1: Morphology of PLLA fibers - a. electrospun PLLA mesh, b. 3 hours aminolysis, c. 6 hours aminolysis

Following conjugation of AcrBP onto aminolysed fibers, the amount of alendronate conjugation could be tuned by controlling the duration of aminolysis time between 2h and 6h (Fig. 2).

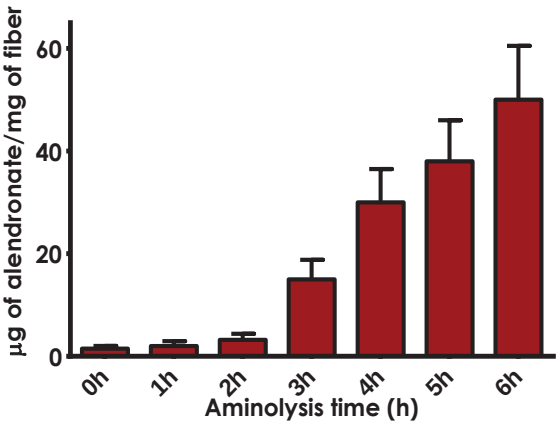

Fig. 2: Detection of phosphorous on bisphosphonate fibers as a function of aminolysis time.

Conclusions: PLLA sub-micron fibers were successfully functionalized with calcium-binding BP groups by aminolysis of electrospun fiber meshes and subsequent Michael addition reaction between AcrBP and aminolyzed PLLA fibers.

References: [1] R. Krüger, J. Groll (2012) Biomaterials 33:5887-00. [2] T.G. Kim, T.G. Park (2008) Macromol. Rapid Commun. 29:1231–36. [3] O.P. Varghese, W. Sun, J. Hilborn, D.A. Ossipov (2009) J. Am. Chem. Soc.:8781-83.

Developing 3D bone scaffolds for *in vitro* bone resorption

S.J.A. Remmers[a], M.C.M. Sleddens[a], K. Ito[a,b], S. Hofmann[a,c]
a Orthopaedic Biomechanics, Department of Biomedical Engineering and the Institute for Complex Molecular Systems, Eindhoven University of Technology, Eindhoven, The Netherlands
b Department of Orthopaedics, UMC Utrecht, Utrecht, The Netherlands
c Institute for Biomechanics, ETH Zurich, Zurich, Switzerland

Introduction

In vitro models have been designed to study the processes underlying bone resorption and formation, but commonly use animal cells or cell lines in 2D culture, which may not be fully representative of human bone remodeling[1]. To more closely mimic human bone remodeling, we aim to develop a system in which human primary osteoblasts and osteoclasts can be cultured on decellularized trabecular bone plugs that allows quantification of bone resorption and formation using micro computed-tomography (µCT). The aim of the present study is to obtain a suitable scaffold enabling *in vitro* bone resorption. To achieve that, we investigated various preparation protocols to i) extract bone scaffolds from porcine femurs, ii) remove bone marrow and cells and iii) sterilize the scaffold in a way that still enables monocytes to attach.

Materials and Methods

Trabecular bone plugs were prepared from porcine femurs using a 4 mm trephine drill. Trabecular bone plugs were treated with various combinations of defatting[2] and cell removal cocktails[3-7]. The plugs were sterilized by autoclaving or peracetic acid-ethanol sterilization. The plugs were scanned using µCT both prior to and after the treatments to quantify total bone volume and changes as a result of the treatment. Afterwards, they were decalcified, paraffin embedded, and used for histology. Finally, monocytes were seeded onto new decellularized and sterilized plugs using a static or dynamic method, and relative cell attachment and distribution was visualized using an MTT assay.

Results

Earlier experiments have shown that it is essential yet challenging to prepare sterile and decellularized 3D mineralized constructs from bone, and to culture osteoclasts on them that resorb quantifiable amounts of tissue. Histology showed that a defatting step is necessary to remove bone marrow and bone lining cells from the plugs (Fig. 1A+B). Osteocyte removal was achieved using all methods, with defatting and incubating with triton x-100, NH_4OH and benzonase[6] resulting in the best decellularization. Both sterilization methods resulted in sterile scaffolds, with autoclaving being less elaborate.. µCT (Fig. 1C) showed a consistent but statistically not significant trend of decreased total bone volume after the treatments. The MTT assay showed that both static seeding and dynamic seeding led to monocyte attachment (Fig. 1D). More cells seemed to attach using the static conditions. While dynamic seeding seems to hold potential for anchored cells, static seeding seems to be more reproducible for monocytes. Different sterilization techniques did not lead to a different outcome.

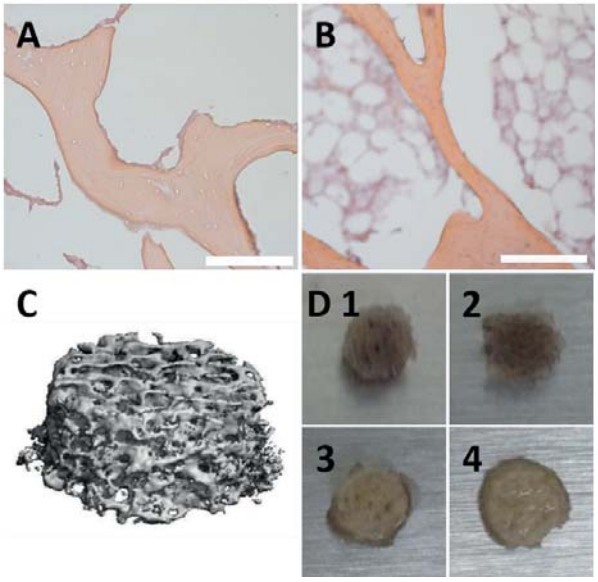

Fig. 1: A+B) H&E staining of bone plugs defatted and decellularized (A) or not (B). Orange: trabeculae. Purple dots in trabeculae: osteocytes. White areas in trabeculae: empty osteocyte lacunae. C) Trabecular bone plug scanned using µCT. D) MTT assay of static (1+2) and dynamic (3+4) seeding of cells (1+2) or vector. Purple color indicates presence of cells. Scale bars are 200 µm. Bone plugs are 4 mm in diameter.

Discussion and conclusion

Our results indicated that the preferred method for decellularization, sterilization and seeding is as follows: First defatting[2], then incubation in Triton X-100, NH_4OH and benzonase[6] followed by autoclaving and static cell seeding. Monocyte attachment to a scaffold is the first step towards *in vitro* bone resorption. In a next step we need to show that the monocytes can actually differentiate into osteoclasts in 3D on bone scaffolds, and that they can resorb quantifiable amounts of bone. Only then can we monitor *in vitro* osteoclastic bone resorption in 3D[8].

References

[1] Edmondson et al. *Assay Drug Dev Technol*. (2014)
[2] Scheffler et al. *Cell and Tissue Banking* (2005)
[3] Marcos-Campos et al. *Biomaterials* (2012)
[4] Smith et al. *Acta Biomaterialia* (2014)
[5] Sadr et al. *Biomaterials* (2012)
[6] Chen et al. *J Bone Miner Res* (2007)
[7] Chen et al. *ACS Appl Mater Inter* (2015)
[8] Hagenmüller et al. *Ann Biomed Eng* (2007)

Acknowledgements

This project was supported by the European Union's Seventh Framework Programme (FP/2007-2013) / grant agreement No. 336043.

Computational Evaluation of Bioreactor, Medium, and Cell-Related Parameters in a Static Bioreactor for Bone Tissue Engineering

A. Saatchi[1,2,3], G. Amoabediny[1,2], M.N. Helder[4], B. Zandieh-Doulabi[3], J. Klein-Nulend[3]
[1] Faculty of Chemical Engineering, College of Engineering, University of Tehran, Enqelab Avenue, Tehran, Iran
[2] Department of Biomedical Engineering, Research Center for New Technologies in Life Science Engineering, University of Tehran, 16 Azar street, Tehran, Iran
[3] Department of Oral Cell Biology, Academic Centre for Dentistry Amsterdam, University of Amsterdam and VU University Amsterdam, MOVE Research Institute Amsterdam, Gustav Mahlerlaan 3004, 1081 LA Amsterdam, The Netherlands
[4] Department of Oral & Maxillofacial Surgery, VU University Medical Center, MOVE Research Institute Amsterdam, PO Box 7057, 1007 MB Amsterdam, The Netherlands

Introduction: Bone tissue engineering uses bioreactors to support efficient oxygen supply and nutrition of cells, in combination with mechanical stimuli. How bioreactor, medium, and cell-related parameters control cell growth in a bioreactor is still unclear. The aim of this study was to investigate the effects of changes in bioreactor, medium, and cell-related parameters by computational evaluation of cell density and oxygen distribution within a 3D-porous cylindrical scaffold in a static bioreactor over time.

Methods: Cell density and oxygen concentration were assessed by modeling of cell proliferation and oxygen transport using the finite element method. The modelling and simulation was done for a cylinder-shaped scaffold with a radius of 0.7 cm and a height of 0.1 cm during 17 days.

Results: After 17 days, increased cell density was obtained by enhancing initial cell number seeded, medium oxygen concentration, maximum specific cell growth rate, and molecular diffusivity of oxygen in cell phase, but cell motility coefficient nor cell volume changes had an effect (Figure 1). Oxygen concentration in the scaffold decreased by enhancing initial cell number seeded, and maximum specific cell growth rate, while enhancing medium oxygen concentration and molecular diffusivity of oxygen in cell phase had the opposite effect (Figure 1). Nor increasing cell motility coefficient nor changes in cell volume did affect oxygen concentration (data not shown).

Discussion and conclusion: Modeling and simulation were used to investigate the effects of changes in bioreactor, medium, and cell-related parameters on cell proliferation and oxygen transport within a 3D-porous scaffold in a static bioreactor. We found significant changes in distribution of cell density and oxygen within 3D-porous scaffolds as a result of changes in these parameters, which might have implications for bone tissue engineering. In conclusion, our data showing that cell density and oxygen distribution within a 3D-scaffold in a static bioreactor were enhanced by increasing medium oxygen concentration, initial cell number seeded, and cell motility coefficient simultaneously, indicate that these parameters might play a crucial role in the creation of densely cell-populated constructs with uniform spatial distribution in 3D-porous scaffolds in a static bioreactor.

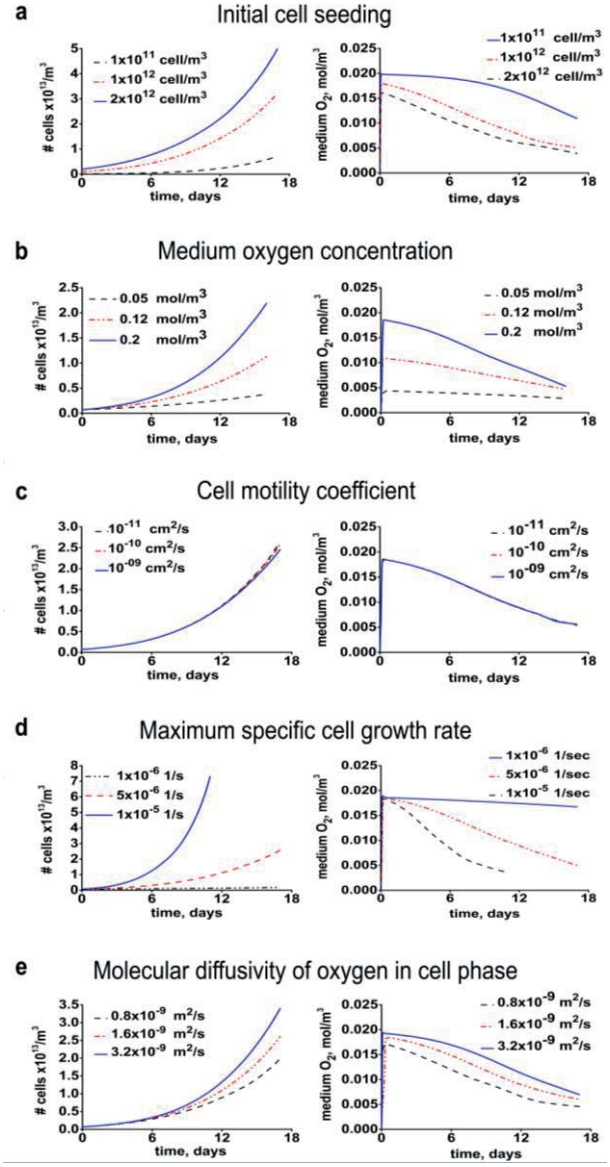

Figure 1. Finite element modelling of the effect of changes in bioreactor, medium, and cell-related parameters on oxygen and cell density in a 3D porous scaffold in a static bioreactor during 17 days. Effect of a) initial number of cells seeded (10^{11}, 10^{12}, $2x10^{12}$ cells/m^3), b) Medium oxygen concentration (0.05, 0.12, 0.2 mol/m^3), c) Cell motility coefficient (10^{-11}, 10^{-10}, 10^{-9} cm^2/s), d) Maximum specific cell growth rate (10^{-6}, $5x10^{-6}$, $10^{-5}s^{-1}$), and e) Molecular diffusivity of oxygen in cell phase ($8x10^{-10}$, $1.6x10^{-9}$, $3.2x10^{-9}$ m^2s^{-1}).

Glycosaminoglycan (GAG)-based Microgels for Controlled Release of Proteins from Hydrogel Scaffolds

C.C.L. Schuurmans, A. Abbadessa, W.E. Hennink, T. Vermonden

Department of Pharmaceutics, Utrecht Institute for Pharmaceutical Sciences (UIPS), Faculty of Science, Utrecht University, Utrecht, The Netherlands.

In situ release of growth factors from tissue-engineered hydrogel scaffolds can enhance cell recruitment and differentiation [1]. In this study, composite hydrogels containing microgels were designed to achieve a prolonged release of a cationic model protein, lysozyme. Monodisperse hyaluronic acid based microgels were fabricated by using a co-flowing microfluidic device, post-loaded with lysozyme through electrostatic interaction and further encapsulated into a thermosensitive hydrogel (Figure 1). Particle size (180 to 700 µm) was tuned by changing the continuous phase flow (2 to 6 ml/min) and the needle diameter (85-115 µm). The composite hydrogel showed a sustained release of lysozyme over at least 20 days, which was significantly slower than that from particle-free hydrogels.

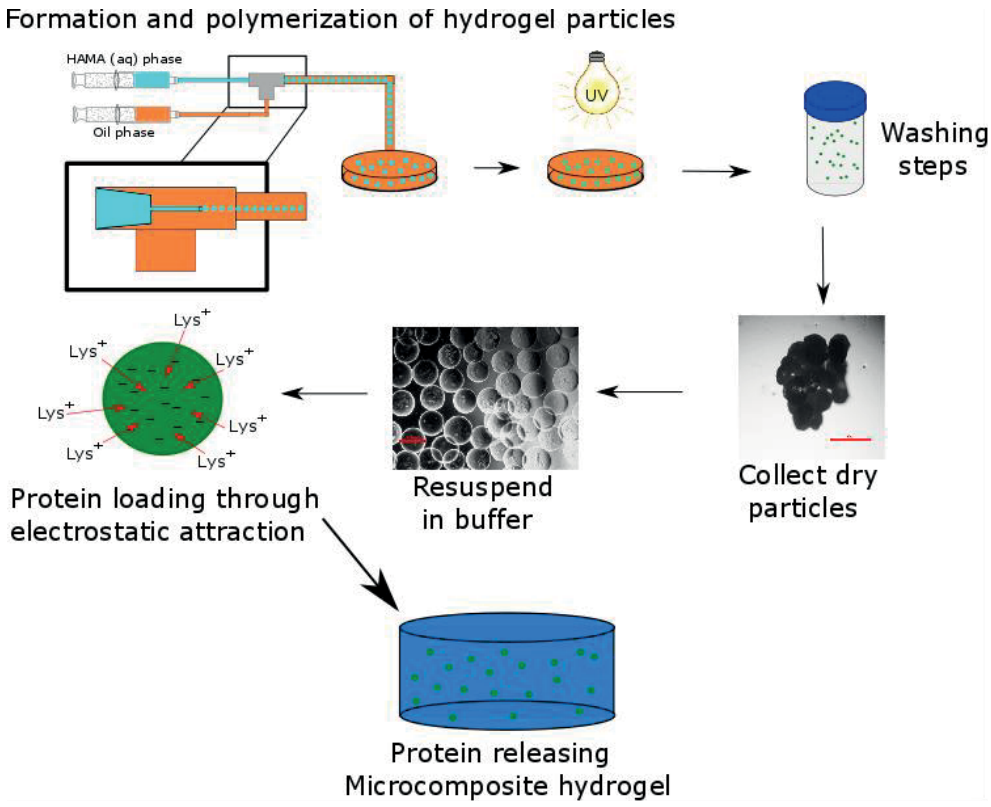

Figure 1. Graphical overview of composite hydrogel preparation.

[1] Lee, K.; Silva, E. A.; Mooney, D. J. Journal of the Royal Society Interface 2011, 8 (55), 153-170.

Adipose-derived Stromal Cells Support and Organize Long Term *in vitro* Connective-like Tissue in 3D Printed Scaffolds

Vincenzo Terlizzi[1,2], Gabriel Liguori[1,3], Martin. C. Harmsen[1]

1 Lab for Cardiovascular Regenerative Medicine (CAVAREM), Dept. Pathology and Medical Biology, University of Groningen, University Medical Center Groningen, The Netherlands

2 Dept. Endocrinology, 5th Medical Department, Medical Faculty Mannheim, University of Heidelberg, Germany

3Laboratory of Cardiovascular Surgery and Circulation Pathophysiology (LIM-11), Heart Institute (InCor), Hospital das Clínicas da Faculdade de Medicina da Universidade de São Paulo

Abstract

Adipose tissue-derived stromal cells (ASC) are adult stem cell-like cells of mesenchymal origin. ASC are exploited for their capacity to differentiate into osteoblasts, chondrocytes, adipocytes, neurons, and mesenchymal lineages such as myofibroblasts, smooth muscle cells and pericytes. Moreover, ASC express a broad therapeutic secretome, that includes stimulation and stabilization of *de novo* formation of endothelial tubes *in vitro*. These characteristics offer a promising ASC application for designing complex multi-tissue co-culture systems to improve research translation to *in vivo* mechanisms. Mainstream systems are based on either monolayers culture or co-culture which limits the cells' capacity to organize into complex, *i.e.* 3D, structures. To facilitate the transition to 3D culturing, we developed a PLA-based (polylactic acid) scaffold to accommodate Matrigel-embedded cells. The scaffold walls offer physical support and anchorage for cells to organize in their natural conformations overcoming contraction issues observed in matrix-based cells systems. This 3D printed scaffold was designed to test the hypothesis that ASC re-organize in stromal fractions as observed in adipose tissue *in vivo* and, in combination with endothelial cells, ASC promote, maintain and connect 3D network of endothelial tubes. The extracellular matrix depositedby ASC comprised fibronectin and collagen IV that ubiquitously surrounded cells and followed the cells' organization in a densely interconnected fashion. Co-culture with endothelial cells showed formation of intersected tubes which maintained their endothelial phenotype as confirmed by CD31 staining. Moreover, this system allowed for culturing for times exceeding 30 days. In summary, we developed a stable and durable ASC 3D culture system to mimic organ-like connective tissue *in vitro*. Extracellular matrix and endothelial cells natural organization in microtubules offer a significant platform to study complex mechanisms in a system closer to *in vivo* organisms.

Design and Fabrication of 3D Porous Tissue Engineering Scaffolds

P. Trepa[1,2], A. Guney[2], P. Ulański[1] and D.W. Grijpma[2]
[1]Institute of Applied Radiation Chemistry, Lodz University of Technology, 93-950, Łódź, Poland
[2]Dept. of Biomaterials Science and Technology, University of Twente, 7522 LG, Enschede, The Netherlands
p.trepa@student.utwente.nl, a.guney@utwente.nl, ulanskip@mitr.p.lodz.pl, d.w.grijpma@utwente.nl

INTRODUCTION

The successful design and fabrication of a complex tissue engineering scaffold with optimum porosity and interconnectivity is significant for tissue engineering applications. The tissue engineering scaffold provides a temporary biomechanical support until the cells produce their own matrix proteins for tissue growth [1]. In tissue engineering, an (interconnected) porosity is a 'must have' property since it provides void volume for vessels formation to transport oxygen, nutrients and metabolic wastes that facilitates new tissue formation [2]. Additive manufacturing based on extrusion of a thermoplastic material is a rapid prototyping technique that is suitable for manufacturing 3D objects with highly-controlled architecture based on CAD models in layer-by-layer deposition process of thermoplastic material [3].

EXPERIMENTAL

Scaffolding structures were prepared by extrusion of solutions of PCL_{16}-b-$PTMC_{42}$-b-PCL_{16} triblock copolymers based on ε-caprolactone and trimethylene carbonate in ethylene carbonate (EC). EC is crystallizable and water-extractable and can be used to prepare structures with microporous strands. The polymer was dissolved in EC at 1/3 and 1/4 weight ratios to obtain different porosities. The constructs were printed using BioBots 3D printer. The solution was extruded in a rectilinear pattern and layers were perpendicular to each other. The extrusion temperature was 60°C. The inner diameter of the nozzle was 234 µm. After printing, the built scaffolds were immediately cooled down (-20°C) with dry ice cooling system to enable fast solidification in order to maintain the pre-designed structure. To form micro- and nanoporosity, extraction of EC in demiwater at ambient temperature was performed for 4-5 days.

RESULTS AND DISCUSSION

The 3D scaffolds were built through additive manufacturing based on extrusion of successive layers (Figure 1). After extraction of EC, the different diluent quantities resulted in different pore sizes in the strands.

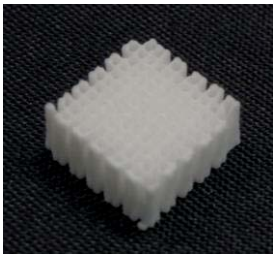

Figure 1. 3D-printed porous tissue engineering scaffold after extraction of EC.

Homogenous pore size distributions were obtained in both cases. The pore size distribution was between 10-50 µm for 1/3 ratio, whereas for 1/4 the range was between 30-50 µm (Figure 2).

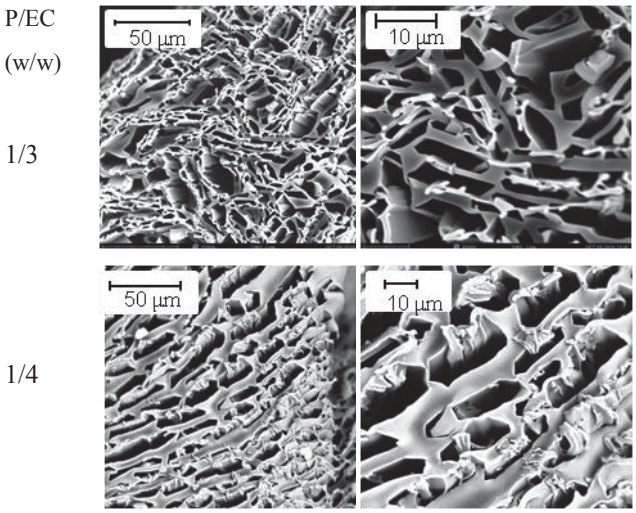

Figure 2. SEM images of built 3D porous tissue engineering scaffolds.

CONCLUSIONS

Additive manufacturing based on extrusion of thermoplastic PCL_{16}-b-$PTMC_{42}$-b-PCL_{16} triblock copolymers allowed us to build porous scaffolds with controlled architectures. By varying the amount of crystallizable ethylene carbonate which is removed in an extraction process, it is possible to adjust pore sizes and porosities of built structures.

REFERENCES

[1] S. H. Masood, J. P. Singh, and Y. Morsi, *Int. J. Adv. Manuf. Technol.*, **27**, 3–4, (2005).
[2] J. Rouwkema, N. C. Rivron, and C. A. van Blitterswijk, *Trends Biotechnol.*, **26**, 8, (2008).
[3] B. Thavornyutikarn, N. Chantarapanich, K. Sitthiseripratip, G. A. Thouas, and Q. Chen, *Prog. Biomater.*, **3**, 2, (2014).

ACKNOWLEDGEMENTS

We would like to acknowledge the EU Erasmus Mundus program for their support.

In Vitro Modulation of the Behavior of Adhering Macrophages by Medications is Biomaterial Dependent

Lizette Utomo[1], Geesien S.A. Boersema[1,2], Yves Bayon[3], Johan F. Lange[2], Gerjo J.V.M van Osch[1,4], Yvonne M. Bastiaansen-Jenniskens[1]

[1]Department of Orthopaedics, Erasmus MC University Medical Center, Rotterdam, the Netherlands
[2]Department of Surgery, Erasmus MC University Medical Center, Rotterdam, the Netherlands
[3]Medtronic-Sofradim Production, Trévoux, France
[4]Department of Otorhinolaryngology, Erasmus MC University Medical Center, Rotterdam, the Netherlands

Introduction: Biomaterials are commonly used in orthopaedics, gynaecology, cardiology, and reconstructive and general surgery. Moreover, the frequency in which bioengineered tissues are being implanted is expanding rapidly. After implantation, the host immune system will immediately interact with the material by inducing an inflammatory response that involves cells such as macrophages. Macrophages play a key role in this initial response, become activated upon receiving stimuli from their environment, and can acquire a phenotype ranging from pro-inflammatory (M1) macrophages to anti-inflammatory (M2). The aim of this study was to assess whether the behavior of human monocyte-derived macrophages activated by biomaterials can be modulated using the compounds rapamycin, dexamethasone, celecoxib or pravastatin. These compounds are members of commonly used medication groups and are in literature described to have effects on inflammation.

Methods: Monocytes were isolated by $CD14^+$ selection from 9 buffy coats (47±15Y). The monocytes were pooled and seeded by rotation in a tube rotator at 20 rpm on monofilament polypropylene (ρ=0.9 g/cm^3; ø=0.10 mm; *l*=8 cm), polyethylene terephthalate (ρ=1.34 g/cm^3; ø=0.09 mm; *l*=8.8 cm,) or polylactic acid (ρ=1.25 g/cm^3; ø=0.10 mm; *l*=8 cm) yarns (Fig. 1). 850,000 monocytes were subjected to each yarn. The materials including adhering monocytes were then cultured in X-VIVO medium/20% FCS in 48-well plates for 3 days to allow for differentiation into macrophages. After this, 1 ng/mL rapamycin, 10^{-8} M dexamethasone, 0.1 µM celecoxib or 0.5 µM pravastatin were added to the biomaterials and cultured for an additional 3 days. DMSO was included as vehicle control for rapamycin and dexamethasone. After culture, the medium was harvested for IL-6, CCL18 and sCD163 protein quantification by ELISA. The macrophages that were adhering to the biomaterials were harvested for DNA quantification and gene expression analysis. Expression of Interleukin-1B (*IL1B*), IL6, Tumor necrosis factor-α (*TNFA*), chemokine (C-C motif) ligand 18 (*CCL18*), Mannose receptor, C type 1/CD206 (*MRC1*/*CD206*) and cluster of differentiation 163 (*CD163*) were assessed. Glyceraldehyde-3-phosphate dehydrogenase (*GAPDH*) was used as housekeeper and the relative expression was determined by the $2^{-\Delta CT}$ formula. The experiments were repeated three times in triplicate using pooled monocytes from 3 buffy coats per experiment.

Results Modulation of the adhering macrophages with rapamycin resulted in a generally pro-inflammatory effect. Dexamethasone caused an overall anti-inflammatory effect on the macrophages cultured on either material, while celecoxib only affected macrophages adhering to polyethylene terephthalate and polylactic acid. Pravastatin increased pro-inflammatory genes of macrophages cultured on polypropylene and polylactic acid. Pairwise comparison showed that macrophages adhering to polylactic acid are more susceptible to modulation, than when adhering to polypropylene or polyethylene terephthalate.

Discussion and conclusion:
The phenotype of macrophages activated by polypropylene, polyethylene terephthalate and polylactic acid can be modulated using commonly used medications. Modulation of macrophages activated by other biomaterials than used in the current study, may be possible as well. The degree of the modulatory capacity however depends on the type of biomaterial that causes initial activation. Combined, this knowledge provides insights into the possibility of using a medication in combination with a certain biomaterial to direct macrophage behavior and thereby possibly avoiding unwanted effects after implantation of a biomaterial.

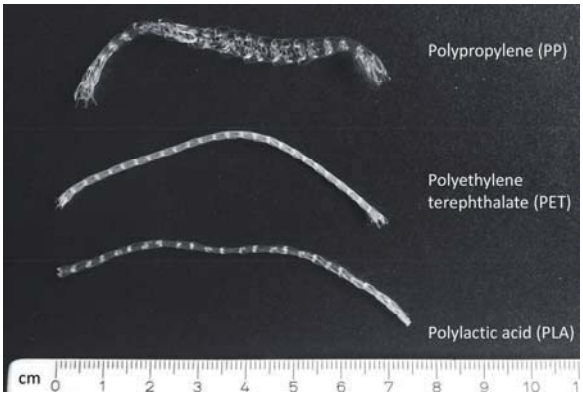

Fig. 1: Biomaterials used in this study

Is morphology a benchmark for instructing cell fate?

Aliaksei S Vasilevich[1], Steven Vermeulen[1], Marloes Kamphuis[1], Nick Beijer[1], Aurélie Carlier[1], Shantanu Singh[2], Jan de Boer[1]
[1]Laboratory for Cell Biology-inspired Tissue Engineering, MERLN Institute, Maastricht University, Maastricht, The Netherlands
[2]Imaging Platform, Broad Institute of MIT and Harvard, Cambridge, MA, USA.

Introduction

Surface topography can affect the morphology, proliferation, gene expression and differentiation of pluripotent cells. Here, we questioned if morphology can be correlated with cell phenotype. For this, we selected 28 surface topographies that elicit distinct cell morphologies in human mesenchymal stromal cells (hMSCs). The cell instructing potential of these surfaces was further evaluated by investigating a multitude of essential cellular functions e.g. migration, proliferation, apoptosis, protein synthesis and differentiation. This knowledge will expand our understanding of the influence of cell morphology on cellular function and opens new opportunities for the development of biomedical materials.

Methods

To obtain a variety of cell shapes, we applied a high-throughput screening with 2176 randomly generated topographies on hMSCs. Using image analysis and data mining methods described previously (1), multiparametric profiles of cell morphologies were obtained. This allowed us to select 28 surfaces that were able to induce the most distinct morphological response. For functional studies, we evaluated proliferation and protein synthesis by Click It EdU and HPG Alexa Fluor (Life Technologies) respectively. Migration and apoptosis were assessed by 24 hours observation using a Life Cell Imaging Microscope. To initiate apoptosis, staurosporine, a potent protein kinases inhibitor is added to the cell culture. Osteogenesis and adipogenesis are induced and quantified as described previously (2).

Results and Discussion

We observed a large diversity in cell responses for morphological distinct cells. Adipogenesis was promoted on topographies (Fig. 1d), while osteogenesis seemed inhibited compared to the blank polystyrene surface. A general trend was observed that surfaces decreased proliferation and protein synthesis, while migration was markedly increased (Fig. 1e). These striking observations illustrate that cell morphology can induce a variety of distinct cellular responses.

Conclusion

The novelty of our approach was to identify surfaces with instructive potential based on cell morphology data. We identified multiple surfaces that induced a variety in cellular response. In the next phase of this project, we explored the causality between cell morphology and phenotype. For this, we aim to expand these assays by targeting the key biomechanical regulatory proteins YAP/TAZ, SRF, MRTF-A, EGR1 and JNK in combination with microarray analysis. This will further extend our knowledge in both signaling pathways and genes involved in mechanotransduction.

Acknowledgement

The research leading to these results has received funding from the Dutch province of Limburg and the People Programme (Marie Curie Actions) of the European Union's Seventh Framework Programme FP7/2007-2013/ under REA grant agreement no.289720.

References

1. Hulsman et al., Acta Materialia (2015)
2. Siddapa et al., Journal of Orthopedic Research (2007)

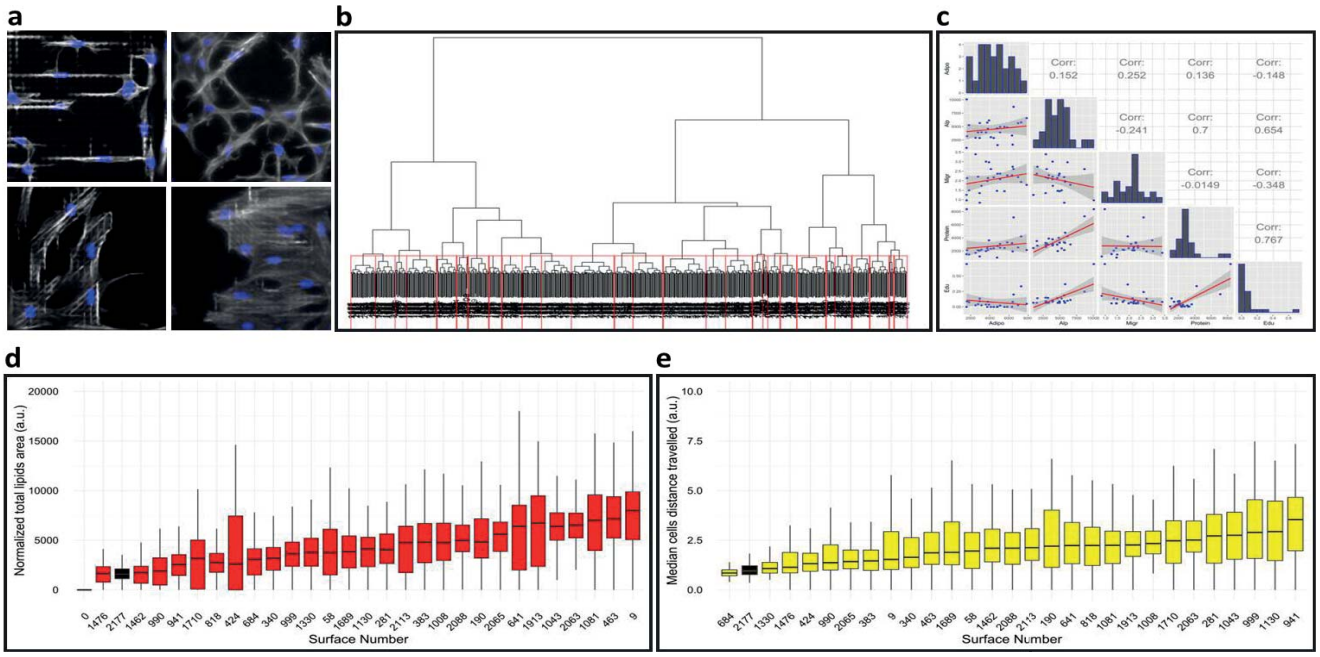

Fig. 1: a) Topographies induce a variety of cell morphologies **b)** Clustering analysis to select 28 topographies that elicit most distinct morphologies. **c)** Correlation analysis between cellular responses. **d)** adipogenesis and **e)** migration analysis of hMSCs cultured on these topographies.

Biomaterial degradation is dependent on macrophage polarization state

T. B. Wissing [a], M.C.P. Brugmans [b], A.I.P.M. Smits [a,c], C.V.C. Bouten [a,c],
[a] *Department of Biomedical Engineering, Eindhoven University of Technology, The Netherlands*
[b] *Xeltis B.V., Eindhoven, The Netherlands*
[c] *Institute for Complex Molecular Systems, Eindhoven University of Technology, The Netherlands*

Introduction

New, acellular, synthetic and biodegradable cardiovascular substitutes are being developed that upon implantation evoke a regenerative response *in situ*, ignited by the host' inflammatory response. For the success of these load-bearing substitutes it is important that the mechanical integrity is warranted throughout the regenerative process, which is highly dependent on the fragile balance between tissue formation and biomaterial degradation[1].

The heterogeneous macrophage population has been shown to play a pivotal role in both these processes, as macrophages contribute to extracellular matrix formation, remodelling and biomaterial degradation. It is the aim of this study to investigate how many degradation products (e.g. esterases, reactive oxygen species (ROS)) are being produced by the different macrophage phenotypes (pro-inflammatory (M1), anti-inflammatory (M2a) and regulatory (M2b)).

Materials and Methods

THP1 cells (human monocytic cell line, 1,25*10^6 cells/well) were seeded in 6-well plates and differentiated into adhering macrophages via phorbol 12-myristate 13-acetate (50 ng/ml, PMA, Sigma Aldrich) stimulation. Subsequently, macrophages were polarized into the pro-inflammatory (M1) (20ng/ml IFN-γ , 100 ng/ml LPS), the anti-inflammatory (M2a) (20 ng/ml IL-4, 20ng/ml IL-13) or the regulatory (M2b) (50 ng/ml IL-10) phenotype. Unstimulated macrophages served as the unpolarized (M0) control group. The 2D cultures were kept in culture for 4 days and cytokine enriched medium was refreshed at day 2. Samples of the medium were collected at day 2 and 4 to determine the esterase production in time. At day 4, the cells were sacrificed and processed for further analysis to 1) visualize active ROS production (CellROX reagent, deep red, Life Technologies), 2) quantify lipid peroxidation as a measure for oxidative stress (Lipid Peroxidation (MDA) assay, Sigma Aldrich), 3) determine the DNA content and 4) confirm macrophage polarization on gene and protein level.

Results

The unpolarised (M0), pro-inflammatory (M1) and regulatory (M2b) macrophages showed pronounced active ROS production at day 4, where hardly any active ROS production was detected in the anti-inflammatory (M2a) macrophage group (fig 1). Furthermore, MDA analysis revealed a 19 ± 1,8% increase in lipid peroxidation (a measure for oxidative stress) for the pro-inflammatory (M1) macrophage group when compared to the unpolarized (M0) and regulatory (M2b) macrophage group (fig 2). In contrast, MDA expression in the anti-inflammatory M2a group was 21,4 ± 3,7% decreased in comparison to the M0 control.

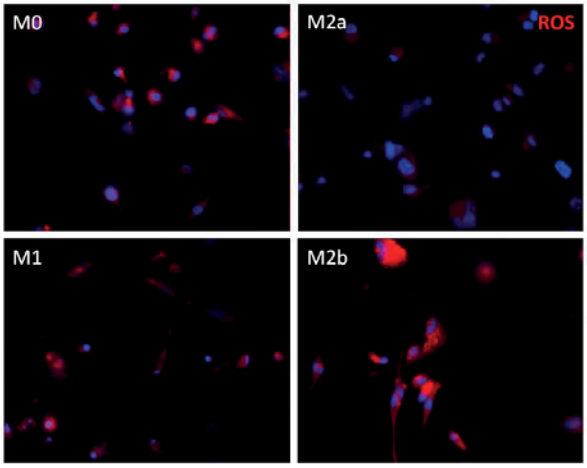

Fig. 1 Immunostainings of the differently polarized macrophages at day 4 to visualize active ROS production. n=2 per group.

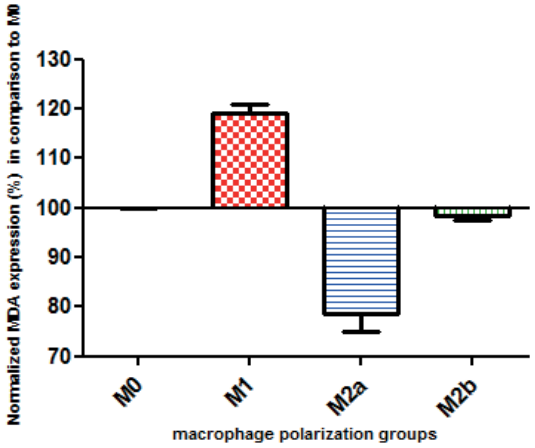

Fig 2. Relative percentages of malondialdehyde (MDA, by-product of lipid peroxidation) expression (day 4) of the differently polarized macrophages in comparison to the unpolarized (M0) group (value set to 100%). Values are corrected for the amount of DNA present and presented as average ± SD. n=2/3 per group.

Conclusions

The current results indicate that the inflammatory macrophage phenotype (M1) may accelerate oxidative degradation, while M2a polarization attenuates it. Future research will focus on the esterase and ROS production of differently polarized macrophages when seeded in 2D and 3D on electrospun synthetic meshes used for in situ tissue regeneration. Ultimately, these insights might be translated towards immunomodulatory design strategies to tune biomaterial degradation.

References

1. Brugmans MCP, (2015) *Acta Biomat*. 2015;27:21 31.

Acknowledgements

We acknowledge the support from the Netherlands Cardio Vascular Research Initiative: The Dutch Heart Foundation, Dutch Federation of University Medical Centres, the Netherlands Organisation for Health Research and Development and the Royal Netherlands Academy of Sciences.

Development of Intelligent Inks for 3D-printing using Supramolecular Polymers for Biomedical Applications

D.J. Wu[1,2], C.V.C. Bouten[1,2], P.Y.W. Dankers[1,2,3]

1 Laboratory for Cell and Tissue Engineering, Department of Biomedical Engineering, Eindhoven University of Technology, PO Box 513, 5600 MB Eindhoven, The Netherlands

2 Institute for Complex Molecular Systems, Eindhoven University of Technology, PO Box 513, 5600 MB Eindhoven, The Netherlands

3 Laboratory of Chemical Biology, Department of Biomedical Engineering, Eindhoven University of Technology, PO Box 513, 5600 MB Eindhoven, The Netherlands

Three-dimensional (3D) printing technology in tissue engineering and regenerative medicine allows the direct generation of complex structured scaffolds in a layer-by-layer fashion through computer-aided design (CAD).[1] This technique is ideal for the fabrication of customized scaffolds with precise control over advanced scaffolds with specific design properties. These scaffolds provide support to the cells and degrade over time as the tissue is formed. Cells are able to migrate and proliferate on scaffolds and excrete extracellular matrix (ECM), that are a crucial processes of forming a functional tissue.[2] 3D cell scaffolding involve various complexities such as: material choice, scaffold's morphology, cell attachment and migration, biological and physical stimuli.

A common used 3D print technique is the fused deposition modeling (FDM) printing technique. It is a low cost technique and makes use of an open source software. However, FDM printers have a few challenges with respect to the production of high resolution complex structures. Moreover, the printers have low resolution (100 micron), limited heating temperature (120 degrees Celsius) and material viscosity dependent. To overcome these problems we propose to use supramolecular polymers. These materials are able to crosslink via specific, directed non-covalent interactions.[3] These polymers can be mixed-and-matched in a modular approach due to our supramolecular polymer toolbox, which allows us to introduce novel printing strategies that are proposed to overcome the printing challenges and improve the complex scaffold production.

[1] Zhang, Y. S. *et al.* (2016). 3D Bioprinting for Tissue and Organ Fabrication. *Annals of biomedical engineering*, 1-16.

[2] Hutmacher, D. W. (2000). Scaffolds in tissue engineering bone and cartilage. Biomaterials, 21(24), 2529- 2543.

[3] Brunsveld, L. *et al* (2001). Supramolecular polymers. *Chemical Reviews*, *101*(12), 4071-4098.

‘Easy access cells’ for intra-operative preparation of cell-based bone regenerative constructs

Y Zhang[1], EC Grosfeld[1], W Camargo[1], H Tang[1,2], AMP Magri[1,3], JA Jansen[1], AC Renno[3], JJJP van den Beucken[1,*]
1 Department of Biomaterials, Radboudumc, Nijmegen, the Netherlands
2 Department of plastic surgery, Tongji Hospital, Huazhong University of Science and Technology, China
3 Department of Bioscience, Federal University of São Paulo, Brazil
* Corresponding author: Jeroen.vandenBeucken@radboudumc.nl

Introduction: Bone defects represent an increasing clinical challenge worldwide. Tissue engineering principles have provided a toolbox to develop suitable strategies based on e.g. scaffolds and bone-forming cells. The general procedure to prepare cell-based constructs involves cell harvest from bone marrow, cell isolation, expansion, seeding and pre-culture on a 3D scaffold, which includes several disadvantages such as time-consumption, high costs, and not patient-friendly with multiple surgical interventions. Lately, adipose tissue is becoming increasingly popular tissue for harvesting mesenchymal stromal cells (ADMSCs) due to the easier and less invasive harvest procedures and larger yield compared to bone marrow. The primary isolate from adipose tissue is known as the stromal vascular fraction (SVF), which is a heterogeneous mixture of predominantly MSCs, endothelial cells, smooth muscle cells, and pericytes [1]. SVF has shown potential for an intra-operative preparation concept due to its easy access and large yield [2]. However, how efficient this intra-operative SVF-based strategy is compared to the ‘conventional’ ADMSC-based approach is not clear [3]. Additionally, a previous study has shown beneficial effects of cell-cell interactions by applying multiple cell types in cell-based constructs [4, 5]. Other cells that can be easily isolated are monocytes (MO) from blood. Interestingly, monocytes have shown to stimulate osteogenic events by attracting MSCs, and stimulating MSCs to proliferate and/or osteogenically differentiate [6]. Consequently, it seems appealing to combine SVF and monocytes as ‘easy access cells’ to heal bone defects in an innovative intra-operative manner.

Objective: Here, we compare the osteogenic performance of SVF- and ADMSC-based constructs either or not in combination with monocytes toward an intra-operative treatment modality for bone defects.

Methods: Six types of bone regenerative constructs were used with calcium phosphate ceramic granules (Cam Bioceramics BV, Leiden, the Netherlands) as a cell carrier: 1) granules (Control); 2) granules + ADMSCs; 3) granules + SVF; 4) granules + MO; 5) granules + ADMSCs & MO; 6) granules + SVF & MO. For *in vitro* evaluation, cell attachment, proliferation and osteogenic differentiation were assessed by immunostaining, DNA content, alkaline phosphatase (ALP) activity and calcium assay. For *in vivo* work, all constructs were implanted bilaterally into rat femoral defects (3 mm diameter) and bone formation was assessed histologically and histomorphometrically after 4 and 10 weeks.

Results: During 4 weeks in vitro culture, co-seeding with monocytes significantly promoted osteogenic differentiation of stromal cells (Figure 1). Additionally, SVF had the same osteogenic potential compared to pure ADMSCs. After subcutaneous implantation, none of the experimental showed bone formation. In the orthotopic model (Figure 2), implants containing SVF or ADMSCs displayed a significant higher rate of bone formation compared to granules alone (Figure 3). More importantly, constructs generated from SVF formed more bone compared to those from ADMSCs. The supplementation of monocytes to the constructs showed no additional improve in bone formation compared to SVF or ADMSCs. Further experiments indicated that the superior bone formation of SVF might result from their immunoregulatory effects.

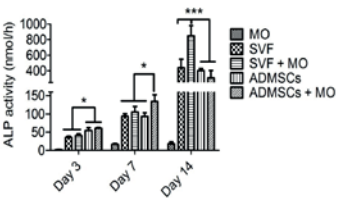

Figure 1 Osteogenic differentiation of SVF and ADMSCs and co-seeding with monocytes was assessed by ALP activity in vitro.

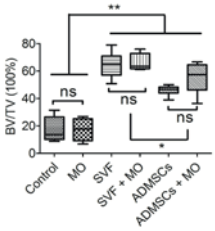

Figure 2 Histomorphometrical analysis of bone formation of different constructs after 10 weeks orthortopic implantation in vivo.

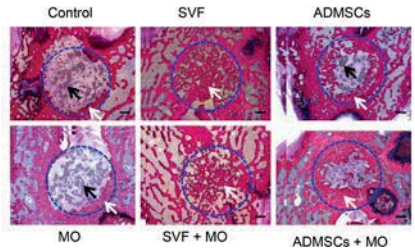

Figure 3: Representative histological sections 10 weeks after construct installment in rat femoral condyles (methylene blue/basic fuchsin stain; blue circle indicates original defect area; black arrow indicates granules; white arrow indicates new bone)

Conclusion: This study demonstrated that intra-operatively prepared SVF-based constructs can effectively be used for bone regeneration with superior bone formation compared to ADMSC-based constructs. No additional effects of intra-operative monocyte supplementation were observed.

References:

1) Varma et al. Stem Cells Dev. 2007 Feb;16(1):91-104.
2) Saxer et al. Stem Cells. 2016 Aug 19. doi: 10.1002/stem.2478. Epub ahead of print
3) Jurgens et al. J Orthop Res. 2011 Jun;29(6):853-60.
4) Ma et al. J Tissue Eng Regen Med. 2015 Jul;9(7):779-88.
5) Hayrapetyan et al. Tissue Eng Regen Med 2016;13(6):1-10
6) Kovach et al. J Immunol Res 2015; 752510.

Acknowledgements: YZ was supported by a grant from the China Scholarship Council (No. 2013622061); JB was financially supported by a grant from ZonMw-TAS (No. 40-41400-98-1401).